

**Optimizing Surface Texturing for YSZ Thermal-Barrier-Coating on Inconel
718 Substrate to Mitigate High Stresses/Strains**

A Technical Report submitted to the Department of Materials Science & Engineering

Presented to the Faculty of the School of Engineering and Applied Science
University of Virginia • Charlottesville, Virginia

In Partial Fulfillment of the Requirements for the Degree
Bachelor of Science, School of Engineering

Nico Fonseca Alva

Spring, 2025

Technical Project Team Members

Iris Boateng

Lara Ojha

Alice Pandaleon

Chris Recuperero

On my honor as a University Student, I have neither given nor received unauthorized aid on this assignment as defined by the Honor Guidelines for Thesis-Related Assignments

Dr. James Fitz-Gerald, Department of Materials Science & Engineering

Contact Information

Collaborators

Dr. Robert Golden, of Rolls-Royce Corporation (Robert.Golden@rolls-royce.com)

Matthew Gold, of Rolls-Royce Corporation (Matthew.Gold@liberty.rolls-royce.com)

Jason Kalishek, of PulseTex (jkalishek@pulsetex.com)

John Sions, of CCAM (john.sions@ccam-va.com)

Grant Sowels, of CCAM (grant.sowels@ccam-va.com)

Dan Cunningham, of CCAM (dan.cunningham@ccam-va.com)

UVA Mentorship

Dr. James Fitz-Gerald, Capstone Advisor (jmf8h@virginia.edu)

Dr. Elizabeth Opila, Subject Matter Expert (ejo4n@virginia.edu)

Authors

Iris Boateng (zga9sh@virginia.edu)

Nicolas Fonseca Alva (uyf4cp@virginia.edu)

Lara Ojha (ssa3yw@virginia.edu)

Alice Pandaleon (fdc3dj@virginia.edu)

Christopher Recuperero (qkk5vr@virginia.edu)

Table of Contents

| | | |
|------|--|----|
| I. | Executive Summary | 14 |
| II. | Project Timeline..... | 16 |
| A. | Gantt Chart..... | 16 |
| III. | Cost Data and Constraints..... | 19 |
| A. | Cost Analysis | 19 |
| 1. | Original Estimated Costs | 19 |
| 2. | Final Cost Analysis..... | 20 |
| B. | Constraints | 22 |
| IV. | Project Challenges | 23 |
| A. | Sample Prep | 23 |
| 1. | EDM..... | 23 |
| 2. | Cutting of Mounted Samples | 23 |
| 3. | Auto polishing..... | 24 |
| B. | Spray Parameter Confusion | 24 |
| C. | Adapting Furnace Procedures | 25 |
| V. | Technical and Detailed Drawings & Sample Design | 25 |
| A. | Textures..... | 25 |
| B. | Sample Generation Pathway | 27 |
| 1. | Sectioning of IN718..... | 27 |
| 2. | Grit Blasting & Bond Coat Application at CCAM..... | 28 |
| 3. | Lasering..... | 30 |
| 4. | Spray Parameter Selection & Coating Procedure | 30 |
| VI. | Experiments Conducted and Equipment Used | 32 |
| A. | Thermal Cycling | 32 |
| B. | Accelerated Thermal Cycling | 33 |
| C. | Adhesion Testing | 33 |
| D. | Characterization Process & Equipment | 34 |
| 1. | Sample Preparation | 34 |
| 2. | Microscopy | 35 |
| VII. | Results: Characterization and Analysis Conducted | 36 |
| A. | Substrate Characterization | 36 |
| B. | Bond Coat Characterization..... | 41 |

| | | |
|-------|--|-----|
| 1. | Profilometry of the Bond Coat..... | 41 |
| 2. | SEM of the Bond Coat..... | 42 |
| 3. | ImageJ Analysis of Bond Coat Thickness after TBC Spraying..... | 43 |
| C. | Pre-Spray Characterization | 45 |
| 1. | Optical Micrographs from PulseTex..... | 45 |
| 2. | SEM | 46 |
| 3. | Profilometry | 47 |
| D. | Analyzing Spray Parameters..... | 49 |
| E. | As-Sprayed Sample Analysis..... | 51 |
| 1. | Grit Blasted | 51 |
| 2. | T1 | 53 |
| 3. | T2 | 55 |
| 4. | T3 | 58 |
| 5. | Overview of Cracking..... | 59 |
| F. | Thermal Cycling Results and Characterization | 60 |
| 1. | Grit Blasted Sample Characterization..... | 67 |
| 2. | T1 | 70 |
| 3. | T2 | 79 |
| 4. | T3 | 82 |
| G. | Accelerated Thermal Cycling Results | 88 |
| 1. | Grit Blasted | 90 |
| 2. | T1 | 91 |
| 3. | T2 | 95 |
| 4. | T3 | 98 |
| H. | Adhesion Testing Results | 101 |
| VIII. | Discussion of Results..... | 105 |
| A. | DVC Induction & Oxidation..... | 105 |
| 1. | Grit Blasted Progression | 105 |
| 2. | T1 Progression | 108 |
| 3. | T2 Progression | 109 |
| 4. | T3 Progression | 110 |
| B. | Adhesion Failure..... | 111 |
| IX. | Conclusions and Future Work | 113 |
| A. | Conclusions..... | 113 |
| 1. | Bond Coat Thickness | 113 |
| 2. | TBC Spray Parameters..... | 113 |
| 3. | Mechanical Interlocking is Improved from Texturing..... | 113 |

| | | |
|------|---|-----|
| 4. | YSZ Powder Size..... | 114 |
| 5. | Regular DVC Spacing is Possible..... | 114 |
| B. | Suggested Future Work..... | 114 |
| X. | Acknowledgements..... | 115 |
| XI. | References..... | 115 |
| XII. | Appendices..... | 116 |
| | Appendix A: Bond Coat Powder and Spray Parameters | 116 |
| | Appendix B: Thermal Cycling..... | 118 |
| | Appendix C: Sample Preparation Equipment..... | 119 |
| | Appendix D: Characterization Equipment..... | 120 |
| | Appendix E: TBC Spray Parameters | 121 |

List of Figures and Tables

| | |
|---|----|
| Figure 1: Dense Vertical Cracks (DVCs) as seen in a thermal barrier coating system | 15 |
| Figure 2: Finalized Gantt chart (a) compared to original Gantt (b). | 17 |
| Table 1: Predicted experimental costs. | 19 |
| Table 2: Predicted sample preparation costs..... | 20 |
| Table 3: Predicted total costs. | 20 |
| Table 4: Actual experimentation costs..... | 21 |
| Table 5: Actual sample preparation costs. | 21 |
| Table 6: Actual final cost. | 21 |
| Figure 3: Mounted sample after being cut too fast, showing burnt TBC and some epoxy melting. After the saw was slowed down, the rest of the sample remained unburned. | 24 |
| Figure 4: Dimensioned view of rounded spikes design. | 26 |
| Figure 5: Dimensioned view of grid pattern design..... | 26 |
| Figure 6: Dimensioned view of grown columnar texture. Dimensions are a rough estimate as the process is less controlled than ablation. | 27 |
| Figure 7: Sample generation pathway..... | 27 |
| Figure 8: Samples after grit blasting; (a) comparison of machined (left) and grit blast (right) samples, (b) grit blast samples on a tray after being taken out of chamber. | 28 |
| Figure 9: (a) Samples in holders being placed on magnetic board for spraying, (b) Robotic arm used for spraying, (c) Plasma powders fed into the gun. | 29 |
| Figure 10: (a) Plasma spraying of the bond coat, (b) Monitoring of spray parameters on Tecnar software, (c) Samples after bond coat application. | 29 |
| Table 7: Nine distinct spray parameters for TBC steel samples. | 31 |
| Figure 11: (a) 3 steel samples after TBC application, (b) Staggered samples on board after TBC spraying..... | 31 |

| | |
|--|----|
| Figure 12: (a) Scale used to measure masses of steel samples before TBC spraying, (b) Caliper used to measure sample thicknesses before and after spraying. | 31 |
| Figure 13: Thermal cycling experimental setup. | 33 |
| Figure 14: Tensile adhesion testing setup. | 34 |
| Table 8: Polishing procedure for TBC samples | 35 |
| Table 9: Sample Thickness Statistics..... | 36 |
| Figure 15: Micrographs of a lathe-cut IN718 sample taken by the Hirox Optical microscope at various magnifications; (a) overview of machined sample at 5X, (b) center of machined sample at 140X, (c) lathe marks at 50X, and (d) lathe marks at 1000X. | 37 |
| Figure 16: Micrographs of a lathe-cut IN718 sample after polishing with 180 grit sandpaper taken by the Hirox Optical microscope at various magnifications; (a) overview at 10X, (b) edge of sample at 30X, (c) polish of sample at 1000X, (d) polish of sample at 30X. | 38 |
| Figure 17(a), (b), (c), (d), (e), (f): Micrographs of a lathe-cut IN718 sample after polishing with 180 grit sandpaper taken by the Quanta 650 scanning-electron-microscope in BSE mode at various magnifications. | 39 |
| Figure 18: EDS compositional analysis performed on IN718 sample. (a) Inspected region and (b) Corresponding spectrum. | 40 |
| Table 10: EDS Compositional breakdown for the IN718 sample. | 40 |
| Table 11: Known IN718 composition ranges, from specialmetals.com. | 41 |
| Table 12: Profilometry Results Averaged from 40 Measurements on 2 Samples | 41 |
| Figure 19: BSE SEM micrographs of bond coat/substrate interface. (a) Wide view of interface at 1000X, (b) High magnification view of interface taken at 5000X showing the roughness of the substrate, (c) Peaks and valleys seen in the bond coat profile, and (d) Porosity found in the coating. | 42 |
| Figure 20: Examples of the area selection utilized for determining the average bond layer thickness of each texture. (a) GB, (b) T1, (c) T2, and (d) T3. | 43 |
| Table 13: Tabulated results of bond layer thickness analysis on SEM Micrographs at 100X. | 43 |
| Figure 21: Optical micrograph of rounded spikes texture produced by PulseTex. | 45 |

| | |
|---|----|
| Figure 22: Optical micrographs of grid pattern texture produced by PulseTex. | 45 |
| Figure 23: Optical micrographs of grown texture produced by PulseTex. | 46 |
| Figure 24(a), (b): SEM micrographs of rounded spike textured sample. | 46 |
| Figure 25(a), (b): SEM micrographs of grid pattern texture sample. | 46 |
| Figure 26: (a), (b): SEM micrographs of grown texture sample. | 47 |
| Figure 27: Zygo profilometry scan of rounded spike texture at 20X. | 48 |
| Figure 28: Zygo profilometry scan of grid pattern at 20X. | 48 |
| Figure 29: Zygo profilometry scan of grown texture at 20X. | 49 |
| Figure 30: Optical Micrographs of the as-sprayed TBC surface; (a) at 1000X, and (b) 140X. | 49 |
| Figure 31: Cross-sections of the nine different TBC steel samples corresponding to spray parameters in Table 7. Seen is the IN718 substrate, Amdry 386-4 bond coat, and YSZ topcoat. | 50 |
| Figure 32: BSE SEM taken for the non-textured, grit-blasted as-sprayed sample. It is observed that the DVCs tend to follow a random pattern. | 52 |
| Figure 33: EDS of as-sprayed GB sample. Shows the expected three regions of TBC, bond coat, and IN718. | 52 |
| Table 14: Compositional results for EDS on as-sprayed GB sample. Compositions given in atomic concentration (%). | 53 |
| Figure 34: BSE SEM micrographs of coated rounded spike textured sample at (a) 50X and (b) 250X. Micrographs show that most of the bond coat was removed during ablation. | 54 |
| Figure 35: Map EDS of rounded spike coated sample. Shows four distinct regions: IN718 substrate, bond coat, intermediate phase, and TBC topcoat. Point EDS was conducted on regions with red X. | 55 |
| Table 15: Point EDS results from rounded spike coated sample in three different regions. | 55 |
| Figure 36: BSE SEM of T2 grid pattern at different magnifications (a,b). It is observed that the laser went through the entire bond coat at spots, allowing the TBC to be in contact with the surface. | 56 |

| | |
|--|----|
| Figure 37: EDS of T2 sample. Shows four distinct regions that include IN718, bond coat, TBC, and an intermediate phase between the bond coat and TBC. | 57 |
| Table 16: Compositional results for EDS on as-sprayed T2 sample. Compositions given in atomic concentration (%). | 57 |
| Figure 38: BSE SEM of as-sprayed T3 grown texture sample at (a) 50X and (b) 400X. Micrographs show some porosity at bond coat/TBC interface. | 58 |
| Figure 39: EDS map of grown texture coating system. Shows distinct substrate, bond coat, and TBC layers with some porosity at bond coat/TBC interface. | 59 |
| Table 17: Table of calculated vertical crack linear density. | 59 |
| Figure 40: BSE micrographs of as-sprayed samples at 100X; (a) GB, (b) T1, (c) T2, and (d) T3. | 60 |
| Figure 41: Overview shots of each sample after they had been removed from furnace cycle testing due to reaching >50% spallation. | 61 |
| Table 18: Final percent spallation of samples after being cycled in the furnace | 61 |
| Figure 42: Samples after 1 cycle (left) vs after 2 cycles (right). All T1 samples have surpassed 50% spallation. | 62 |
| Figure 43: Samples after 9 cycles, showing T3-B1 and T3-B2 with over 50% spallation and T3-B3 beginning to fail. | 63 |
| Figure 44: (a) Samples after 13 cycles, showing failure of GB samples and the last T3 sample. Note: the missing samples are because the team removed the samples that had previously failed (T1-B1—T1-B4 and T3-B1—T3-B4) to begin characterization, and (b) Side view of samples 3-4 cycles before GB failure, showing the beginning of peeling. | 64 |
| Figure 45: (a) Samples after cycle 15, showing that only GB-B3, T2-B3, and T2-B4 remain (circled), and (b) Samples after cycle 16, all samples have reached 50% spallation threshold. | 65 |
| Table 19: Failure summary table for results of thermal cycling. | 65 |
| Figure 46: (a) Plot of mass loss of each sample over time, and (b) histogram showing starting and ending masses of each sample. | 66 |

| | |
|---|----|
| Figure 47: Optical micrographs of TBC remnants on grit blasted samples at (a) 100X and (b) 150X..... | 67 |
| Figure 48: BSE SEM of GB long furnace cycled samples. The remaining bond coat and TGO are visible. The TBC spalled off the sample..... | 68 |
| Figure 49: EDS of cycled GB sample. Shows residual TBC, TBC/bond coat oxide, dark layer within the bond coat, underlying bond coat, and IN718..... | 69 |
| Table 20: Compositional results for EDS on cycled grit blast sample. Compositions given in atomic concentration (%)...... | 69 |
| Figure 50: Cycled grit blast map EDS separated by element. (a) Oxygen, (b) Aluminum, (c) Chromium, and (d) Zirconium. Highlights remaining TBC, chromium oxide at TBC/bond coat interface, and aluminum oxide within the bond coat. | 70 |
| Figure 51: Optical micrographs of T1 sample surfaces after furnace cycling: (a) a sample edge showing chipping of TBC and crack profiles at 50X, (b) edge of TBC showing cracking at 50X, (c) mid-TBC surface crack at 50X, and (d) microcrack in the TBC at 3000X..... | 71 |
| Figure 52: BSE SEM micrographs of T1 samples. A new layer formed between the substrate and the TBC, resulting in the delamination of this layer from the substrate, pinching the spikes in the process..... | 72 |
| Figure 53: Map and point EDS of thermally cycled rounded spike sample. Map shows distinct chromium-rich region at substrate/bond coat interface and composition gradient in rounded spikes..... | 75 |
| Figure 54: Select EDS maps of thermally cycled rounded spike sample. Shows concentration gradients and segregation within the spikes. (a) Iron, (b) Aluminum, (c) Oxygen, (d) Cobalt, and (e) Chromium. | 76 |
| Table 21: Point EDS results for thermally cycled rounded spike samples. Results shown for 7 regions on the sample..... | 77 |
| Figure 55: Line scan EDS of thermally cycled rounded spike samples. Line (1) captures chromium rich region and Line (2) captures concentration gradient up the spike. | 78 |
| Figure 56: Line scan (1) results showing pure chromium rich region suggestion a chromium oxide..... | 78 |
| Figure 57: Line scan (2) results. Shows decrease in iron and nickel going up the spike, slight chromium deficiency at the bottom of the spike, and cobalt increase going up the spike.... | 78 |

| | |
|--|----|
| Figure 58: Optical micrographs of T2 sample surfaces after furnace cycling: (a) TBC edge showing zig-zag failure at 150X, (b) grid pattern in bond coat revealed with remaining TBC following this grid payment at 50X, (c) TBC and bond coat failure at 50X, and (d) a substrate surface where the bond coat grid pattern had been destroyed at 35X. | 79 |
| Figure 59: BSE SEM micrographs of the T2 long furnaced cycled sample. The TBC completely delaminated, and the bond coat appears to have remained partially on the substrate. | 80 |
| Figure 60: EDS of cycled T2 sample. Shows oxidized bond coat, substrate/bond coat oxide, dark regions within the substrate, and IN718. | 81 |
| Table 22: Compositional results for EDS on cycled T2 sample. Compositions given in atomic concentration (%). | 81 |
| Figure 61: Cycled T2 map EDS separated by element. (a) Oxygen, (b) Aluminum, (c) Chromium, and (d) Nickel. Highlights oxidized bond coat, chromium oxide at substrate/bond coat interface, and aluminum oxide within the substrate. | 82 |
| Figure 62: Optical micrographs of T3 sample surfaces after furnace cycling: (a) cracks around an area where a piece of TBC chipped off at 50X, (b) edge of TBC peeling off substrate at 50X, (c) crack geometry in TBC at 100X, and (d) base metal that TBC has come off from at 50X. | 83 |
| Figure 63: BSE SEM micrographs of T3 sample after furnace cycling. The delaminated topcoat/bond coat from the substrate can be observed along with the DVCs and an unknown interlayer. | 84 |
| Figure 64: EDS map of spalled off coating. Shows 2 distinct regions within the bond coat, including an aluminum rich region. | 85 |
| Table 23: Point EDS for T3 cycled coating | 86 |
| Figure 65: Individual EDS maps of T3 coating. (a) Oxygen, (b) Aluminum, and (c) Chromium. | 86 |
| Figure 66: Substrate/bond coat interface EDS map for T3. Shows chromium remnants on surface after complete delamination. | 87 |
| Table 24: Point EDS for bond coat/substrate interface on failed T3 sample. | 87 |
| Figure 67: Individual EDS maps of T3 substrate. (a) Oxygen, (b) Aluminum, and (c) Chromium. | 88 |

Figure 68: (a) Samples after one accelerated thermal cycle, first column retired. (b) Samples after two accelerated cycles, second column retired. (c) Samples after 3 accelerated thermal cycles, third column retired. At this point, some burning of the GB sample in the 4th column was observed. (d) Samples after 4 accelerated thermal cycles. No failure or spallation can be seen after the completion of the accelerated thermal cycling. 89

Figure 69: BSE SEM for the GB sample undergone 4 short furnace cycles. The TGO has started growing between the bond coat/TBC interface. 90

Figure 70: EDS of grit blast sample after 4 cycles. Shows early formation of aluminum oxide at TBC/bond coat interface. (a) Full EDS map, (b) Oxygen map, and (c) Aluminum map. 91

Table 25: Compositional results for EDS on grit blast sample after 4 cycles. Compositions given in atomic concentration (%). 91

Figure 71: BSE SEM for the T1 sample subjected to 4 short furnace cycles. TGO appears to have grown in between the rounded spikes deep into the substrate along the bond coat/TBC interface. 92

Figure 72: EDS of T1 after 4 cycles. Shows early formation of aluminum, chromium, and iron oxides at different interfaces within the coating system. (a) Full EDS map, (b) Oxygen map, (c) Aluminum map, (d) Chromium map, and (e) Iron map. 94

Table 26: Compositional results for EDS on T1 after 4 cycles. Compositions given in atomic concentration (%). 95

Figure 73: BSE SEM for the T2 sample subjected to 4 short furnace cycles. TGO appears to have grown in the trenches where the TBC is in contact with the substrate and in the interface between the bond coat and the TBC. 95

Figure 74: EDS of T2 after 4 cycles. Shows early formation of aluminum and chromium oxides at different interfaces within the coating system. (a) Full EDS map, (b) Oxygen map, (c) Aluminum map, and (d) Chromium map. 97

Table 27: Compositional results for EDS on T2 after 4 cycles. Compositions given in atomic concentration (%). 98

Figure 75: BSE SEM for the T3 sample subjected to 4 short furnace cycles. TGO appears to have grown on the interface between the bond coat and the TBC. 99

| | |
|--|-----|
| Figure 76: EDS of T3 after 4 cycles. Shows early formation of aluminum and chromium oxides at different interfaces within the coating system. (a) Full EDS map, (b) Oxygen map, (c) Aluminum map, (d) Chromium map. | 100 |
| Table 28: Compositional results for EDS on T3 after 4 cycles. Compositions given in atomic concentration (%). | 101 |
| Table 29: Tabulated bond strength results (psi) from adhesion testing. Largest and smallest reported values in green and red, respectively. | 101 |
| Figure 77: Fracture surfaces of adhesion tested samples. Samples exhibit failure though the TBC as well as through the bond coat. | 102 |
| Figure 78: Optical micrographs of the metal side of a GB sample, post-adhesion testing; (a) surface showing mostly TBC failure, and (b) section of the surface where some bond coat has been torn out. | 103 |
| Figure 79: Optical micrographs of the coating side of a GB sample, post-adhesion testing; (a) what most of the coating-side surface looks like, showing that most of what was pulled off was coating, with only some small amounts of bond coat, and (b) a region of the coating-side surface showing a section of bond coat that was torn out – likely corresponding with the area torn out from the metal-side surface in Figure 78(b). | 104 |
| Figure 80: Optical micrographs of the metal side of a T1 sample, post-adhesion testing; (a) what most of the metal-side surface looks like, showing that virtually all failure is within the TBC, and (b) edge exposing top of bond coat texture. | 104 |
| Figure 81: Optical micrographs of the metal side of a T2 sample, post-adhesion testing; (a) a region showing TBC failure, interface failure, as well as bond coat failure, and (b) what left over bond coat looked like. | 105 |
| Figure 82: Optical micrographs of the metal side of a T3 sample, post-adhesion testing; (a) a region of exposed bond substrate and (b) an area showing failure within TBC as well as at the bond coat/TBC interface. | 105 |
| Figure 83: Bond coat/TBC interface progression of GB sample from (a) as-sprayed, (b) 4 short thermal cycles, and (c) failure after long thermal cycles. Shows TGO growth that contributed to coating failure. | 107 |
| Figure 84: (a) BSE SEM micrograph of the test steel sample sprayed using spray parameter 4, and (b) BSE SEM micrograph of an as-sprayed grit blast sample which had TBC applied using supposedly the same spray parameters. | 108 |

| | |
|---|-----|
| Figure 85: Bond coat/TBC interface progression of T1 from (a) as-sprayed, (b) 4 short thermal cycles, and (c) failure after long thermal cycles. Shows TGO growth that contributed to coating failure. | 109 |
| Figure 86: Bond coat/TBC interface progression of T2 from (a) as-sprayed, (b) 4 short thermal cycles, and (c) failure after long thermal cycles. Shows TGO growth that contributed to coating failure. | 110 |
| Figure 87: Bond coat/TBC interface progression of T3 from (a) as-sprayed, (b) 4 short thermal cycles, and (c) failure after long thermal cycles. Shows TGO growth that contributed to coating failure. | 111 |
| Figure 88: Comparison of adhesion tested metal surfaces; (a) GB, (b) T1, (c) T2, and (d) T3.. | 112 |
| Table A.1: Amdry 386-4 Composition. | 116 |
| Table A.2: Bond coat spray parameters. | 117 |
| Figure B.1: One of the two furnaces in the Opila lab used for thermal cycling. | 118 |
| Table B.1: Furnace schedule used to divide responsibility for taking samples out of the furnace and putting them back after an hour, every 12 hours. | 118 |
| Figure C.1: Samples placed in epoxy for mounting post-furnace-cycling. | 119 |
| Figure C.2: Image of resin bond Al ₂ O ₃ blade. | 119 |
| Figure C.3: Cressington 108 Auto Sputter Coater | 119 |
| Figure D.1: Hirox RH-8800 used for optical microscopy. | 120 |
| Figure D.2: (a) Phenom XL G2 SEM and (b) Quanta 650 SEM. | 120 |
| Table E.1: Recorded TBC Spray Parameters..... | 121 |

I. Executive Summary

This project is a UVA Materials Science and Engineering capstone project in partnership with Rolls-Royce Corporation, PulseTex, and the Commonwealth Center for Advanced Manufacturing (CCAM). High temperature material systems, such as turbine engines manufactured by Rolls-Royce, require thermal barrier coatings (TBCs) with low thermal conductivity to protect engine components from heat damage. These coating systems are

composed of a metallic bond coat for proper adhesion and a ceramic topcoat composed of Yttria-Stabilized-Zirconia (YSZ) with low thermal conductivity, as seen in Figure 1. While effective at reducing the amount of heat to which the substrate is exposed, the varied coefficients of thermal expansion (CTEs) of the different components within the coating system, when combined with thermal cycling, make the system susceptible to high stresses and, subsequently, coating spallation, oxidation, and failure.

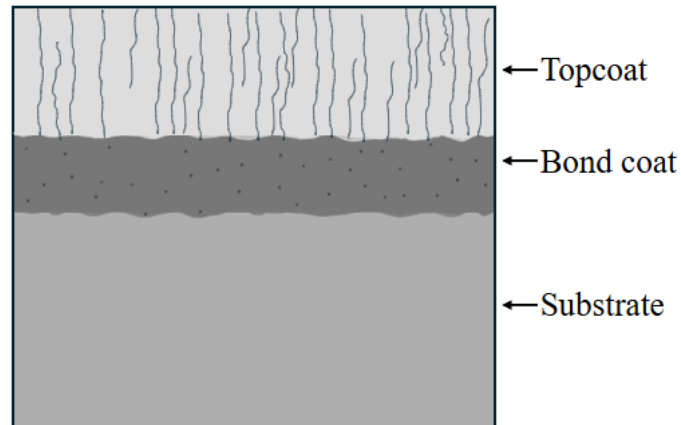


Figure 1: Dense Vertical Cracks (DVCs) as seen in a thermal barrier coating system

The induction of Dense Vertical Cracking (DVC) is the primary method for improving strain tolerance of the coating, as it allows for the accommodation of the different CTEs. DVCs in the coating are currently generated through manipulating air plasma spray parameters close to the substrate surface; however, this is not conducive to coating complex geometries. Rolls-Royce has thus tasked the team with designing an alternate method of producing DVCs within the TBC topcoat.

The goal of this project is to investigate how varying surface texture variables, including texturing method, geometry, and depth, can be leveraged to improve adhesion and performance in high temperature environments. Based on existing literature and industry discussions, the team designed textures to induce DVCs and help mitigate spallation after differential thermal expansion at high temperatures, as well as to improve mechanical interlocking at the TBC-bond coat interface. The team selected three distinct textures: rounded spikes, grid pattern, and grown columns. Samples were created with each of these textures using an ultra-short pulsed laser

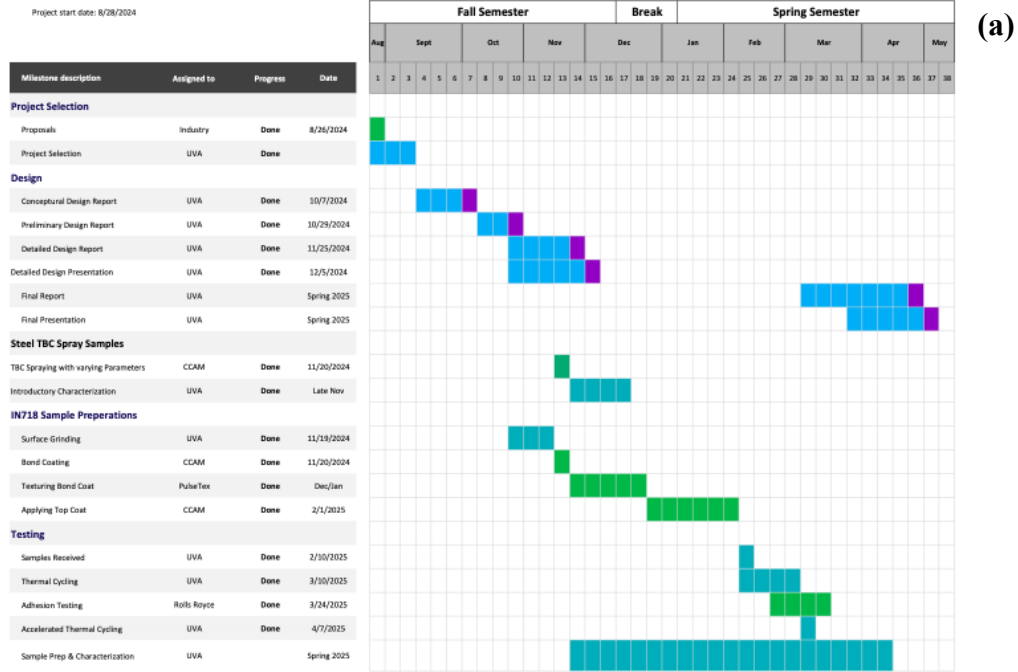
technique, along with the industry standard grit blast as a control, in collaboration with the team at UVA, CCAM, and PulseTex. Testing was conducted to produce samples using the correct plasma spray parameters, coating thicknesses, and texture dimensions.

The team at UVA performed extensive as-sprayed characterization to understand the texture's effects on the coating system. Then, the team performed testing to understand coating system behavior in response to the high temperature and stress environments these coatings are designed for — including thermal cycling testing, accelerated thermal cycling testing, and adhesion testing. The team did optical and SEM microscopy and EDS analysis on these tested samples throughout the project.

The team has found potential in the three chosen textures to induce controlled DVCs and improve mechanical interlocking. Adhesion testing results indicate all textures produced increased mechanical interlocking as compared to the industry standard grit blast samples. Despite thermal cycling testing resulting in far lower coating lifetimes than Rolls-Royce had expected for all textures, the team has identified ways to avoid this in the future: adjusting spray parameters and ensuring the preservation of the bond coat. Microstructural and compositional analysis reveals the potential for these textures to induce controlled, periodic DVCs. In the future, the team hopes that these results can inform the next iteration of texture testing using improved coating system parameters.

II. Project Timeline

A. Gantt Chart



Thermal Barrier Coating Capstone Project

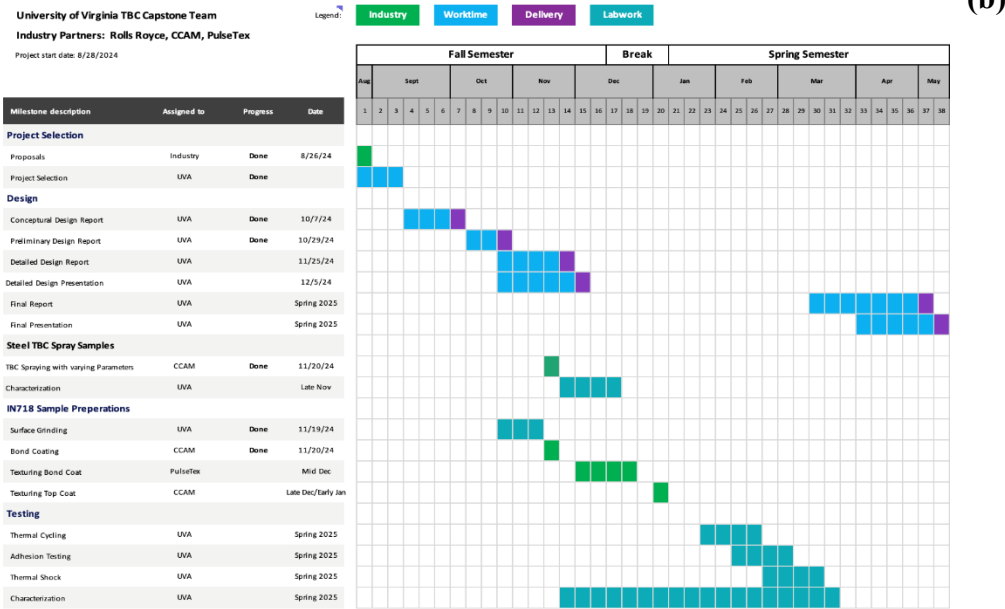


Figure 2: Finalized Gantt chart (a) compared to original Gantt (b).

A proposed timeline was followed throughout the project, and goals were accomplished in a timely manner. There were only minor changes made to the Gantt chart caused by slight delays or changes in the testing procedures.

The first notable change in the schedule was a result of longer sample production time than anticipated. Originally, the timeline estimated for the UVA team to receive the fully prepared samples was early to mid-January, coinciding with the end of the academic winter break. The team received the samples in early February instead, thus the testing timeline was shifted. The team adapted to this delay by taking the extra time to fully define the procedure for the first test – thermal cycling – before receiving the samples. This allowed the team to immediately begin the first round of testing as soon as the samples arrived.

The adhesion testing portion of the testing phase was also adjusted. Originally, the UVA team planned to acquire the necessary materials and conduct the adhesion testing in house. However, this proved to be more complicated than originally thought because the team lacked the necessary attachments for the tensile frame to conduct the testing. The UVA team, with industry partners, agreed that the samples should be sent to Rolls-Royce for adhesion testing. This deviation from the original plan had been considered during the proposal period, making schedule adjustment easy.

The last significant change came from the decision to replace thermal shock testing with an accelerated thermal cycling test. During the first thermal cycling test, the UVA team noticed that the samples were failing much more rapidly than expected. This was an interesting behavior that the team wanted to explore more thoroughly. With the industry partners' advice, the team decided to conduct another round of thermal cycling to better understand failure mechanisms.

The original timeline was well-planned and realistic. The team remained flexible and proactive, adapting to developments throughout the project to ensure each step was completed within a reasonable timeframe.

III. Cost Data and Constraints

A. Cost Analysis

1. Original Estimated Costs

Planned costs associated with this project are shown in the tables below. The experimentation costs were expected to be paid for by the University of Virginia Department of Materials Science & Engineering, while the costs associated with the bond coating, laser processing, and top coating were to be paid for by Rolls-Royce. All costs incurred by the team through shipping and on-site travel were reimbursed by the University of Virginia Department of Materials Science & Engineering.

Table 1: Predicted experimental costs.

| Experimentation Costs | | | | | |
|---|-----------|---------|--------------|---------|----------------|
| | Cost | Use | Total/Sample | Samples | Total |
| Thermal Cycling* | \$0.20/hr | 250 hrs | - | - | \$50 |
| Adhesion Testing | - | - | \$2.50 | 12 | \$30 |
| Thermal Shock* | \$0.20/hr | 25 hrs | - | - | \$5 |
| Optical Microscopy | \$17/hr | 0.5 hrs | \$8.50 | 56 | \$476 |
| Electron Microscopy | \$45/hr | 0.5 hrs | \$22.50 | 56 | \$1,260 |
| Sample Preparation | - | - | \$5 | 56 | \$280 |
| Total Exp. Cost | | | | | \$2,102 |
| *Testing conducted in batches, rates from NMCF website (White, 2024 and Thompson, 2024) | | | | | |

Table 2: Predicted sample preparation costs.

| Sample Preparation Costs | | | |
|---------------------------------|--------------|-------------|-----------------|
| | Cost/Time | Use Time | Total |
| Sectioning Coupons | \$75/hour | 20 | \$1,500 |
| Blades for Sectioning | \$200/blade | 2 Blades | \$400 |
| Bond Coating | \$3000/day | 1 Day | \$3,000 |
| Laser Processing | \$3000/day | 2 Days | \$6,000 |
| Top Coating | \$3000/day | 1 Day | \$3,000 |
| Shipping | \$60/package | 3 Shipments | \$180 |
| Total Prep Cost | | | \$14,080 |

Table 3: Predicted total costs.

| Total Cost | |
|--------------------|-----------------|
| Preparation | \$14,080 |
| Experimentation | \$2,102 |
| Travel (\$0.67/mi) | \$146 |
| Total Cost | \$16,328 |

2. Final Cost Analysis

Actual costs associated with this project are shown in the tables below. Increased experimentation cost is attributed to outsourcing adhesion testing, though this cost is absorbed by Rolls-Royce and not the UVA Department of Materials Science & Engineering. Costs absorbed by UVA are limited to thermal cycling, microscope use, sample preparation (including mounting, polishing, and sectioning equipment), and travel costs.

Table 4: Actual experimentation costs.

| Experimentation Costs | | | |
|---|-----------|----------|----------------|
| | Cost | Use | Total |
| Thermal Cycling* | \$0.20/hr | 210 hrs | \$42 |
| Adhesion Testing** | - | - | \$3471 |
| Optical Microscopy | \$17/hr | 6 hrs | \$102 |
| Electron Microscopy (Phenom) | \$45/hr | 9 hrs | \$405 |
| Electron Microscopy (Quanta) | \$50/hr | 11.5 hrs | \$575 |
| Sample Preparation*** | - | - | \$20 |
| Total Cost | | | \$4,615 |
| *Testing conducted in batches, rates from NCMF website (White, 2024 and Thompson, 2024) | | | |
| **Outsourced to Rolls-Royce | | | |
| ***Cost of Epoxy and Polishing/Grinding Pads | | | |

Table 5: Actual sample preparation costs.

| Sample Preparation Costs | | | |
|---------------------------------|-----------------|-------------|-----------------|
| | Cost/Time | Use Time | Total |
| Sectioning Coupons | \$75/hour | 4 | \$300 |
| Blades for Sectioning | \$216/10 blades | 4 Blades | \$87 |
| Bond Coating | \$3000/day | 1 Day | \$3,000 |
| Laser Processing | \$3000/day | 2 Days | \$6,000 |
| Top Coating | \$3000/day | 1 Day | \$3,000 |
| Shipping | \$60/package | 5 Shipments | \$300 |
| Total Prep Cost | | | \$12,687 |

Table 6: Actual final cost.

| Total Cost | |
|--------------------|-----------------|
| Preparation | \$12,687 |
| Experimentation | \$4,615 |
| Travel (\$0.67/mi) | \$146 |
| Total Cost | \$17,448 |

B. Constraints

In the early development of this project, several constraints were considered to guide the goals and decisions of the team. Rolls-Royce first provided the team with a project proposal in which the team was tasked with evaluating the effect of surface texture variables on DVC microstructure and performance. The project proposal provided by Rolls-Royce outlined several constraints, including using CCAM coating capabilities and materials, using PulseTex laser ablative capabilities, and the requirement to complete ASTM C633 bond strength testing and furnace cycle testing. The predetermined coating procedure helped to narrow the scope of the team's work solely to the surface texture variables that could be induced via texturing. The partnership with PulseTex constrained the team to using ultra-short pulsed laser ablation as the texturing method, though previous reports from the team indicate that this still would have been the preferred method of texturing in the absence of this constraint. Provided testing requirements narrowed the extent of evaluation expected from the team. PulseTex also required that all desired textures be straightforward and feasible to produce using laser ablation, given the laser constraints of xy-plane accuracy up to 70 μ m and z-plane accuracy up to 1nm.

Constraints inherent to the nature of a capstone project primarily centered around time and resources. Testing and characterization were limited to the facilities at UVA and those of industry partners. All work was to be completed prior to the end of the Spring 2025 semester, which would culminate in a comprehensive report and presentation. Furthermore, the team must be able to test and characterize all samples produced; the sample pool size was dictated by the size and training capabilities of the five-person team. Production time was a significant constraint, as CCAM needed 1 day for bond coating, PulseTex needed 1 week for texturing, and CCAM needed 1 week for TBC coating. The Coating and texturing pathway required that samples be shipped between CCAM and PulseTex, lengthening the entire production process. As such, the team's ability to test and characterize efficiently was critical to the success of the project.

Texture constraints were determined by the team during the Fall 2024 semester. The team decided that in order to preserve the desirable oxidation inhibiting properties of the bond coat layer of the coating system, the thinnest part of the texture must be at least 127 μ m in compliance

with Rolls-Royce specifications. Texture dimensions must allow for the TBC powder particles to fully fill the space between texture features during application. Powder diameter was $45 \pm 15\mu\text{m}$, and when considering the laser processing restrictions, this limited texture dimensions.

IV. Project Challenges

A. Sample Prep

1. EDM

The team's original plan to section the IN718 rods received from Rolls-Royce was to utilize UVA's wire EDM machine. It is an accurate, quick, and efficient tool for sectioning. However, just before receiving the samples from Rolls-Royce the wire EDM machine malfunctioned for unknown reasons and was temporarily unavailable. A new method of cutting the samples from the rod was devised; the UVA team took advantage of the in-house machine shop and had samples cut using a lathe. While it took longer than the EDM, the team was able to quickly reorganize and receive assistance from an Engineering Technician to deliver the samples on schedule.

2. Cutting of Mounted Samples

Sectioning of mounted samples was first attempted using the same cutting speeds (0.15 mm/s) and saw blade (Aluminum Oxide) as the unmounted IN718. This proved to be too fast, and the epoxy mounted around the samples prevented heat dissipation from the sample, resulting in some TBC burning and epoxy melting (Figure 3). To prevent this, cutting speed was reduced to 0.015-0.03 mm/s, resulting in a 40-minute sectioning time per sample. This posed a severe bottleneck in the sample characterization process, so cutting had to be planned out well in advance.

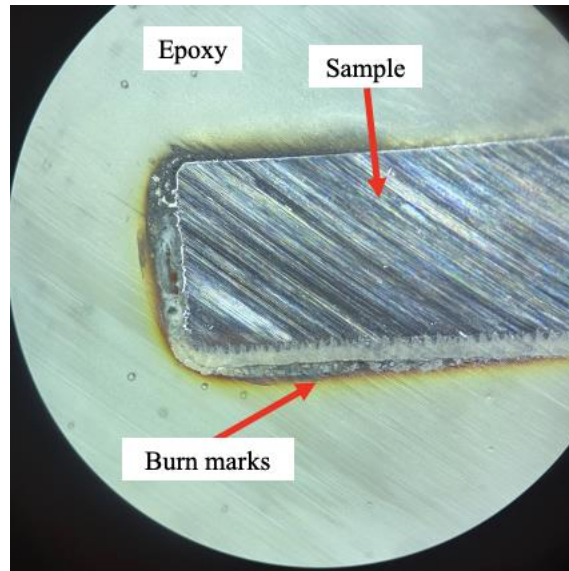


Figure 3: Mounted sample after being cut too fast, showing burnt TBC and some epoxy melting. After the saw was slowed down, the rest of the sample remained unburned.

3. Auto polishing

After furnace testing of the samples, any remaining coating was very fragile. This prevented direct cutting of sample cross sections for mounting and polishing. Instead, samples were first mounted to preserve the coating. Due to the size of whole, uncut, IN718 samples, they were mounted in larger epoxy cups that prevent the use of the auto polisher. Instead, these samples had to be hand polished, adding considerable time to sample preparation.

B. Spray Parameter Confusion

There was some confusion regarding the chosen spray parameters and the actual spray parameters used on the IN718 samples. Using the steel samples, the team selected spray parameter 4 which corresponded with 550A and 85mm. However, CCAM informed the team that the spray parameters in the spreadsheet were mixed up and spray parameter 4 actually corresponded with 550A and 65mm. The team therefore went with these corrected spray parameters given by CCAM. However, IN718 samples showed more numerous DVCs and horizontal branching, and the team questioned the actual spray parameters corresponding to chosen spray parameter 4. Further on this can be found in the Discussion of Results.

C. Adapting Furnace Procedures

Furnace size and availability constrained the team's furnace testing considerably, causing adaptations to original plans. Initially, 20 samples, 5 of each texture, had been reserved for 23-hour thermal cycles repeated until 50% coating spallation. However, Rolls-Royce advised that they expected spallation at 50-100 cycles. Based on this benchmark, 23-hour cycles would mean this portion of testing lasting for 2-3 months, which was not feasible in the remaining time.

Therefore, the team opted for 11-hour cycles that allowed for 2 cycles per day rather than 1, shortening total testing time to about a month, which was within an acceptable timeframe for the project. Furnaces from the Opila lab were utilized and had space for 8 samples in each. Given the lab only has 3 furnaces, the team could not reserve all of them and hinder other student projects that require furnaces. Therefore, the number of samples was reduced from 20 to 16, reducing the number of furnaces required to 2. Results from this modified testing plan can be found in the Thermal Cycling Results and Characterization section.

V. Technical and Detailed Drawings & Sample Design

A. Textures

For this project, the team conducted a literature review to see what textures had been tested for adhesion and DVC inducing properties in the past. Based on this review and industry partner discussions, three textures were developed and were to be laser ablated into the bond coat before TBC application. These textures are the rounded spikes (T1), grid pattern (T2), and grown texture (T3), shown with dimensions in Figure 4, Figure 5, and Figure 6. The grown texture was not seen in literature, but PulseTex has reported promising adhesion results with its use. Note that dimensions were provided in imperial units to comply with Rolls-Royce standards. These drawings were submitted to PulseTex and used as their reference for producing the textures.

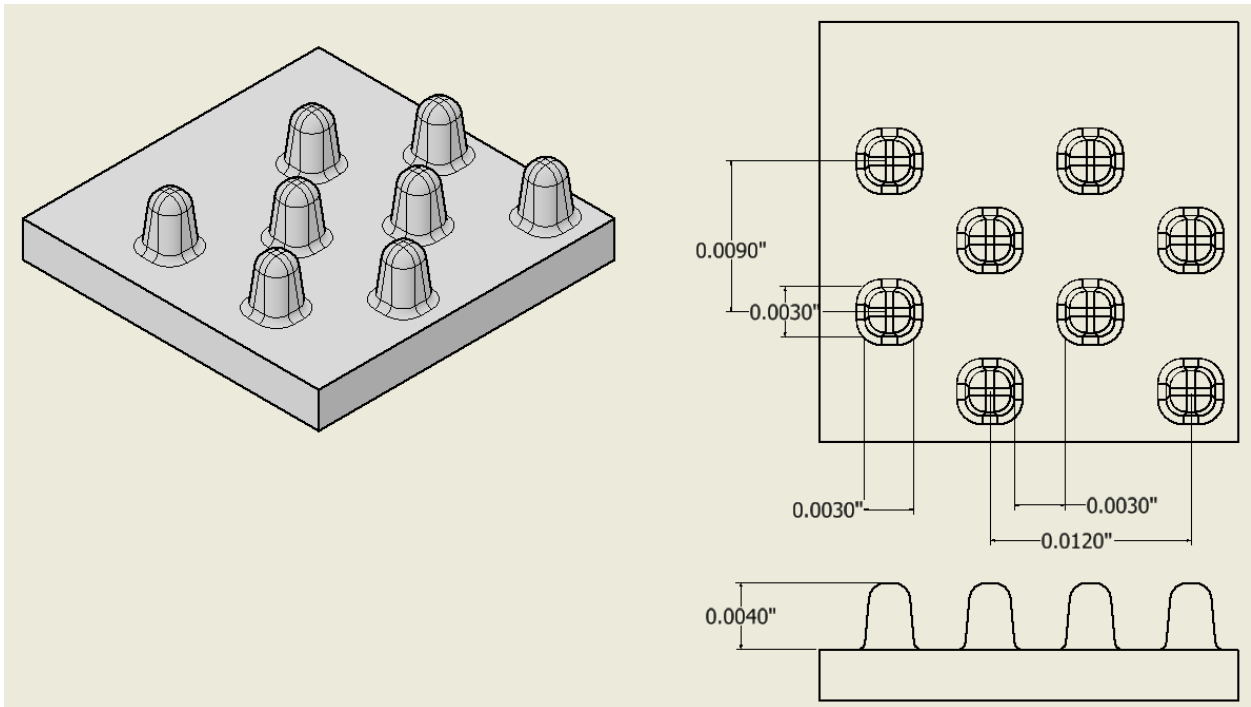


Figure 4: Dimensioned view of rounded spikes design.

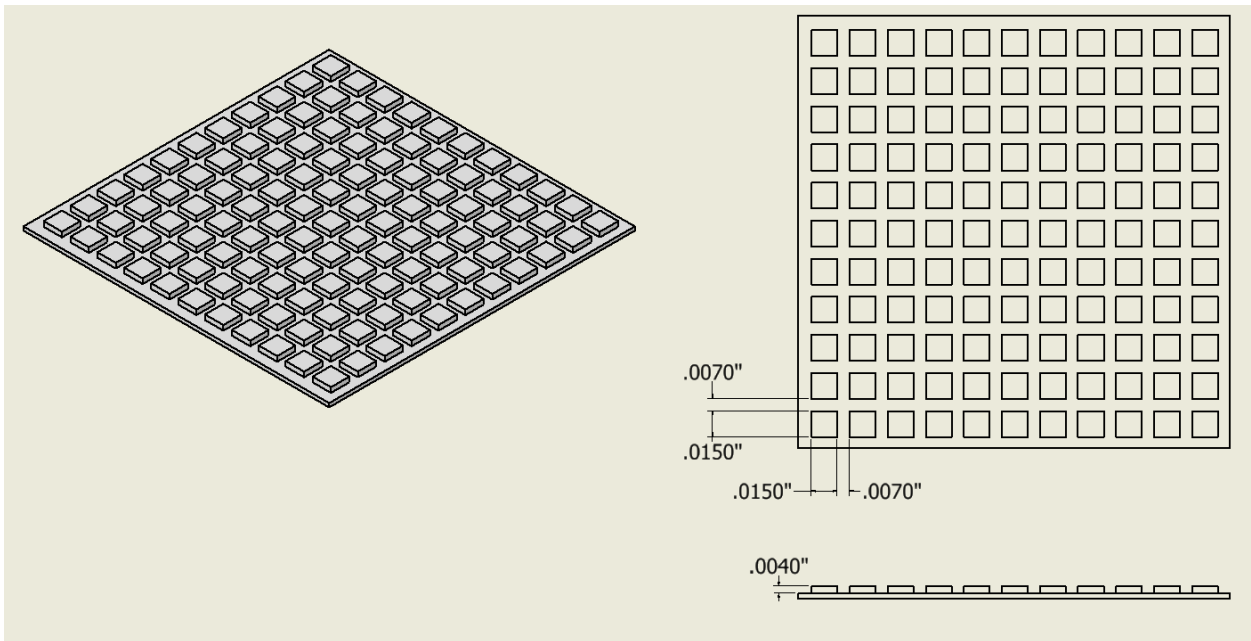


Figure 5: Dimensioned view of grid pattern design.

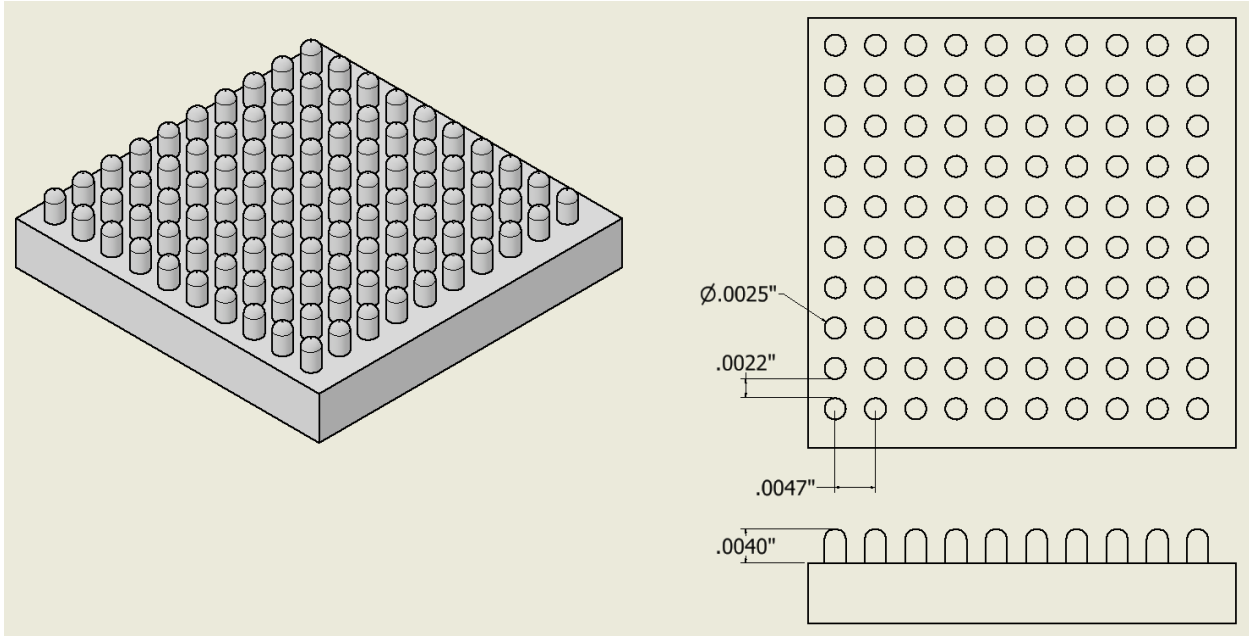


Figure 6: Dimensioned view of grown columnar texture. Dimensions are a rough estimate as the process is less controlled than ablation.

B. Sample Generation Pathway

In order to produce samples with the desired textures built into the coating system, the following sample generation pathway was used (Figure 7).

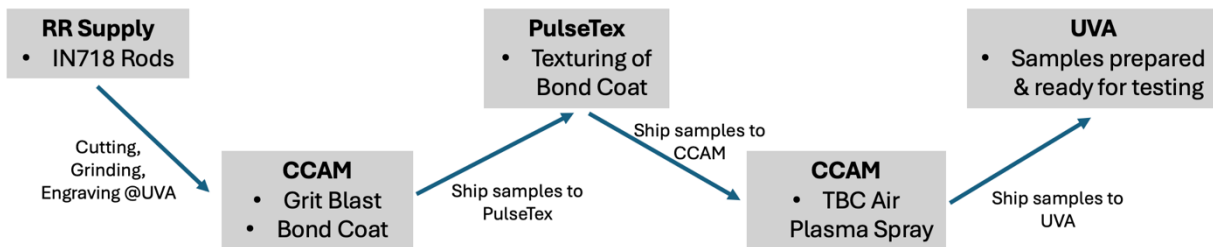


Figure 7: Sample generation pathway.

1. Sectioning of IN718

In late September, the team received two, 12” long, 1” diameter rods of IN718 from Rolls-Royce. This served as the substrate material for all texture testing. These rods were cut into 1/8” thick, disc-shaped samples using a lathe. 70 samples were cut in total. One side of each sample

was ground using 180 grit sandpaper until all lathe marks were gone to properly prepare the surface for grit blasting and subsequent bond coat application. Grinding was done one at a time, by hand, by applying pressure for approximately 5 minutes each at 400-500 rpm.

After polishing, each sample was labeled using an engraver. The naming standards divide the samples by texture (GB for grit blast; T1, T2, T3 for each chosen texture), testing procedure (A-D), and then enumerated for identical samples that will be used for different trials. Some samples were also labeled for characterization of bond coat and texture application alone. Seven extra samples remained. The final thicknesses of all samples were measured to ensure uniformity. Substrate thickness distribution data can be found in the Substrate Characterization section.

2. Grit Blasting & Bond Coat Application at CCAM

On November 20th, the team traveled to the CCAM facility in Disputanta, VA to oversee the grit blasting and bond coat application of the samples. To prepare the samples for bond coat application, they were grit blast to roughen the surfaces and improve adhesion. Grit blasting was done in a chamber at CCAM using Aluminum Oxide 60 grit at 50 psi. CCAM decided to use a manual grit blaster due to the simple surface geometry of the samples and to avoid time required to program the automatic grit blaster. Thicknesses and masses were measured after this step to use as a baseline to calculate bond coat thicknesses after application.

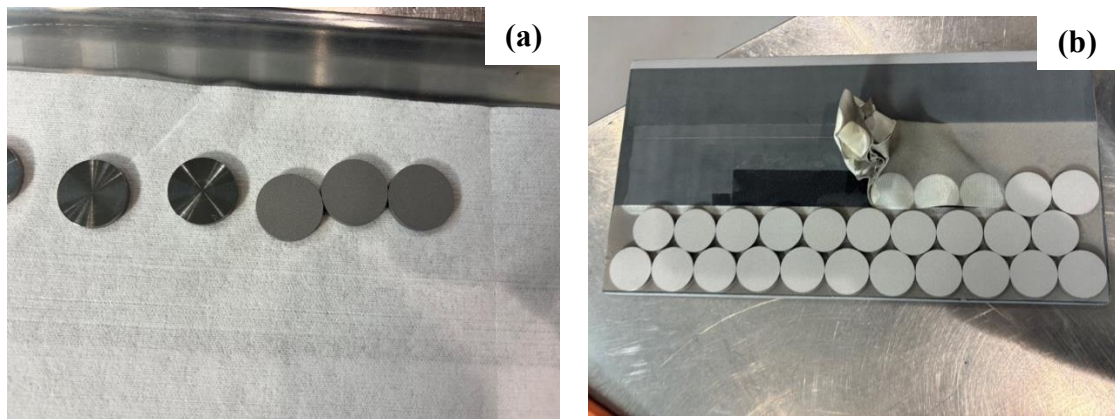


Figure 8: Samples after grit blasting; (a) comparison of machined (left) and grit blast (right) samples, (b) grit blast samples on a tray after being taken out of chamber.

The bond coat spray parameters were chosen based on input from Rob Golden with Rolls-Royce. These are the bond coat spray parameters that have been used as the standard at Rolls-Royce for the IN718 substrate. The Amdry 386-4 powder was used for the application of the bond coat. Bond coat composition and spray parameters dictated by CCAM and Rolls-Royce can be found in Appendix A.

At CCAM, the team put all grit blasted samples into sample holders. These holders clamped samples and were placed onto a magnetic board in the spray chamber. The bond coat was then sprayed according to specified bond coat parameters using a robotic arm. The plasma spraying itself was very bright, so the chamber was blacked out to prevent eye damage. Tecnar software was used to monitor spray particle velocity and temperature, complimented by an in-house software to monitor more parameters. The samples were sprayed in two batches due to space limitations within the chamber.



Figure 9: (a) Samples in holders being placed on magnetic board for spraying, (b) Robotic arm used for spraying, (c) Plasma powders fed into the gun.



Figure 10: (a) Plasma spraying of the bond coat, (b) Monitoring of spray parameters on Tecnar software, (c) Samples after bond coat application.

Once completed, samples cooled for about 15 minutes, and then the team used compressed air to remove dust and bond coat debris from the sample holders. Then, samples were removed from their holders and measured for their changed thickness and masses. Samples were then individually bagged to prevent scratching.

3. Lasering

Bond coated samples, apart from the samples set aside as the Grit Blast control samples, were shipped to PulseTex in Texas for lasering of textures based on the drawings (see Textures). PulseTex uses an ultra-short pulsed lasering technique to achieve these textures. They were then shipped back to CCAM for TBC plasma spraying.

4. Spray Parameter Selection & Coating Procedure

Nine different TBC spray settings were tested on steel samples in order to compare DVC induction and inform the selection of spray parameters for the textured Inconel samples. 9 steel samples in 3 rounds were plasma sprayed with different spray gun power used for each round (450A, 500A, 550A). Within one round, each of the 3 steel samples were offset from one another to produce 3 separate spray distances (65mm, 75mm, 85mm). This setup resulted in 9 distinct combinations of spray parameters to analyze. The team measured each sample's thickness and mass before and after TBC application. The 9 distinct combinations are shown in Table 7. There was some confusion regarding these combinations, which can be seen in the Project Challenges section, but Table 7 shows the correct parameter combinations, to the best of the team's knowledge.

Table 7: Nine distinct spray parameters for TBC steel samples.

| Steel Sample | Gun Current (Set point) (A) | Distance (mm) | TBC Thickness | | TBC Mass (g) |
|--------------|-----------------------------|---------------|---------------|-------------------|--------------|
| | | | (mils) | (μm) | |
| 1 | 500 | 85 | 13.20 | 335 | 2.277 |
| 2 | 500 | 75 | 11.50 | 292 | 3.340 |
| 3 | 500 | 65 | 7.60 | 193 | 2.817 |
| 4 | 550 | 85 | 12.20 | 310 | 3.532 |
| 5 | 550 | 75 | 14.15 | 359 | 3.684 |
| 6 | 550 | 65 | 10.20 | 259 | 3.145 |
| 7 | 450 | 85 | 10.55 | 268 | 3.073 |
| 8 | 450 | 75 | 11.25 | 286 | 3.144 |
| 9 | 450 | 65 | 8.15 | 207 | 2.719 |

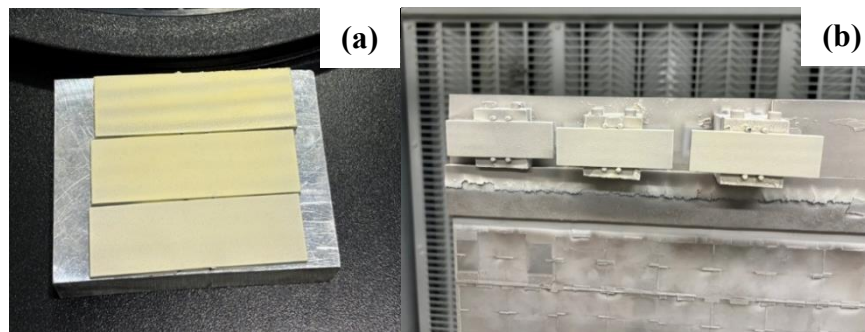


Figure 11: (a) 3 steel samples after TBC application, (b) Staggered samples on board after TBC spraying.

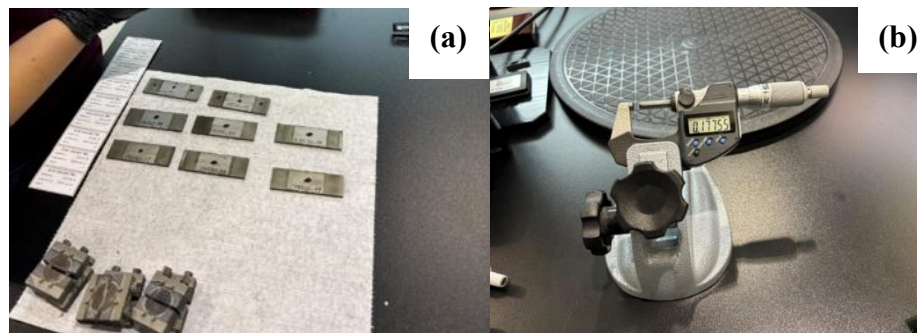


Figure 12: (a) Scale used to measure masses of steel samples before TBC spraying, (b) Caliper used to measure sample thicknesses before and after spraying.

Results from this testing can be seen in the Analyzing Spray Parameters section, including SEM micrographs of each resulting TBC microstructure, and the spray parameters ultimately chosen. Once this spray parameter decision was made, the team informed CCAM, and the plasma spraying was completed to those specifications. On February 6th, the fully prepared, TBC coated samples were received by the UVA team.

VI. Experiments Conducted and Equipment Used

A. Thermal Cycling

In order to test the efficacy of the textures in improving coating performance, thermal cycling tests were conducted. With modifications made to the original testing plan (see Project Challenges), 2 furnaces were reserved from February 10th- March 7th. During each cycle, samples were heated in each furnace (CM Rapid Temp Furnace 1200 Series, Bloomfield, NJ) to 1135°C for 11 hours, then taken out for 1 hour to cool on a block of alumina before being put back in for another cycle. During cycling, 2 of each texture were put in each furnace to eliminate the possibility of an entire set of textures failing due to an individual furnace malfunction. Samples were individually weighed after each cycle to monitor mass change possible associated with oxide growth and TBC spallation. Significant analysis regarding mass loss/gain was not conducted as it was not possible to distinguish between mass gain from oxide growth and mass loss from spallation. After each cycle, a picture was taken of all the samples to track coating behavior. Further information regarding equipment and cycle timing can be found in Appendix B. The experimental procedure is shown in the diagram depicted in Figure 13.

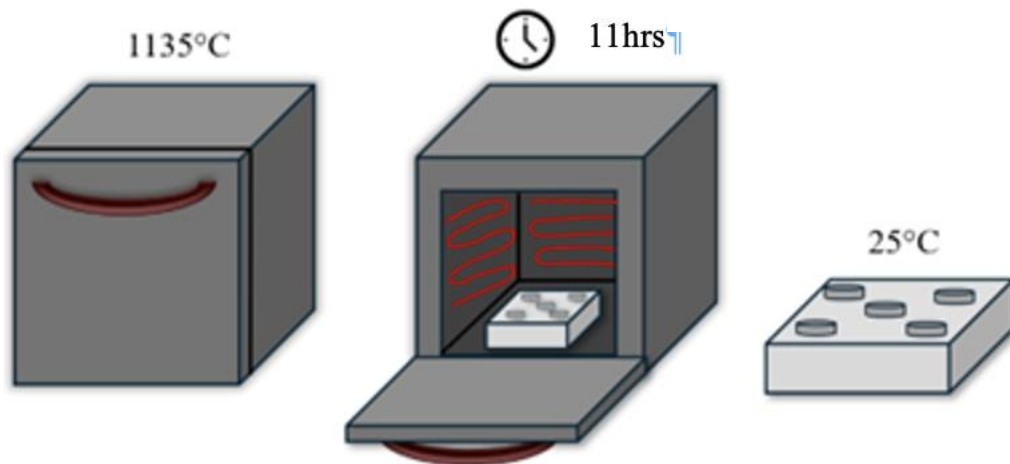


Figure 13: Thermal cycling experimental setup.

B. Accelerated Thermal Cycling

Initial thermal cycling testing yielded failure far sooner than the team or Rolls-Royce anticipated. All coatings failed after 15 cycles, based on the criterion of a 50% spallation threshold. Short cycles and cycling to failure prevented observation of the evolution of failure. In the case of the GB samples, there was virtually no coating left adhered to characterize.

Although this thermal cycling testing was valuable in providing comparative cycle lives for the four coating texture types, subsequent characterization could only reveal end state (failure stage) microstructures. Thus, it was decided to augment these results with shorter, accelerated thermal cycling experiments that aimed at capturing intermediate interface microstructures of each coating texture type in the steps leading up to failure. Preliminary characterization of failed samples suggested that oxide growth is key to failure at interfaces and documenting intermediate oxide growth could enhance understanding of the progression of this failure mechanism.

Using the same furnaces from the Opila lab (CM Rapid Temp Furnace 1200 Series, Bloomfield, NJ), four samples of each texture were subjected to four accelerated thermal cycles of 2 hours, each separated by a 30-minute cooling period. After each 2-hour cycle, one of each textured sample was removed from cycling. This resulted in having one sample for each texture that had experienced 1, 2, 3, and 4 accelerated thermal cycles.

C. Adhesion Testing

The team sent 12 samples to Rolls-Royce for adhesion sampling. This is made up of three samples of each of the three laser produced textures and three grit blasted samples. The samples underwent tensile adhesion testing in accordance with ASTM standard C633. The adhesive used for the testing was FM1000. Bond strength of the adhesive was recorded to be a minimum of 9900psi, which was used to compare the values measured for coated samples. All coated samples were found to have failed at significantly lower stresses, eliminating the possibility of failure within the glue. Thus, all tested samples failed somewhere in the coating system. The tensile adhesion testing setup is shown in Figure 14.

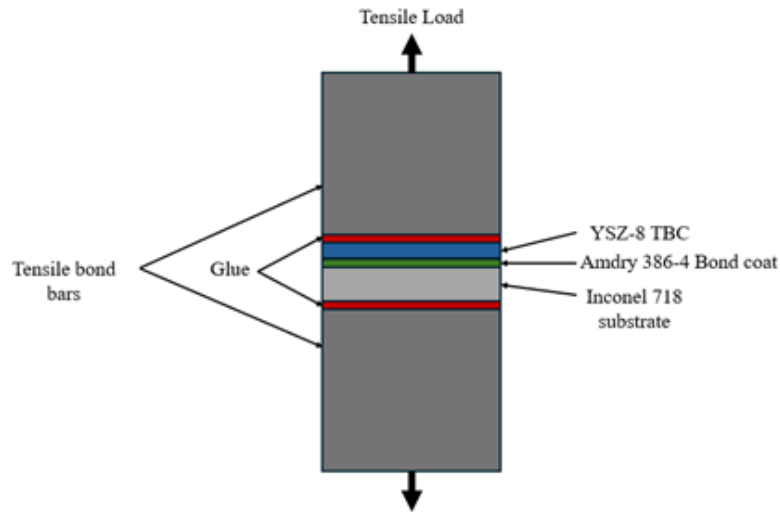


Figure 14: Tensile adhesion testing setup.

D. Characterization Process & Equipment

1. Sample Preparation

All sample preparation equipment can be found in Appendix C.

Mounting

The mounting procedure for the coated samples consisted of the same procedure used for the TBC steel samples. This included using Buehler Epothin Slow Cure Epoxy (Epothin 2 Epoxy Resin & Epothin 2 Epoxy Hardner, Buehler (Illinois Too Works), Lake Bluff, IL) to mount the sectioned sample for 24 hours before proceeding to grinding and polishing. The large mounting cups necessary for mounting the samples prevented the team from using the autopolisher for grinding and polishing.

Cutting

The team contacted three suppliers (Allied High Tech, Buehler, Hudson Supply) to inquire about the optimal blade for sectioning IN718. Based on their advice, the team decided to order resin bond aluminum oxide (Al_2O_3) blades from Allied High Tech. The specifications of the blade, HV < 450, 7" x 0.030" x .5" (175 x 0.76 x 12.7 mm), are designed for the high-speed saw available in Jesser Hall. Ten blades were purchased.

Sectioning of mounted samples was done using the aluminum oxide blade with a cutting speed of 0.015-0.03 mm/s, resulting in a 40-minute sectioning time per sample. Challenges associated with finding these cutting parameters can be found in the Project Challenges section.

Grinding & Polishing

The grinding and polishing procedures which were used on the samples after sectioning are outlined in Table 8.

Table 8: Polishing procedure for TBC samples

| Step | Time |
|------------------|--|
| 220 grit | 10 min (until sample exposed from epoxy) |
| 600 grit | 4 min |
| 1200 grit | 4 min |
| 9 μ m polish | 2 min |
| 3 μ m polish | 2 min |
| 1 μ m polish | 1.5 min |

Sputter Coating

Once the samples were polished, they were sputter coated using the Cressington Sputter Coater located in Jesser Hall (Cressington 108 Auto Sputter Coater, Cressington Scientific Instruments Ltd, Watford, United Kingdom). They were sputter coated with a current of 30A for 45 seconds.

2. Microscopy

All equipment used for microscopy can be found in Appendix D.

Optical (Hirox)

Optical microscopy was completed using the Hirox microscope in Jesser Hall (Hirox RH-8800, Hirox-USA Inc., Hackensack, NJ). This was used to obtain overview optical micrographs of the sample surface before and after experiments.

SEM (Quanta & Phenom)

Scanning electron microscopy was completed using the Phenom desktop SEM (Phenom XL G2, Thermo Fisher Scientific, Waltham, Massachusetts) and the Quanta 650 SEM (Quanta 650, Thermo Fisher Scientific, Waltham, Massachusetts). Micrographs were taken at varying magnification. Most micrographs were taken using the Quanta 650 SEM with additional micrographs taken using the Phenom SEM. Micrographs were taken in Backscattered Electron mode (BSE).

EDS

Electron Dispersion Spectroscopy (EDS) was completed using the Phenom (Phenom XL G2, Thermo Fisher Scientific, Waltham, Massachusetts). This was used to gather compositional information for the samples before and after experimentation. This system is not calibrated against standards, so compositional results are not to be taken as an exact measurement of actual composition.

VII. Results: Characterization and Analysis Conducted

A. Substrate Characterization

Following the sectioning and polishing of IN718 buttons, the team measured button thicknesses to ensure uniformity between samples. The results of these measurements can be seen in Table 9.

Table 9: Sample Thickness Statistics

| Average Thickness (mm) | Range (mm) | Standard Deviation |
|------------------------|------------|--------------------|
| 3.23 | 0.68 | 0.084 |

Before coating the IN718 substrates for testing, it was important to establish its baseline properties. Optical micrographs of the IN718 samples were taken as-cut (by the lathe) and after grinding to verify desired surface quality.

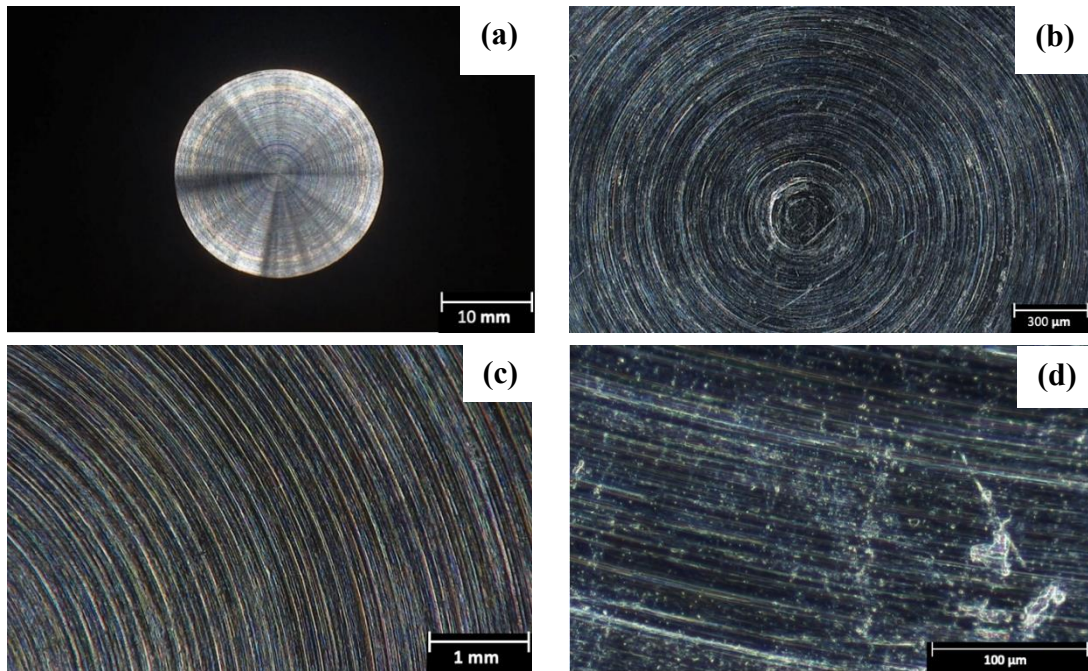
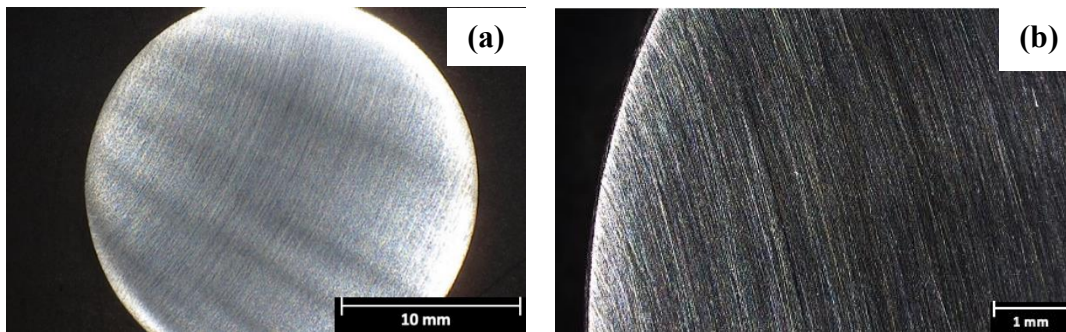


Figure 15: Micrographs of a lathe-cut IN718 sample taken by the Hirox Optical microscope at various magnifications; (a) overview of machined sample at 5X, (b) center of machined sample at 140X, (c) lathe marks at 50X, and (d) lathe marks at 1000X.



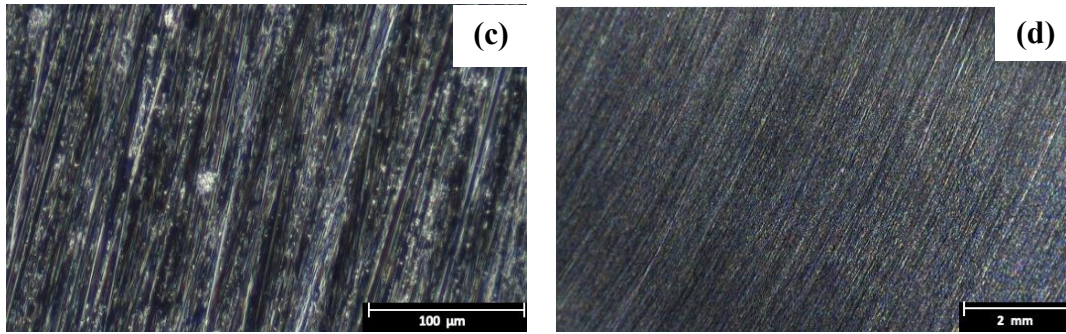


Figure 16: Micrographs of a lathe-cut IN718 sample after polishing with 180 grit sandpaper taken by the Hirox Optical microscope at various magnifications; (a) overview at 10X, (b) edge of sample at 30X, (c) polish of sample at 1000X, (d) polish of sample at 30X.

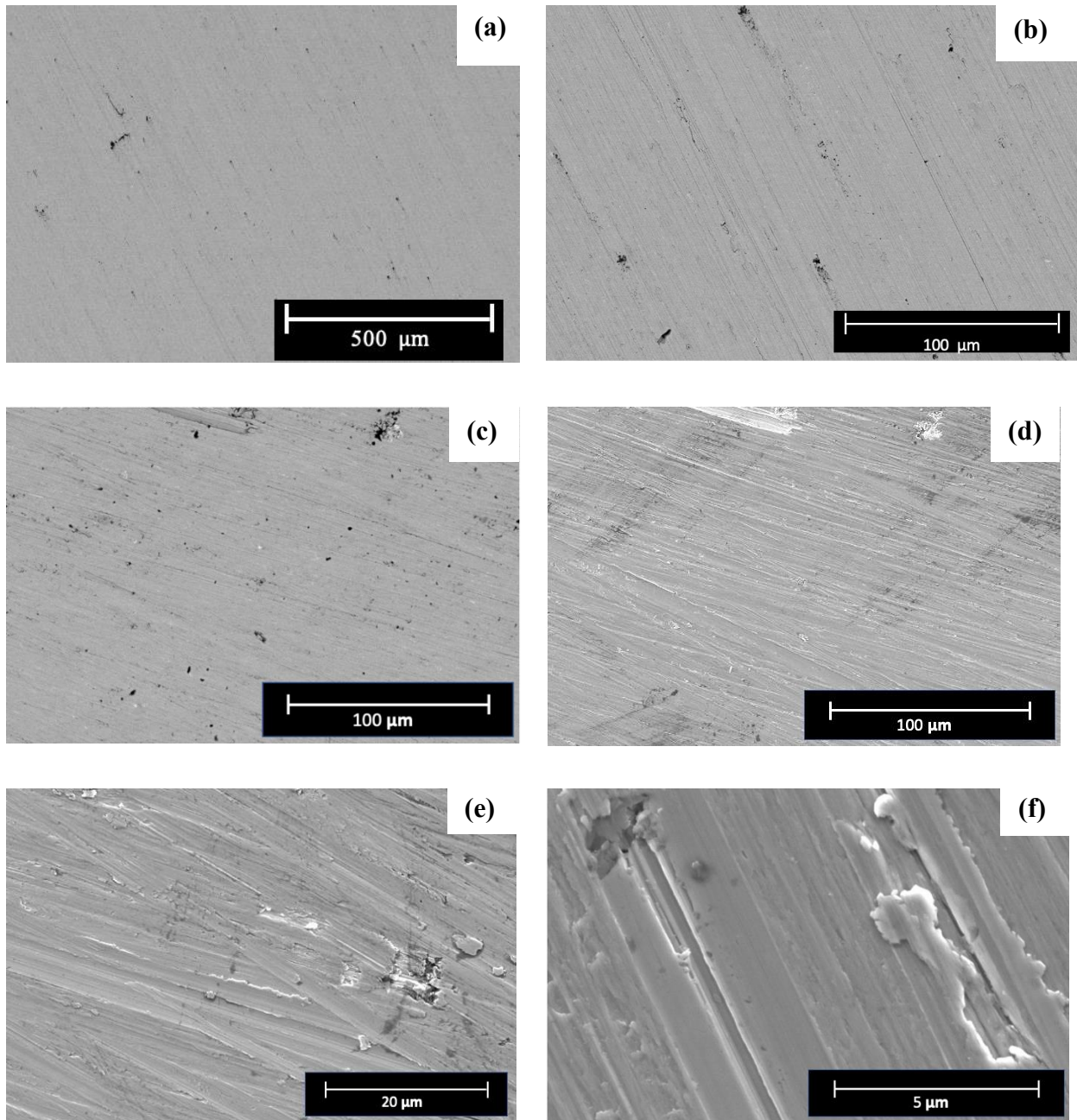


Figure 17(a), (b), (c), (d), (e), (f): Micrographs of a lathe-cut IN718 sample after polishing with 180 grit sandpaper taken by the Quanta 650 scanning-electron-microscope in BSE mode at various magnifications.

The team also studied the substrate using the SEM (Figure 17) and conducted EDS analysis (Figure 18) to verify composition. Understanding the substrate composition was critical in order

to later understand how the coating system was impacted by the elements of the substrate, especially after thermal testing. The EDS results (Table 10) showed elemental composition within normal range for IN718, as can be seen in Table 11.

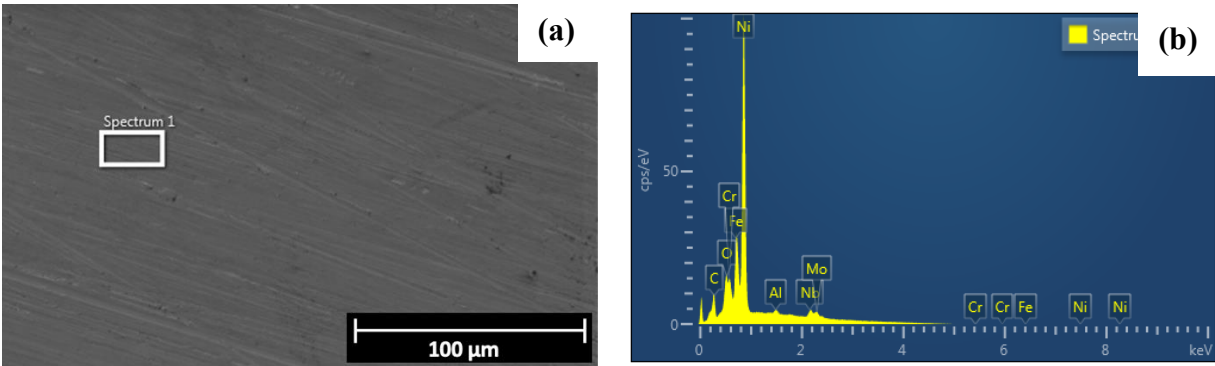


Figure 18: EDS compositional analysis performed on IN718 sample. (a) Inspected region and (b) Corresponding spectrum.

Table 10: EDS Compositional breakdown for the IN718 sample.

| Element | Line Type | Apparent Concentration | k Ratio | Wt% | Wt% Sigma | Standard Label | Factory Standard |
|---------|-----------|------------------------|---------|--------|-----------|----------------|------------------|
| O | K series | 2.42 | 0.00813 | 0.92 | 0.05 | SiO2 | Yes |
| Al | K series | 0.52 | 0.00371 | 0.45 | 0.05 | Al2O3 | Yes |
| Cr | L series | 13.22 | 0.13217 | 17.61 | 0.47 | Cr | Yes |
| Fe | L series | 13.34 | 0.13341 | 18.87 | 0.28 | Fe | Yes |
| Ni | L series | 37.31 | 0.37308 | 54.18 | 0.43 | Ni | Yes |
| Nb | L series | 3.38 | 0.03378 | 5.01 | 0.27 | Nb | Yes |
| Mo | L series | 1.97 | 0.01967 | 2.94 | 0.32 | Mo | Yes |
| Total: | | | | 100.00 | | | |

Table 11: Known IN718 composition ranges, from specialmetals.com.

| | |
|-------------------------|-------------|
| Nickel (plus Cobalt) | 50.00-55.00 |
| Chromium | 17.00-21.00 |
| Iron | Balance* |
| Niobium (plus Tantalum) | 4.75-5.50 |
| Molybdenum | 2.80-3.30 |
| Titanium | 0.65-1.15 |
| Aluminum | 0.20-0.80 |
| Cobalt | 1.00 max. |
| Carbon | 0.08 max. |
| Manganese | 0.35 max. |
| Silicon | 0.35 max. |
| Phosphorus | 0.015 max. |
| Sulfur | 0.015 max. |
| Boron | 0.006 max. |
| Copper | 0.30 max. |

B. Bond Coat Characterization

1. Profilometry of the Bond Coat

Bond coated samples were characterized with a profilometer to evaluate surface roughness, summarized in Table 12. Two samples were characterized with twenty measurements per sample. Roughness was not expected to be dependent on sample orientation. A random direction was selected and ten measurements were performed in that direction. An additional ten were conducted perpendicular to the random direction.

Table 12: Profilometry Results Averaged from 40 Measurements on 2 Samples

| Average Roughness (μm) | RMS Roughness (μm) | Average highest Peak-to-Valley (μm) |
|-------------------------------------|---------------------------------|--|
| 8.3 | 10.2 | 45.1 |

Average and RMS roughness offer two averages of surface roughness, while average highest peak-to-valley offers information regarding the most extreme variations in surface roughness. The surface roughness tends towards 8-10 μm , with the most extreme variations at around 45 μm . While most of the surface does not display variations this intense, the team used this variation number to inform texture dimensions (see the Textures section), as textures must be larger than

bond coat roughness variations to be able to confidently distinguish effects of the texture from the normal surface roughness.

2. SEM of the Bond Coat

One of the bond coated samples was then cross-sectioned and imaged using the Phenom SEM to inspect the bond coat-substrate interface and the profile of the bond coat before TBC application. Micrographs are shown below in Figure 19. The micrographs show a distinct, mildly rough interface between bond coat and substrate, peaks and valleys at the top of the layer, visible splats, and porosity formed during the spraying process. Microscopy also revealed “speckles” throughout the bond coat.

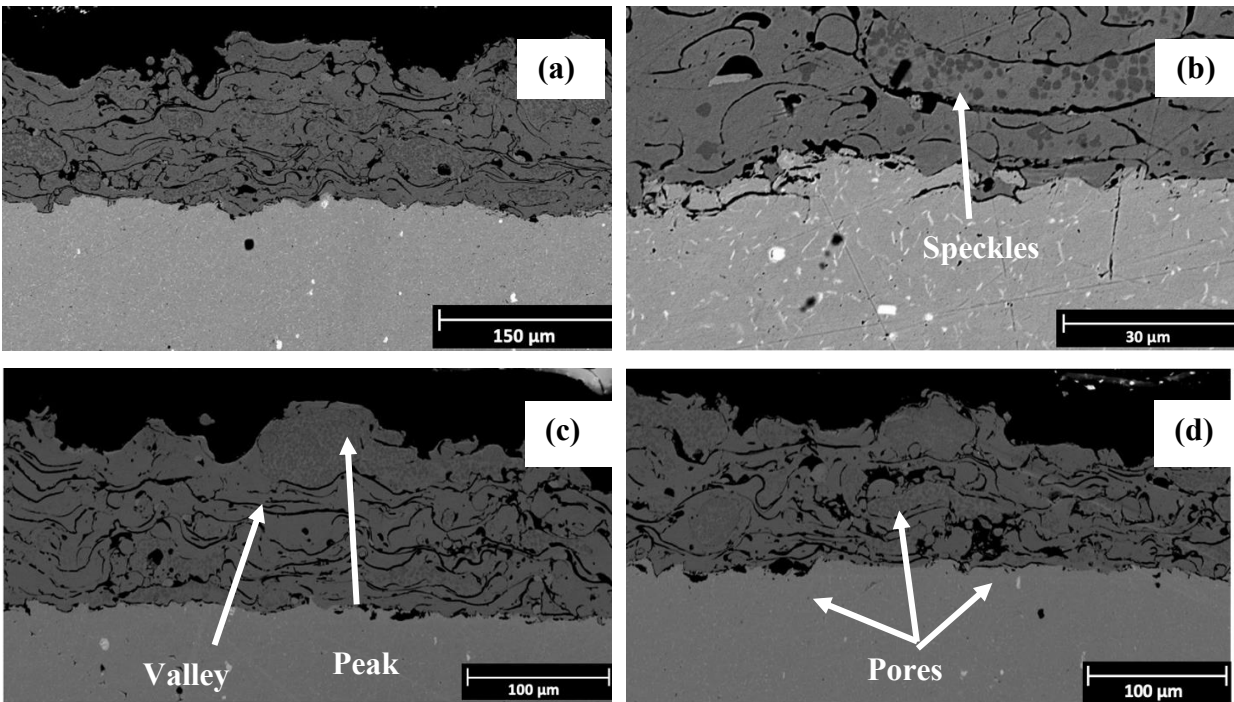


Figure 19: BSE SEM micrographs of bond coat/substrate interface. (a) Wide view of interface at 1000X, (b) High magnification view of interface taken at 5000X showing the roughness of the substrate, (c) Peaks and valleys seen in the bond coat profile, and (d) Porosity found in the coating.

3. ImageJ Analysis of Bond Coat Thickness after TBC Spraying

The average bond coat thickness of the as-sprayed samples for each texture was measured from 3-4 SEM micrographs taken at 100X magnification. Utilizing the ImageJ software, the area of the bond coat in each image was determined. Below, in Figure 20, is a representation of the area selection. The average length was then determined utilizing the formula below:

$$t_{avg} = \frac{\sum A_i}{\sum l_i}$$

Dividing the total area across the micrographs by the total length of the micrographs results in a thickness measurement averaged across all the micrographs.

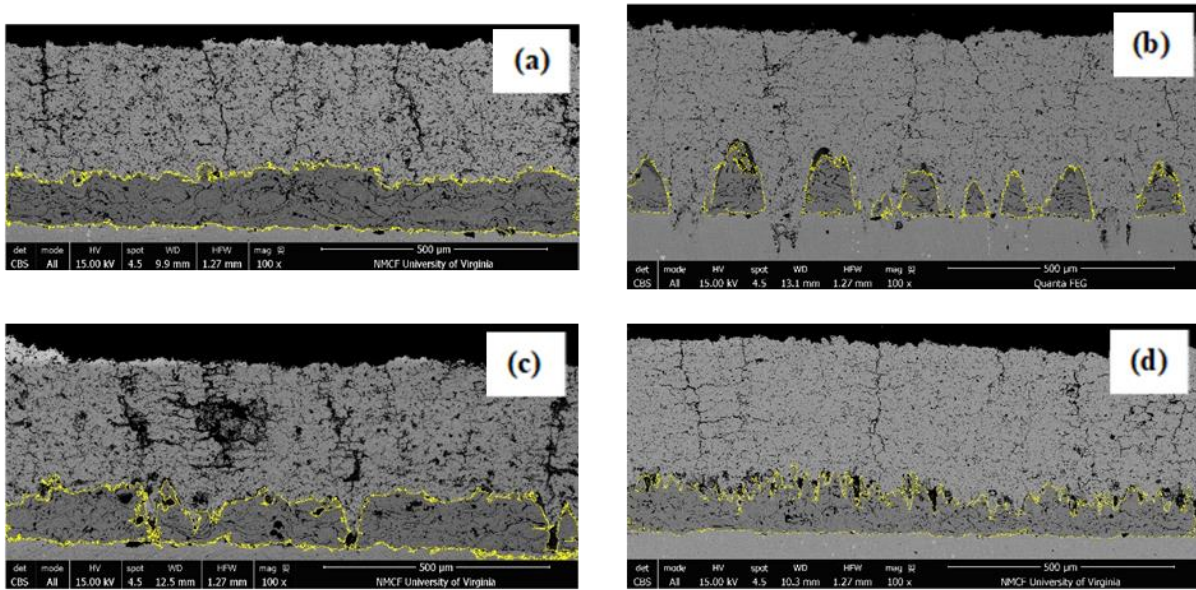


Figure 20: Examples of the area selection utilized for determining the average bond layer thickness of each texture. (a) GB, (b) T1, (c) T2, and (d) T3.

Table 13: Tabulated results of bond layer thickness analysis on SEM Micrographs at 100X.

| Sample | GB-B5 | T1-B5 | T2-B5 | T3-B5 |
|--------------|-------|-------|-------|-------|
| Average (µm) | 117 | 46.1 | 97.4 | 88.5 |
| Min (µm) | 77 | 0 | 0 | 33 |
| Max (µm) | 166 | 158 | 161 | 167 |

From the ImageJ analysis, the team notes that the maximum bond coat thicknesses represent close to the bond coat thickness before any laser processing or grit blasting. The fact that the distribution of maximum thicknesses between sample types demonstrates that the initial bond coat application was relatively uniform across sample types. The T1, T2, and T3 average thicknesses are significantly less than the GB thicknesses due to their subsequent laser processing to generate distinct geometric shapes. However, it is important to note that the desired bond coat thickness of 127 μm after laser ablation, was not achieved. Coating was expected to produce a bond coat that was approximately 180 μm thick, and ablation aimed to keep most of this thickness intact. An average unablated bond coat thickness of 117 μm combined with texture dimensions designed for a thicker bond coat, resulted in significantly thinner textured bond coats and reduced the protective ability of bond coat. Analysis confirmed this theory, with post-ablation average thickness assuming values less than 100 μm , very clearly not aligning with standard bond coat thickness dictated by Rolls-Royce.

The most important results of this ImageJ analysis are the minimum thicknesses. At the minimum, the T1 and T2 sample analyzed had a minimum bond coat thickness of 0 μm . In fact, outside of these sampled micrographs, there were many areas where missing bond coat was noted throughout analysis for the project. This meant that in several locations, the laser ablated all the way through the bond coat into the substrate – something that was not intended and facilitated oxidation mechanisms that contributed to poor performance in thermal cycling tests (See Discussion of Results).

One important limitation of this analysis is that only one micrograph was analyzed from one of each of the texture types. These micrographs were chosen to roughly be representative of the cross sections of each sample type, but variation undoubtedly exists that is not captured in this analysis.

C. Pre-Spray Characterization

1. Optical Micrographs from PulseTex

Using ablative laser technology, PulseTex produced selected textures. Preliminary optical micrographs taken at an angle were supplied by PulseTex and are in Figure 21, Figure 22, and Figure 23. The team then took more detailed SEM micrographs to examine the textures from a top-down view. These micrographs can be seen in the following section in Figure 24, Figure 25, and Figure 26.

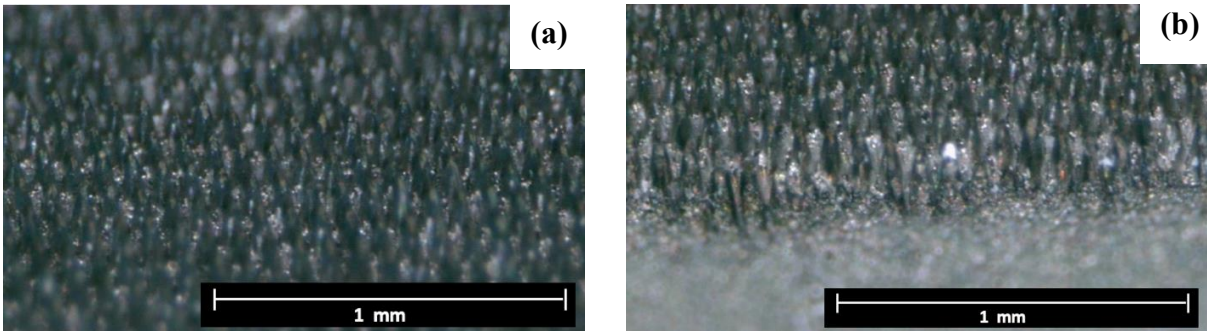


Figure 21: Optical micrograph of rounded spikes texture produced by PulseTex.

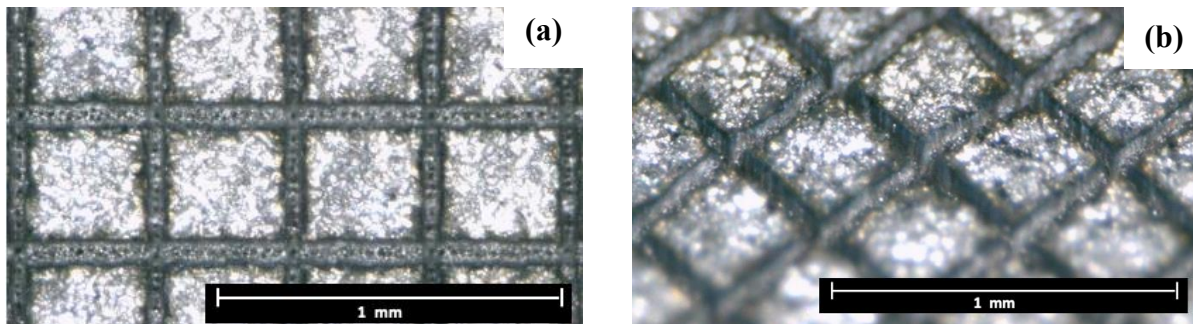


Figure 22: Optical micrographs of grid pattern texture produced by PulseTex.

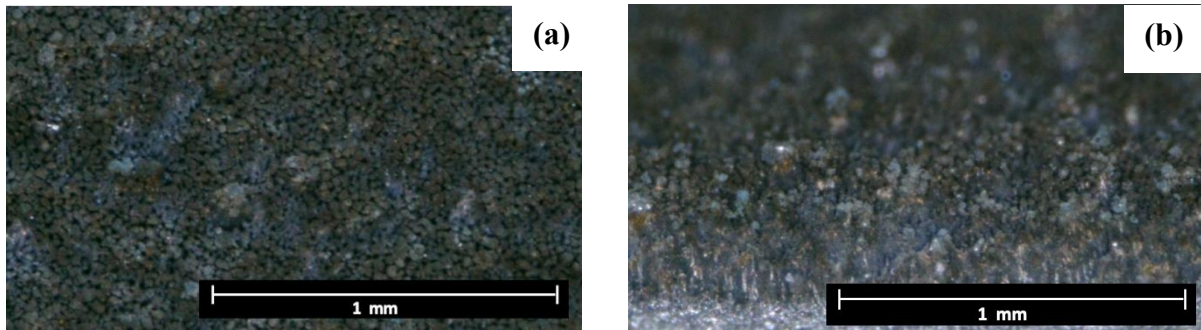


Figure 23: Optical micrographs of grown texture produced by PulseTex.

2. SEM

The micrographs shown below are the results from SEM completed using the Quanta 650 to inspect the textured samples prior to bond coat application. The secondary electron detectors were used in order to capture micrographs that best showed the surface topography.

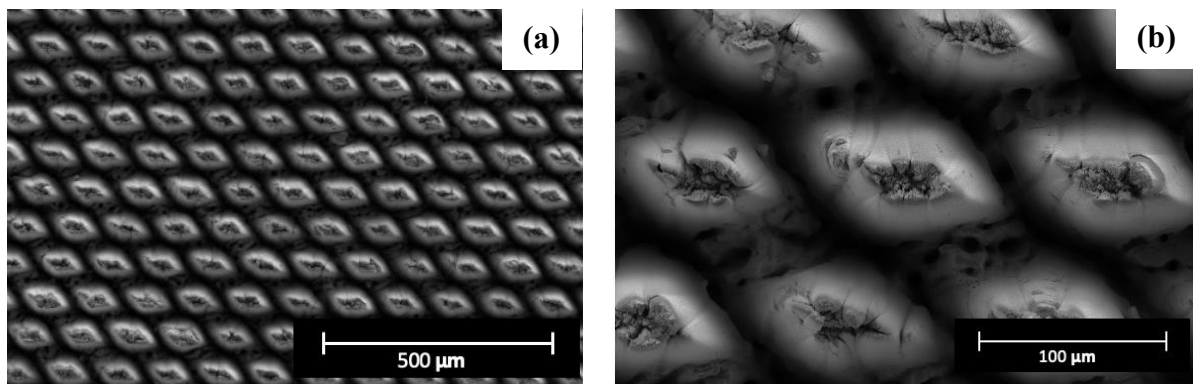


Figure 24(a), (b): SEM micrographs of rounded spike textured sample.

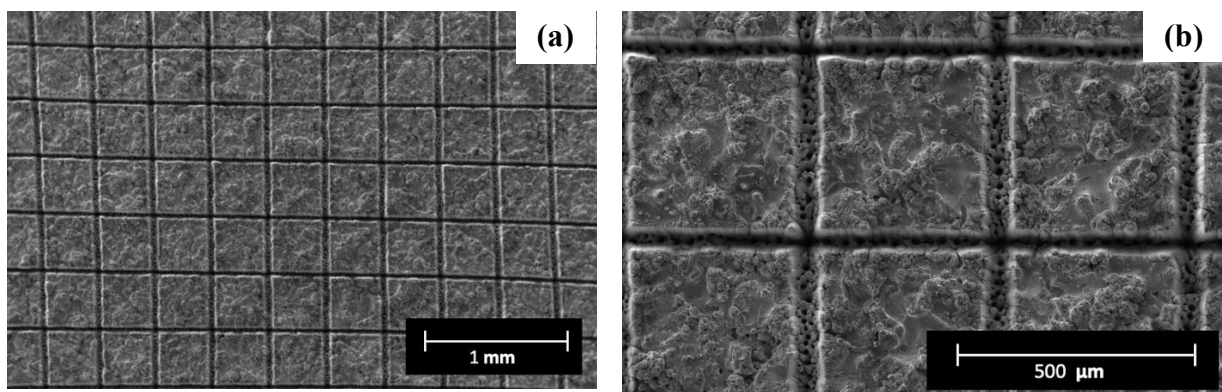


Figure 25(a), (b): SEM micrographs of grid pattern texture sample.

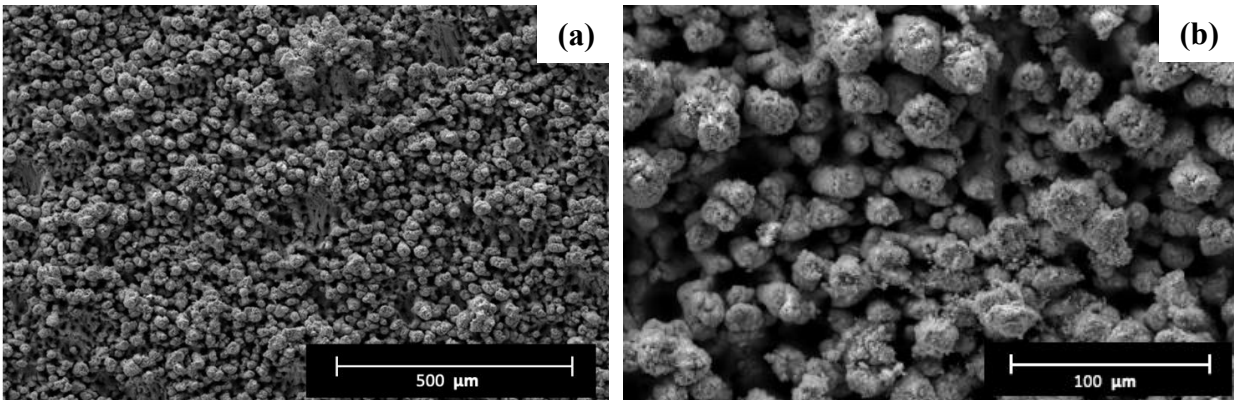


Figure 26: (a), (b): SEM micrographs of grown texture sample.

3. Profilometry

The team wanted to measure the depth of the textures and decided to perform profilometry on one sample of each of the three textures using the Zygo NewView 7300 Optical Surface Profilometer and MetroPro Software. This was done in the dual light stitch mode with a 20X objective lens for all three samples. Profilometry was used to obtain 3D images and measurements of surface topography via scanning white-light interferometry. The objective is mounted in a piezo scanning device that moves vertically and the camera detects interference patterns and stores data as 3D interferogram. Profilometry was performed on the textured samples without any topcoat application.

The main complication encountered while running these scans was setting optimal measurement parameters for the instrument to obtain enough data points to generate a full 3D model of the surface topography. Specifically, the “grooves”, or the lowest levels of the textures, did not show up very well. In the dual light offset stitch mode, one can perform measurements at multiple light levels in one scan to maximize the number of data points the instrument can collect on the surface profile. Offset values of 1.2%, 1.8%, and 0.2% were applied to the T1, T2, and T3 scans respectively (ex: the T1 scan was taken at light levels ranging from 2.01% to 3.21%). Additionally, “plane” is removed from the scan to correct for any tilt of the stage during the focusing and nullification process.

The T1 scan required an “extended” scan length of 350μm along with the offset to maximize the number of data points collected. Here, scan length refers to the depth of the scan. The

objective in a regular “bipolar” scan starts at an initial position, moves down half the scan length then scans upward. The objective in an extended scan only scans upwards, starting at a lower initial position. While the peaks of the rounded spikes appear very clearly, the sides and grooves did not, as seen in Figure 27. Based on the surface profile, the rounded spikes have an average depth of about 120 μm .

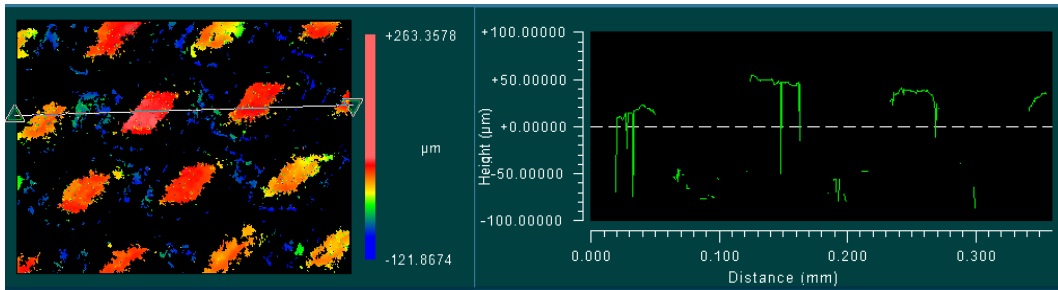


Figure 27: Zygo profilometry scan of rounded spike texture at 20X.

The scans for T2 and T3 required a regular bipolar scan with a scan length of 150 μm . The T2 scan focused on part of two grid squares and the groove in between them, having similar issues to the T1 scan (Figure 28). Based on the surface profile, the depth of the grid pattern is about 80 μm .

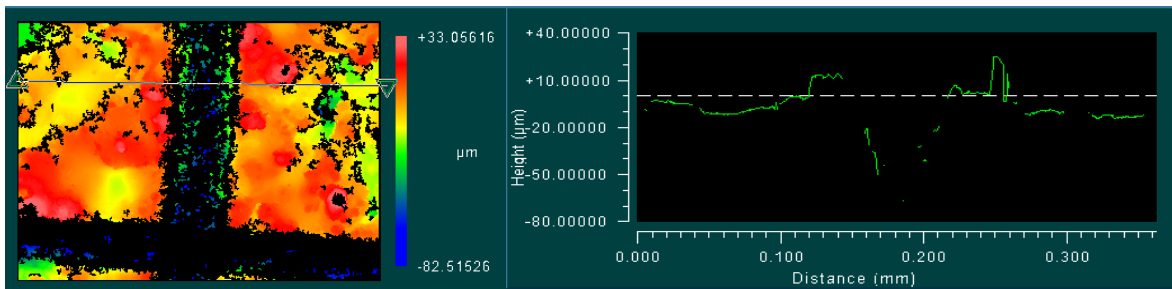


Figure 28: Zygo profilometry scan of grid pattern at 20X.

With the grown column texture, it is extremely difficult to determine the average depth due to the large variation of heights, as seen in Figure 29.

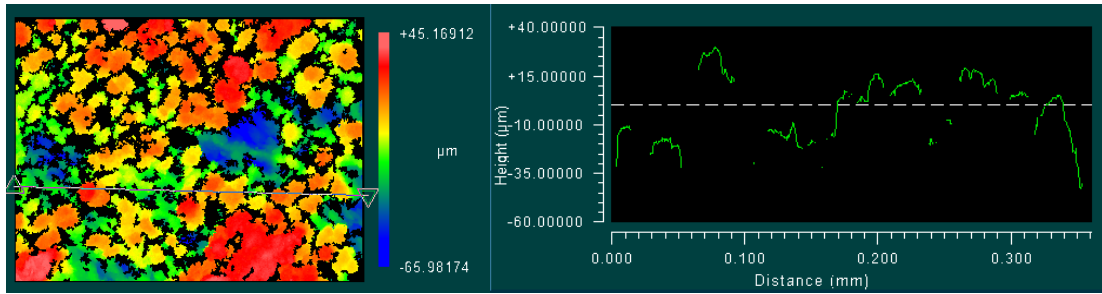


Figure 29: Zygo profilometry scan of grown texture at 20X.

D. Analyzing Spray Parameters

In order to choose a set of TBC spray parameters to use on textured samples, CCAM applied a set of 9 different spray parameters on steel samples. The 9 steel samples with the 9 different spray parameter configurations were analyzed in order to choose the most optimal TBC spray parameter for the IN718 samples. The TBC surface was first observed using optical microscopy, as seen in Figure 30. These micrographs show a rough surface, as expected from the plasma spraying method, and possible burn marks.

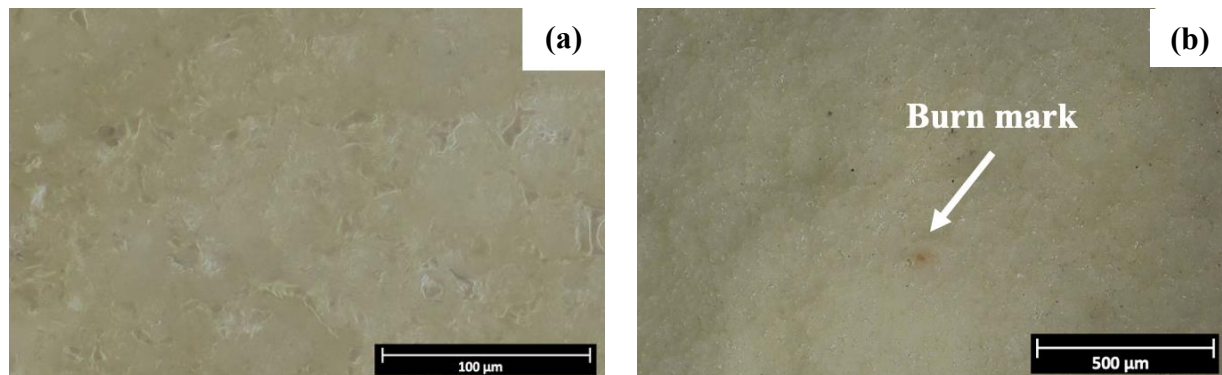


Figure 30: Optical Micrographs of the as-sprayed TBC surface; (a) at 1000X, and (b) 140X.

The group cross-sectioned, mounted, and polished the TBC steel samples for SEM analysis to determine their microstructure. These views are made up of 6 micrographs taken at 150X in Back Scattered Electron mode (BSE) and then stitched together in ImageJ. The 9 different micrographs are shown in

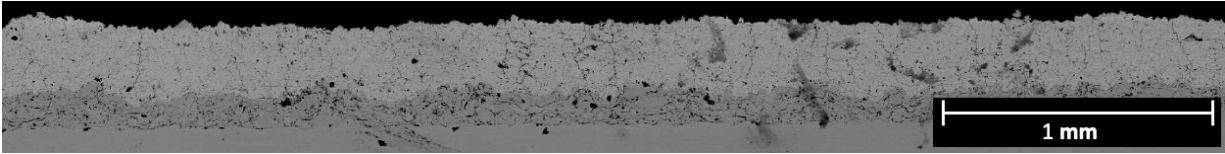
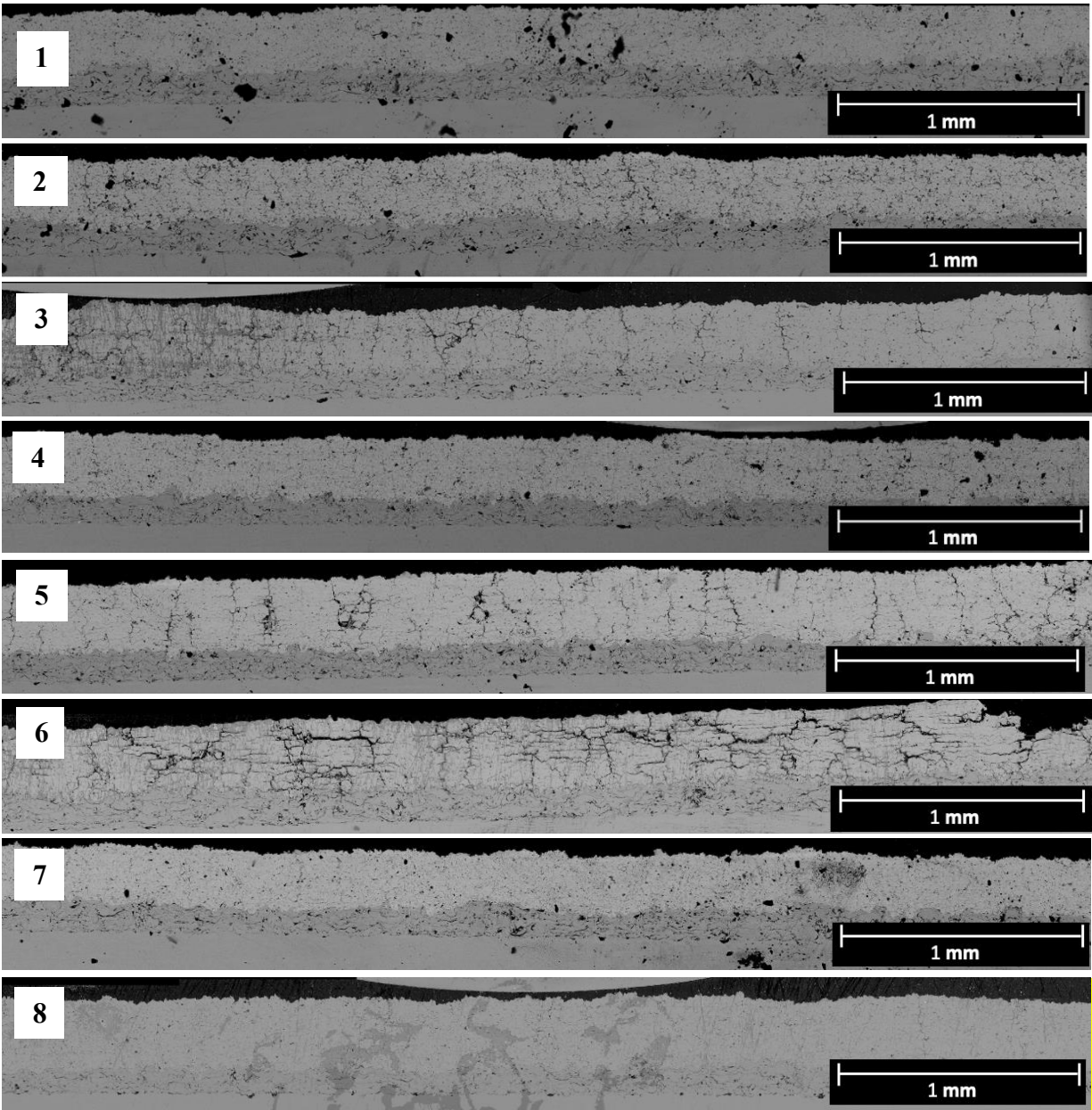


Figure 31: Cross-sections of the nine different TBC steel samples corresponding to spray parameters in



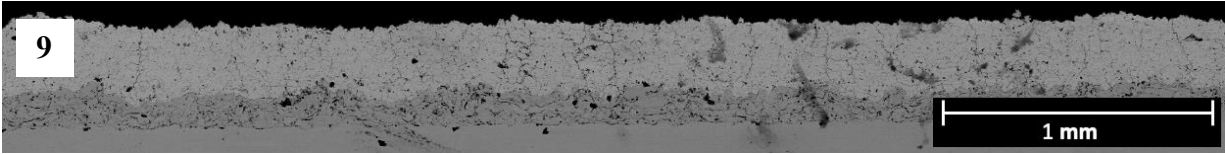


Figure 31: Cross-sections of the nine different TBC steel samples corresponding to spray parameters in

The micrographs were discussed with subject matter experts including Prof. Opila at UVA, and Rob Golden and Matt Gold at Rolls-Royce. After thorough analysis and discussion, it was concluded that the best TBC spray parameters would be one which only slightly induced DVCs. While some spray parameters show a large quantity of DVCs induced, this project is focused on finding the textures which induce the DVCs. Therefore, in order to isolate the effect of bond coat texture, the team wanted to mostly remove the effect that the TBC spray parameters have on inducing the DVCs, so the effect of the textures can be more accurately analyzed. Spray parameter 4 (Gun current: 550A, Distance: 85mm) appeared to produce only a slight number of DVCs, and it would allow an observation of the individual effect the textures have on producing DVCs.

Through this analysis, the team learned what kinds of DVCs may form. The vertical cracks that can be seen prominently in spray parameters 3 and 4 of

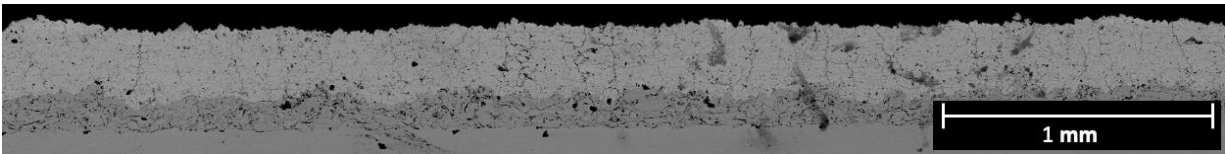


Figure 31: Cross-sections of the nine different TBC steel samples corresponding to spray parameters in

are the kind of DVC formation desired. However, vertical cracks can also develop horizontal branches, as seen in spray parameter 6, which can cause spallation and breaking off of entire sections of coating. This is something that should be avoided.

E. As-Sprayed Sample Analysis

1. Grit Blasted

SEM was conducted for as-sprayed GB, displayed in Figure 32. The micrographs show that the bond coat covers the substrate relatively uniformly. The DVCs appear to be wider than originally anticipated on this unexperimented sample and they fall randomly. There are some pores located in the bond coat.

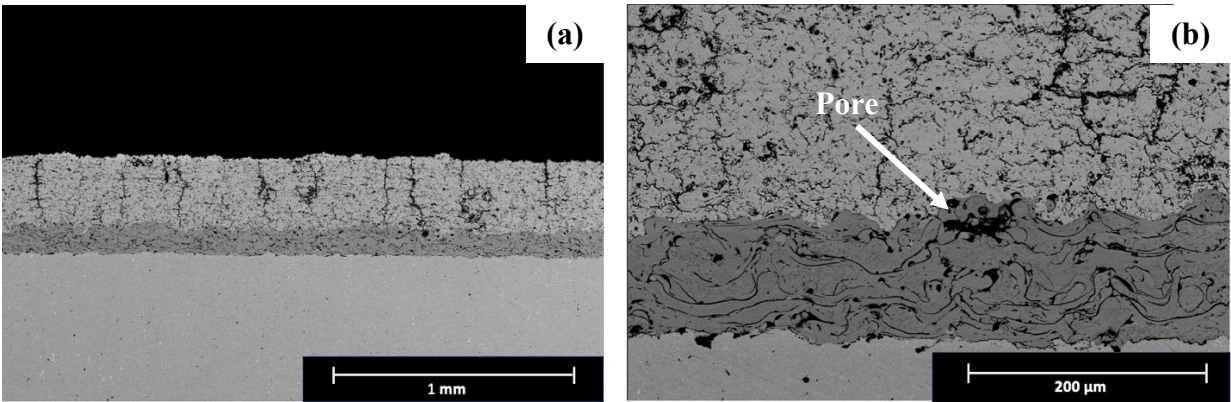


Figure 32: BSE SEM taken for the non-textured, grit-blasted as-sprayed sample. It is observed that the DVCs tend to follow a random pattern.

The team conducted EDS to examine compositional anomalies and supplement SEM micrographs. Note that EDS was conducted on the Phenom SEM XL which is not calibrated for exact values, so compositional information should only be used to compare to other EDS and not nominal compositional values. Figure 33 and Table 14 show EDS obtained for the GB sample. There are three distinct regions—IN718, bond coat, and TBC—as expected.

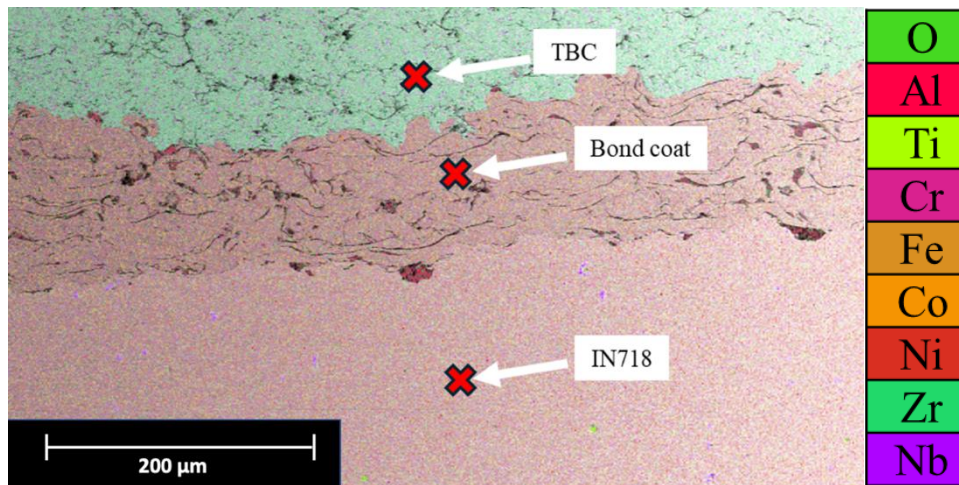


Figure 33: EDS of as-sprayed GB sample. Shows the expected three regions of TBC, bond coat, and IN718.

Table 14: Compositional results for EDS on as-sprayed GB sample. Compositions given in atomic concentration (%).

| Element | Atomic Concentration [%] | | |
|---------|--------------------------|-----------|-------|
| | IN718 | Bond Coat | TBC |
| O | 0.00 | 0.00 | 53.98 |
| Al | 0.00 | 31.77 | 0.00 |
| Ti | 1.09 | 0.00 | 0.00 |
| Cr | 21.82 | 12.24 | 0.00 |
| Fe | 21.46 | 0.00 | 0.00 |
| Co | 0.00 | 16.57 | 0.00 |
| Ni | 50.56 | 39.31 | 0.00 |
| Y | 0.00 | 0.00 | 2.84 |
| Zr | 0.00 | 0.00 | 43.18 |
| Nb | 5.07 | 0.00 | 0.00 |

2. T1

Shown in Figure 34 are micrographs of the untested, fully coated T1 rounded spike samples. As expected, there are three primary regions: (1) IN718 substrate, (2) bond coat with texture, and (3) TBC topcoat. There is also an unexpected intermediate phase that is found at the interface between the bond coat and the TBC. Further investigation into this phase can be found in the following section that covers Energy Dispersive Spectroscopy (EDS).

It is important to note what is missing from the micrograph, namely a continuous layer of bond coat between the texture and the IN718 substrate. According to the designs submitted to PulseTex by the team, it was anticipated that the texture would make up less than half of the bond coat thickness. The micrographs, however, reveal that the entire bond coat is either textured or missing. In the spaces between spikes, there is no bond coat, resulting in contact between the TBC and IN718 substrate. This feature is detrimental and could be the failure initiation site for thermal testing that depends on the strain for differing expansion between layers. Furthermore, in the regions missing the bond coat, there is also damage to the substrate that is not consistent with surface roughness from the grinding and grit blasting previously conducted. This indicates that

laser parameters developed by PulseTex may have been too aggressive for the bond coat and caused its complete removal and laser penetration into the substrate.

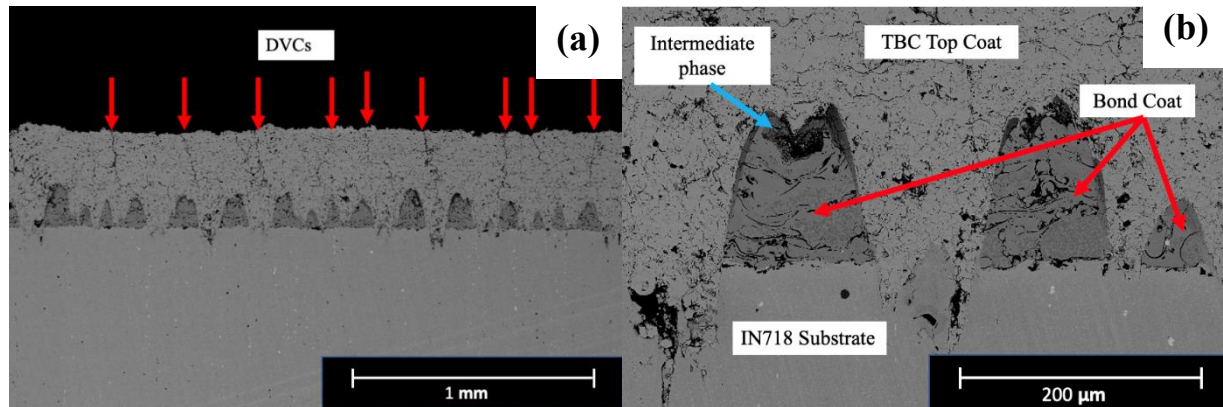


Figure 34: BSE SEM micrographs of coated rounded spike textured sample at (a) 50X and (b) 250X. Micrographs show that most of the bond coat was removed during ablation.

The team supplemented micrographs with EDS to investigate unexpected regions within the coating system. One such region of note is the “intermediate phase” labeled in Figure 34(b). Shown in Figure 35 and Table 15 are the results of EDS analyzing each region of the coating system. EDS was done on the Phenom XL G2 SEM, which is not properly calibrated, meaning that the exact compositions found by the EDS are not to be accepted as accurately reflecting the exact composition of the sample.

These results clearly show that there is a compositional difference between the intermediate region and the rest of the coating system. The most significant differences are that, relative to the bond coat, the intermediate layer is iron and nickel rich, and it is cobalt and aluminum deficient. Note that neither the bond coat nor the TBC contain iron, meaning the only place in the system it could originate from is the substrate. This suggests that at the end of the laser process the substrate may have been ablated resulting in free nickel and iron within the system which then diffused into the top layer of the bond coat, resulting in a layer that is deficient in aluminum and cobalt relative to the rest of the bond coat. This theory is supported by the presence of an intermediate layer on spikes that are next to deep trenches in the substrate. The effects of such a layer are unknown; they could potentially be seen during testing, though given the missing bond

coat, it is expected that this defect will dominate failure initiation sites, offering no insight into the effects of the intermediate layer.

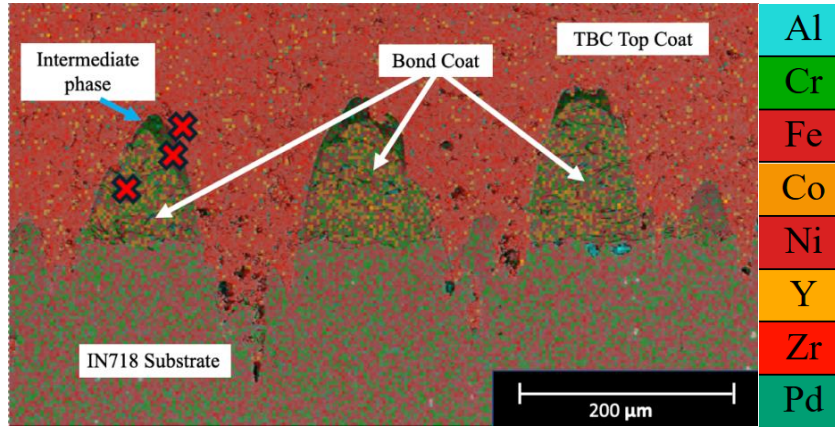


Figure 35: Map EDS of rounded spike coated sample. Shows four distinct regions: IN718 substrate, bond coat, intermediate phase, and TBC topcoat. Point EDS was conducted on regions with red X.

Table 15: Point EDS results from rounded spike coated sample in three different regions.

| Element | Atomic concentration [%] | | |
|---------|--------------------------|-----------|-------|
| | Intermediate | Bond Coat | TBC |
| O | 0.00 | 0.00 | 52.39 |
| Al | 14.78 | 21.86 | 0.00 |
| Cr | 18.85 | 19.42 | 0.00 |
| Fe | 9.26 | 0.00 | 0.00 |
| Co | 9.87 | 20.79 | 0.00 |
| Ni | 43.51 | 37.04 | 0.00 |
| Y | 0.00 | 0.00 | 2.71 |
| Zr | 0.00 | 0.00 | 43.19 |
| Nb | 3.02 | 0.00 | 0.00 |
| Pd | 0.71 | 0.43 | 1.18 |
| Hf | 0.00 | 0.00 | 0.53 |
| Au | 0.00 | 0.44 | 0.00 |

SEM was conducted for as-sprayed T2, displayed in Figure 36. The micrographs show that for some of the grid lines, the laser went all the way through the bond coat and into the IN718 substrate. This allowed the TBC to come into direct contact with the substrate at those points. It is also observed that the DVCs appear wider than originally anticipated, and they tend to fall in line with the grid lines. DVCs appear at the trenches independent of full ablation of the bond coat; even in trenches where bond coat remains, DVCs appear.

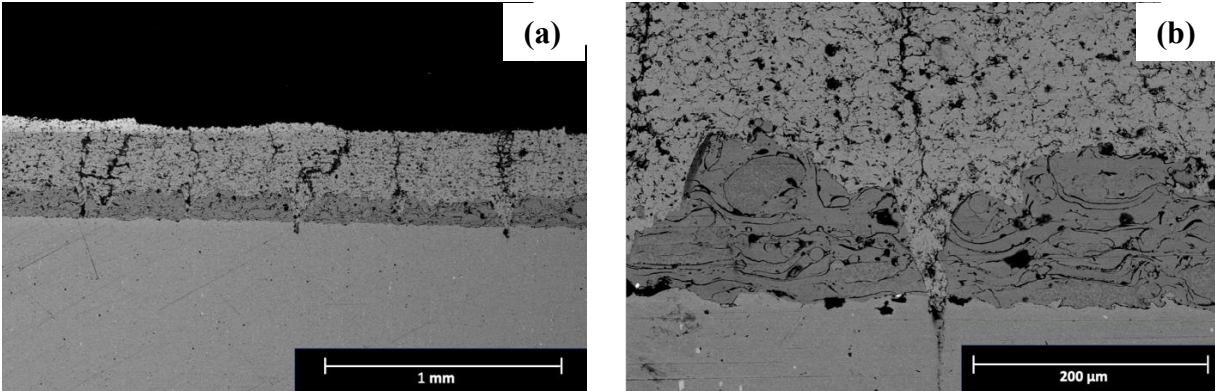


Figure 36: BSE SEM of T2 grid pattern at different magnifications (a,b). It is observed that the laser went through the entire bond coat at spots, allowing the TBC to be in contact with the surface.

EDS conducted on T2, displayed in Figure 37 and Table 16, showed IN718, bond coat, TBC, and an intermediate phase, similar to T1 when the laser penetrated through the bond coat to the substrate. This intermediate phase is found at the interface between the bond coat and the TBC. This phase is a nickel rich, oxidized layer on top of the ablated texture, presumably formed during laser ablation when the laser penetrated through the bond coat to the substrate. The layer is less prominent than it was in T1, likely due to less penetration of the substrate.

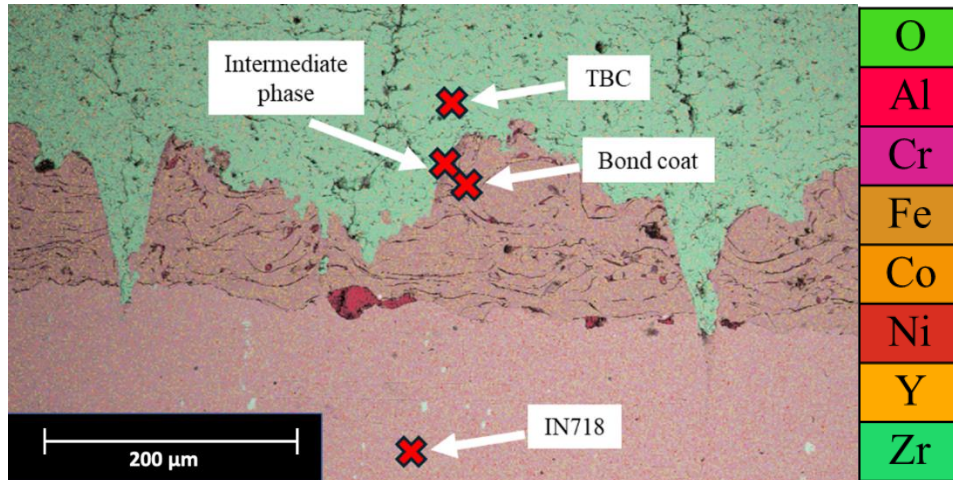


Figure 37: EDS of T2 sample. Shows four distinct regions that include IN718, bond coat, TBC, and an intermediate phase between the bond coat and TBC.

Table 16: Compositional results for EDS on as-sprayed T2 sample. Compositions given in atomic concentration (%).

| Element | Atomic Concentration [%] | | | |
|---------|--------------------------|-----------|--------------------|-------|
| | IN718 | Bond Coat | Intermediate Phase | TBC |
| O | 0.00 | 0.00 | 15.25 | 54.49 |
| Al | 0.00 | 22.72 | 24.18 | 0.00 |
| Ti | 1.09 | 0.00 | 0.00 | 0.00 |
| Cr | 21.84 | 17.52 | 14.35 | 0.00 |
| Fe | 21.58 | 0.00 | 0.00 | 0.00 |
| Co | 0.00 | 20.07 | 15.29 | 0.00 |
| Ni | 50.41 | 39.58 | 30.94 | 0.00 |
| Y | 0.00 | 0.12 | 0.00 | 3.16 |
| Zr | 0.00 | 0.00 | 0.00 | 42.35 |
| Nb | 5.08 | 0.00 | 0.00 | 0.00 |

4. T3

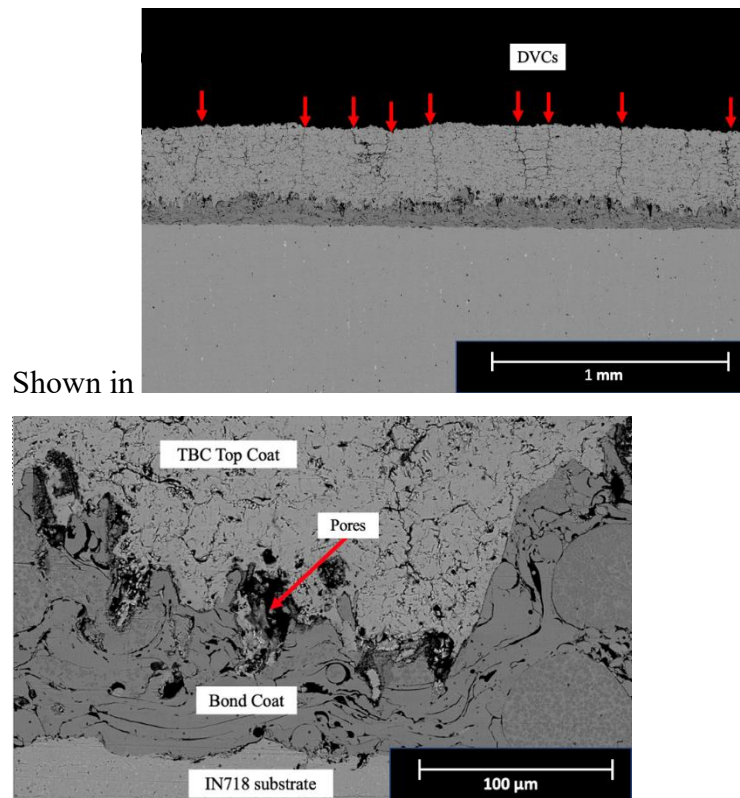


Figure 38 are micrographs of the unexperimented, fully coated T3 grown texture samples. Similar to the T1 texture, there are observable DVCs induced within the topcoat. The grown texture does not follow a uniform pattern, so the bond coat appears to have varying levels of depth. Unlike the T1 rounded spikes texture, it appears that all the substrate is covered in the bond coat. However, there are noticeable pores between the topcoat and the bond coat, indicating that perhaps the powder particle size of the topcoat was not small enough to fill in all the small crevices.

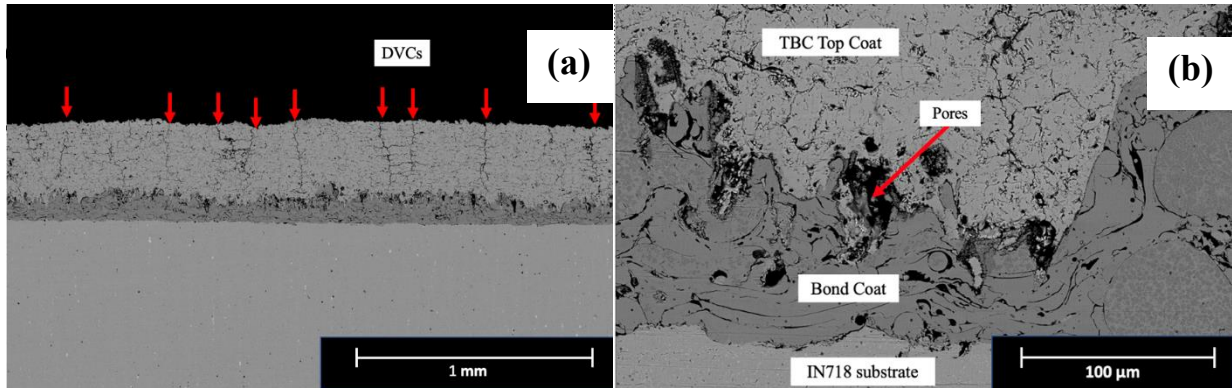


Figure 38: BSE SEM of as-sprayed T3 grown texture sample at (a) 50X and (b) 400X. Micrographs show some porosity at bond coat/TBC interface.

Microscopy for T3 was also supplemented with EDS, shown below in Figure 39. The EDS shows 3 clear phases (substrate, bond coat, TBC), with no intermediate phase seen in T1 and T2. The only abnormal compositional features are aluminum clusters in the bond coat, which were also seen in T1. There are, however, regions with no compositional information which indicates the presence of porosity at the bond coat/TBC interface. This could prove to be detrimental to coating adhesion, offering failure initiation sites.

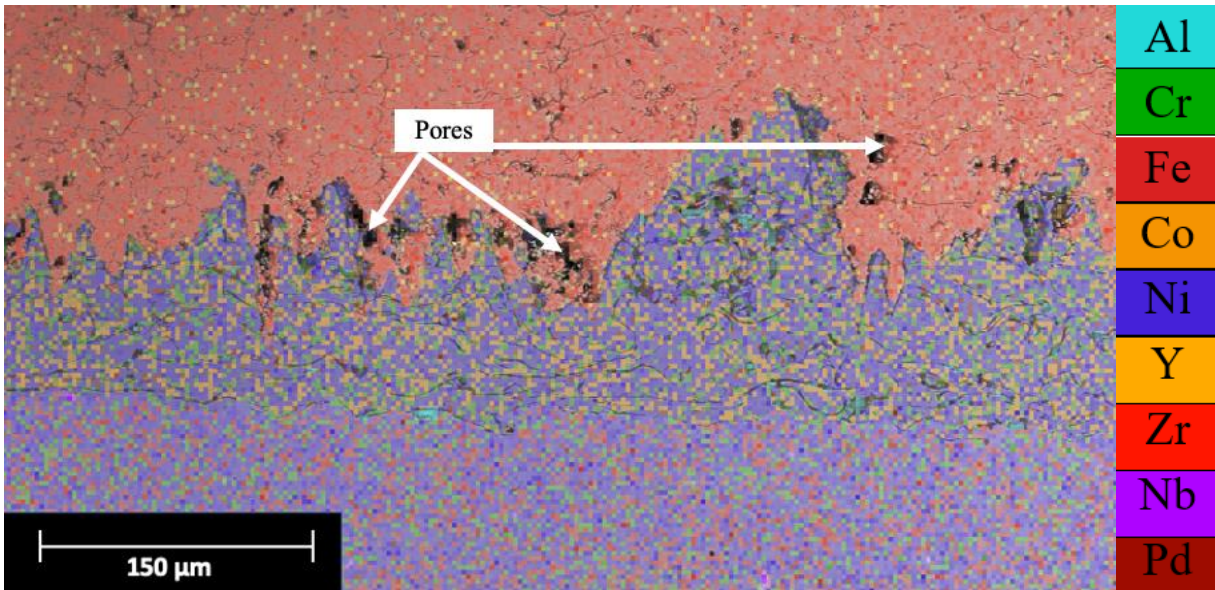


Figure 39: EDS map of grown texture coating system. Shows distinct substrate, bond coat, and TBC layers with some porosity at bond coat/TBC interface.

5. Overview of Cracking

ImageJ software was used to quantitatively analyze arrangement of the DVCs. This was completed by measuring the width of SEM micrographs at 50X (low magnification to increase data points) and counting the number of vertical cracks present in the topcoat of the TBC – vertical cracks were defined as a crack that spans from the outer edge of the topcoat to the bond coat. The spacing of the cracks was then analyzed. The values measured are listed below in Table 17.

Table 17: Table of calculated vertical crack linear density.

| | GB | T1 | T2 | T3 |
|---------------------------------------|------|------|------|------|
| Linear Density (mm ⁻¹) | 3.28 | 3.15 | 3.02 | 3.02 |

There are errors inherent to this analysis. First, the material has a large amount of vertical cracks/voids and the determination of vertical cracks can be biased by the individual conducting the analysis. Secondly, the data set is rather limited, and further characterization with more micrographs would be needed to reliably quantify this variable. Thirdly, the cracks may have

some directional dependence that is not reflected by this methodology since it is all conducted on a singular cross section.

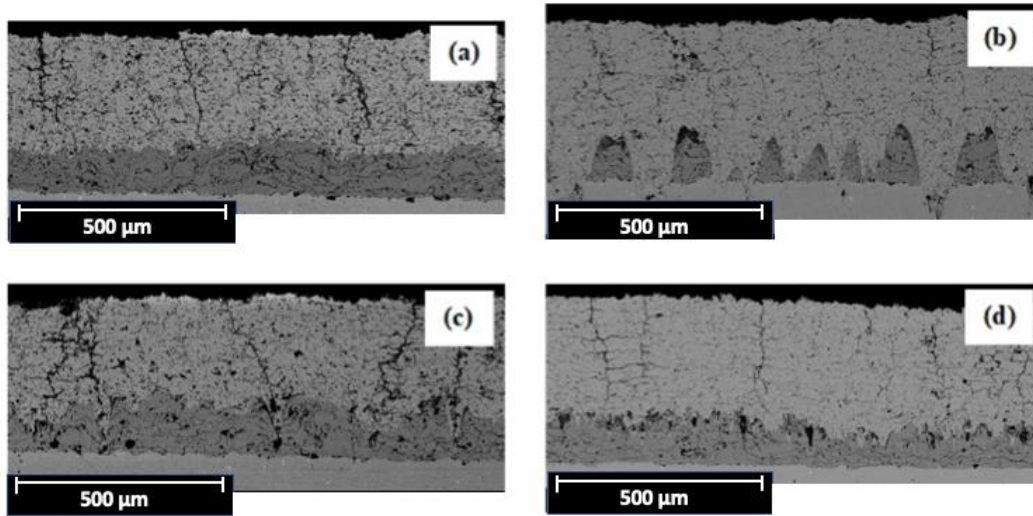


Figure 40: BSE micrographs of as-sprayed samples at 100X; (a) GB, (b) T1, (c) T2, and (d) T3.

The linear density shows that there is not a statistical difference in the spacing of the DVCs. However, some qualitative conclusions can be made; GB and T2 have larger crack widths, and vertical cracks tended to terminate internally in regions with bond coat depressions. This is most notably visualized in T1 and T2 where the cracks seem to prefer terminating in areas where the laser had subtracted bond coat material.

F. Thermal Cycling Results and Characterization

Thermal cycling led to spallation and coating failure far sooner than Rolls-Royce expected. All 16 samples surpassed the 50% limit after 16 cycles, with the first 4 samples reaching this threshold after only 2 cycles. Figure 41 shows optical micrographs of each sample surface at the point where they surpassed the 50% spallation threshold.

The figures are organized by rows. Samples were kept in the same formation for all images taken during testing for simplicity.

- Row 1: GB, or grit blasted samples
- Row 2: T1, or rounded spike texture

- Row 3: T2, or grid texture
- Row 4: T3, or grown texture

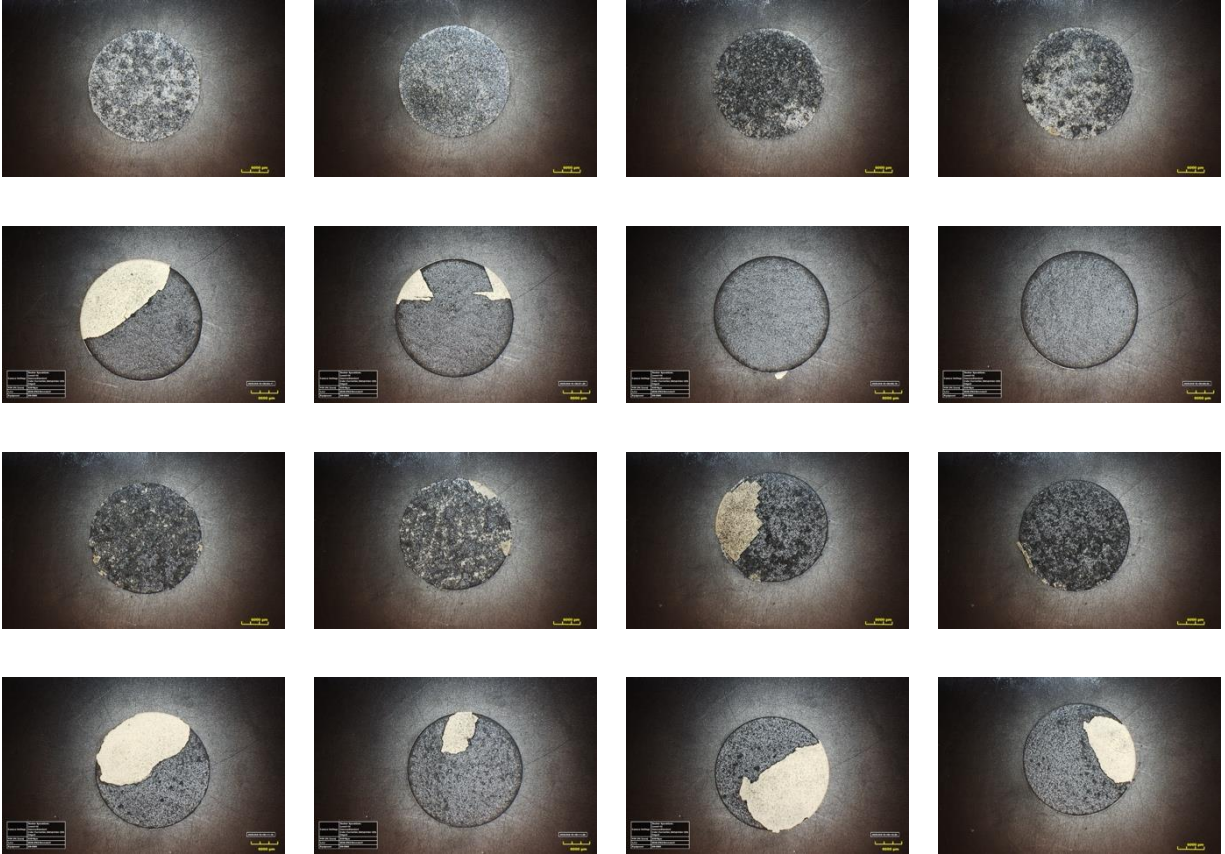


Figure 41: Overview shots of each sample after they had been removed from furnace cycle testing due to reaching >50% spallation.

Using these overview shots, the team conducted image analysis in ImageJ to calculate the final percentage of spallation for each sample. It should be noted that these spallation values are underestimated, as much of the coatings remaining in the overview shots were not fully attached to the substrates.

Table 18: Final percent spallation of samples after being cycled in the furnace

| | B1 | B2 | B3 | B4 | Average |
|-----------|-----------|-----------|-----------|-----------|----------------|
| GB | 100% | 100% | 100% | 99.31% | 99.77% |

| | | | | | |
|-----------|--------|--------|--------|--------|--------|
| T1 | 62.26% | 88.92% | 100% | 100% | 87.80% |
| T2 | 98.86% | 95.83% | 73.78% | 98.10% | 91.64% |
| T3 | 55.19% | 89.17% | 49.50% | 76.13% | 67.50% |

The first samples to fail, after only 2 cycles, were the T1 rounded spike textured samples. All 4 T1 sample coatings fully or partially failed during the cooling period after their second cycle, with coating cracking and popping off over the span of 2-5 minutes after they had been removed from the furnace. Many parts of the coating flew across the room and were collected by hand afterwards.

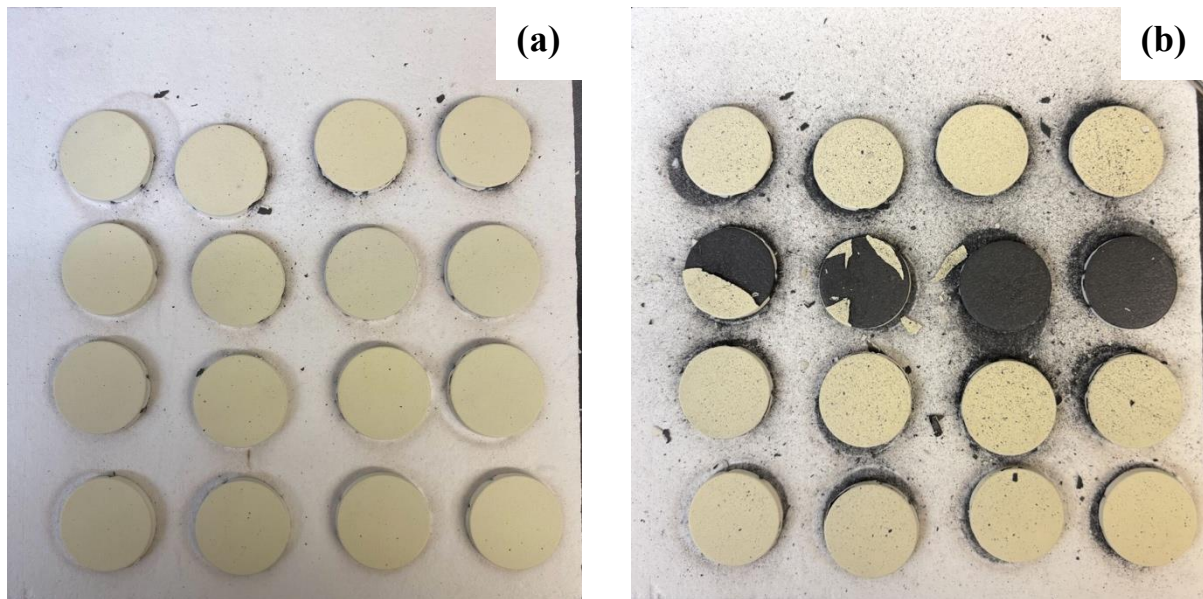


Figure 42: Samples after 1 cycle (left) vs after 2 cycles (right). All T1 samples have surpassed 50% spallation.

The next coatings to fail were T3-B2 (after 7 cycles) and T3-B1 (after 9 cycles). At this point, another T3 coating was also delaminating, as can be seen in Figure 43, but it had not yet reached the 50% threshold. T3-B3 later failed after cycle 10.



Figure 43: Samples after 9 cycles, showing T3-B1 and T3-B2 with over 50% spallation and T3-B3 beginning to fail.

After 13 cycles, GB-B1, GB-B2, and GB-B4 and the final T3 sample, T3-B4, surpassed 50% spallation. As can be seen in Figure 44, the GB samples had coatings come off cleanly in one or two sheets. The team noticed that for 3-4 cycles before failure, the coatings had been peeling off (Figure 44(b)). Note the missing samples in Figure 44 are because the samples that had previously failed were removed (T1 samples and T3-B1-3) to begin characterization.

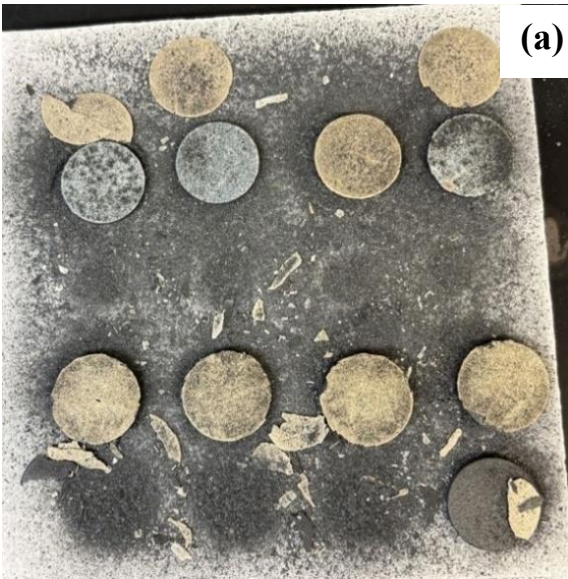


Figure 44: (a) Samples after 13 cycles, showing failure of GB samples and the last T3 sample. Note: the missing samples are because the team removed the samples that had previously failed (T1-B1—T1-B4 and T3-B1—T3-B4) to begin characterization, and (b) Side view of samples 3-4 cycles before GB failure, showing the beginning of peeling.

Lastly, after cycles 15 and 16, all samples had reached the 50% spallation. The last samples to fail were GB-B3, T2-B3, and T2-B4.

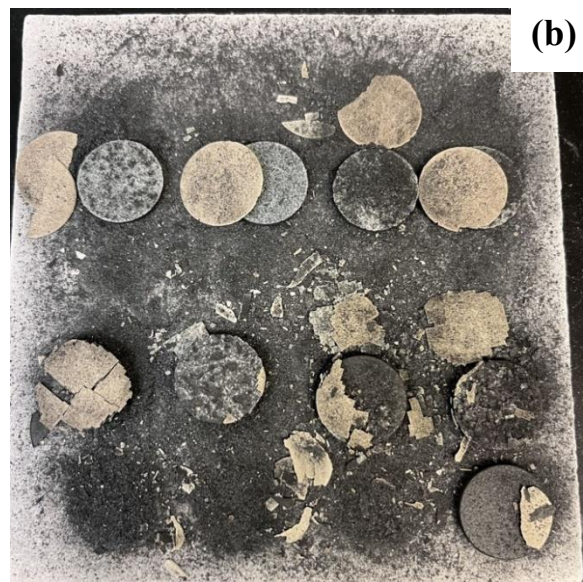
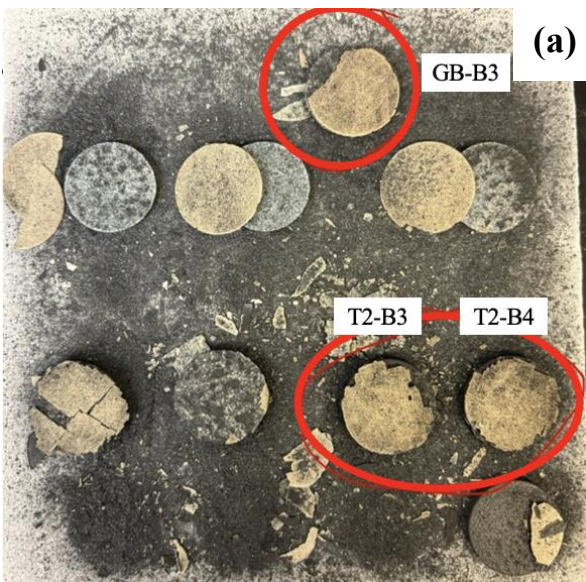


Figure 45: (a) Samples after cycle 15, showing that only GB-B3, T2-B3, and T2-B4 remain (circled), and (b) Samples after cycle 16, all samples have reached 50% spallation threshold.

Table 19: Failure summary table for results of thermal cycling.

| Texture | Average Cycles to Failure |
|---------------------|---------------------------|
| Grit blasted | 13 |
| Rounded spikes (T1) | 2 |
| Grid pattern (T2) | 15 |
| Grown texture (T3) | 9 |

Cycling results showed that on average, the grid pattern performed better than the baseline grit blasted samples. The grown texture showed promising, though not comparable results and the rounded spikes failed completely.

After each of the 16 cycles, masses were taken to track over time. Final masses were also taken after oxide dust was removed during characterization. The team noticed significant mass loss of substrate via oxidation of the exposed substrate which easily fell off.

Figure 46(a) shows a plot of masses over time, grouped by texture type. The mass drop-off at the end of each sample lifetime coincides with when coating was partially or completely lost. Figure 46(b) shows the initial and final masses of each of the samples. Of note, the GB and T2 samples lost more mass than the T1 and T3 samples. This aligns with results in Table 18 showing that these textures suffered higher percentages of spallation at failure.

(a)

(b)

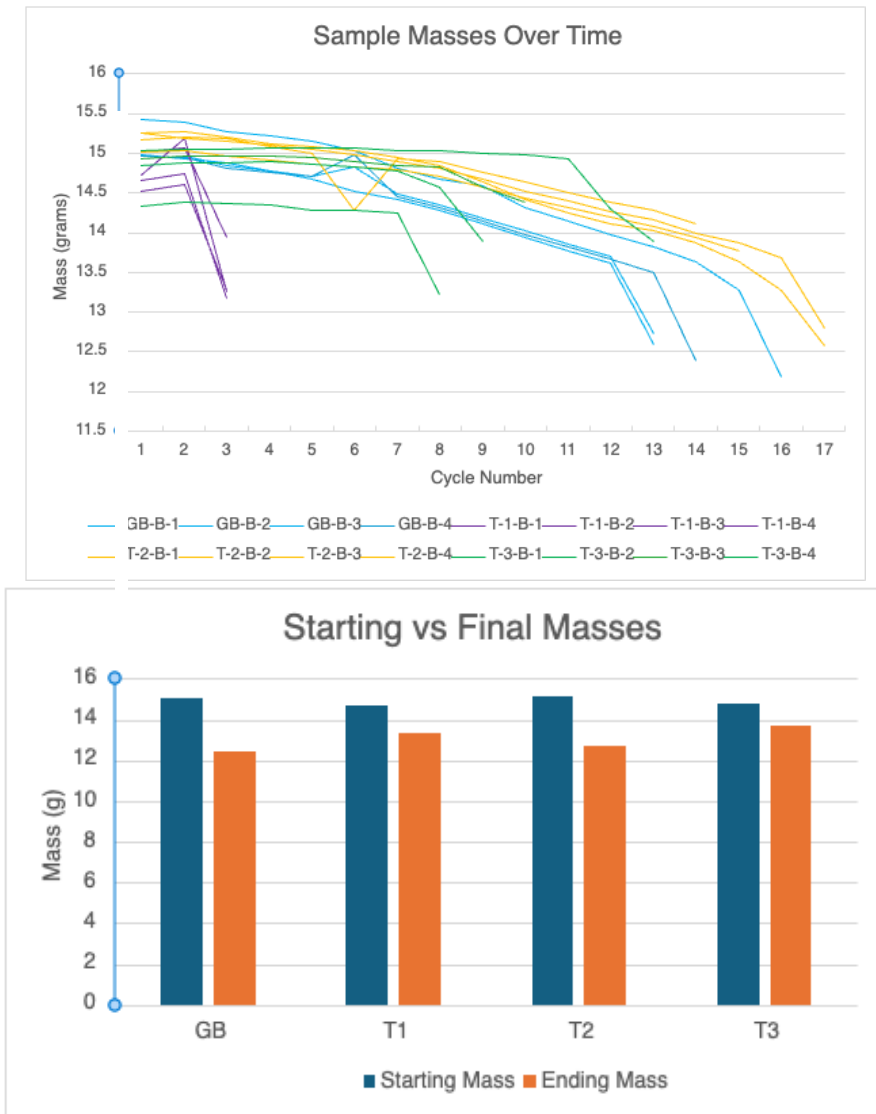


Figure 46: (a) Plot of mass loss of each sample over time, and (b) histogram showing starting and ending masses of each sample.

Qualitatively, it was noted that most of this mass loss was due to oxidization of the IN718 substrate and coating spallation. Although mass was monitored primarily to track oxidation growth between the substrate, bond coat, and TBC – it is impossible to distinguish what amount of the mass fluctuations were due to oxide growth in these areas.

1. Grit Blasted Sample Characterization

Upon inspection of optical micrographs of the grit blasted samples, the team observed that despite the TBC coatings appearing to have peeled off in one or two sheets during furnace testing, some of the ceramic remained attached to the bond coat (Figure 47). This leftover TBC is not visible without looking under the microscope and is only present on some parts of the surface. Rolls-Royce explained that the coating fills surface texture well and confirmed that remnants should be expected to be found on the surface.

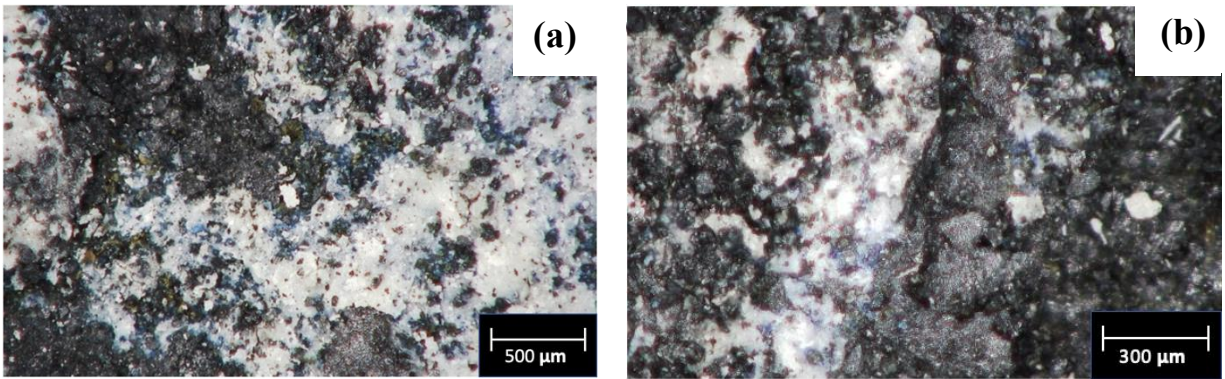


Figure 47: Optical micrographs of TBC remnants on grit blasted samples at (a) 100X and (b) 150X.

SEM micrographs were taken for the GB long furnace cycled samples and are shown in Figure 48. The TBC had completely spalled off from the samples so the remaining substrate with remaining bond coat was imaged. Unlike the as-sprayed sample, contrast in this sample does not show a difference between the bond coat and IN718, suggesting a change in composition from the as-sprayed sample. The bond coat is observed to have remained adhered to the substrate and thermally grown oxide (TGO) grew on the bond coat/TBC interface.

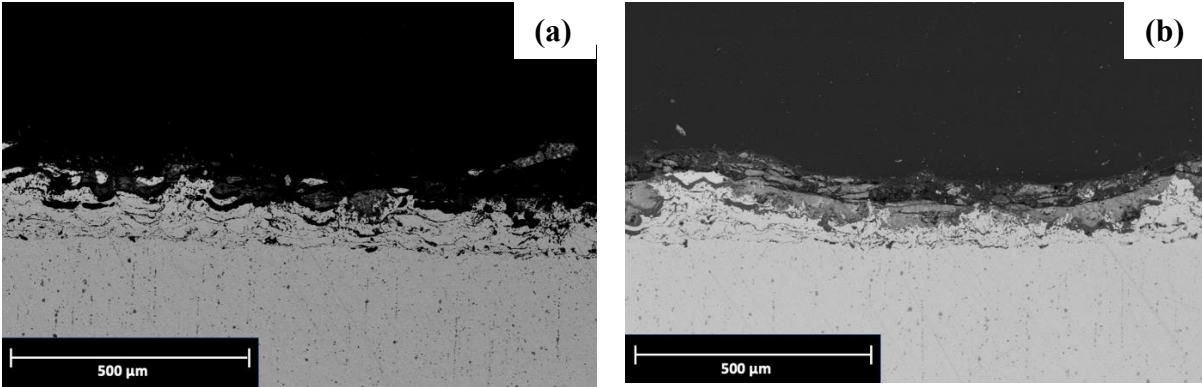


Figure 48: BSE SEM of GB long furnace cycled samples. The remaining bond coat and TGO are visible. The TBC spalled off the sample.

After cycling, samples were analyzed using EDS, seen in Figure 49 and Table 20. The EDS showed five regions within the sample: residual TBC, an oxide at the TBC/bond coat interface, dark layers throughout the bond coat, underlying bond coat, and IN718. In previous discussions, Rolls-Royce explained that after failure, cycled samples should have a small amount TBC still adhered to the bond coat. The GB sample was the first sample to exhibit this, which confirms that this sample had adequate adhesion of the TBC to the bond coat. Below the TBC there is a layer of oxide at the interface between the TBC and the bond coat, as well as the remaining bond coat with dark layers running through it. Compositional values reveal that the oxide at the TBC/bond coat interface is chromium rich, while the dark layers running through the bond coat are aluminum rich. Individual EDS maps that highlight these features are seen in Figure 50.

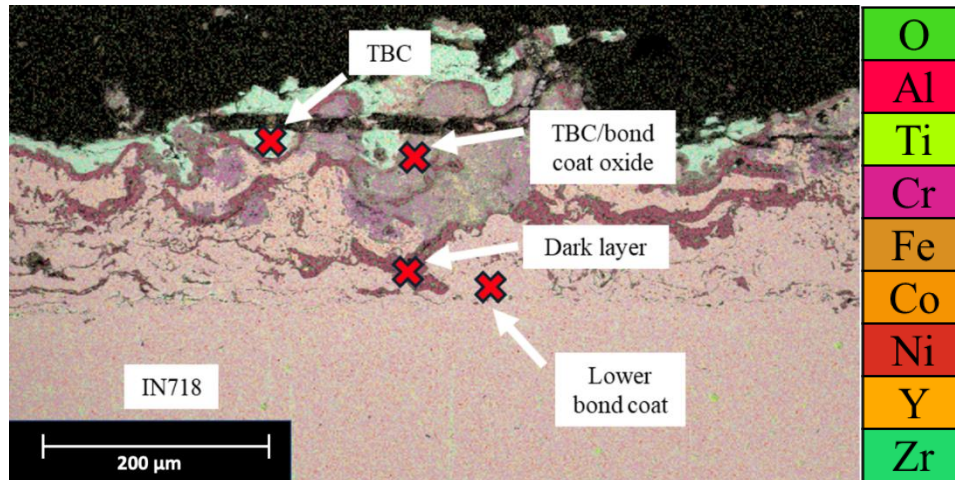


Figure 49: EDS of cycled GB sample. Shows residual TBC, TBC/bond coat oxide, dark layer within the bond coat, underlying bond coat, and IN718.

Table 20: Compositional results for EDS on cycled grit blast sample. Compositions given in atomic concentration (%).

| Element | Atomic Concentration [%] | | | |
|---------|--------------------------|------------|---------------------|-------|
| | Lower bond coat | Dark layer | TBC/bond coat oxide | TBC |
| O | 0.00 | 49.25 | 37.90 | 54.90 |
| Al | 0.00 | 50.49 | 4.10 | 0.00 |
| Cr | 22.80 | 0.00 | 26.40 | 0.00 |
| Fe | 14.82 | 0.00 | 10.42 | 0.00 |
| Co | 9.54 | 0.00 | 10.29 | 0.00 |
| Ni | 49.45 | 0.26 | 10.89 | 0.59 |
| Y | 0.00 | 0.00 | 0.00 | 2.46 |
| Zr | 0.00 | 0.00 | 0.00 | 42.05 |
| Nb | 3.39 | 0.00 | 0.00 | 0.00 |

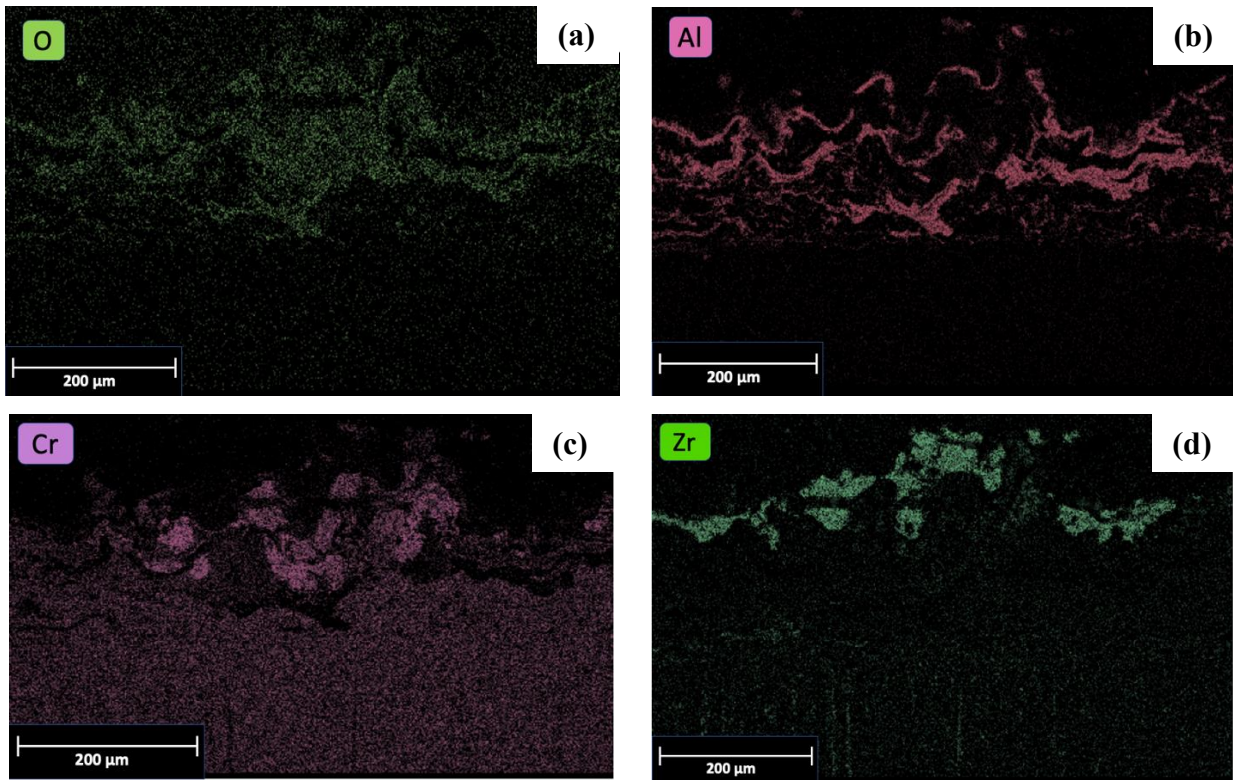


Figure 50: Cycled grit blast map EDS separated by element. (a) Oxygen, (b) Aluminum, (c) Chromium, and (d) Zirconium. Highlights remaining TBC, chromium oxide at TBC/bond coat interface, and aluminum oxide within the bond coat.

2. T1

Optical micrographs taken of the T1, rounded spike, surfaces showed interesting crack patterns in the remaining TBC left after furnace cycling (Figure 51(a-c)). In addition to surface cracks, there was also visible chipping of the TBC on the edges of the sample, Figure 51(a).

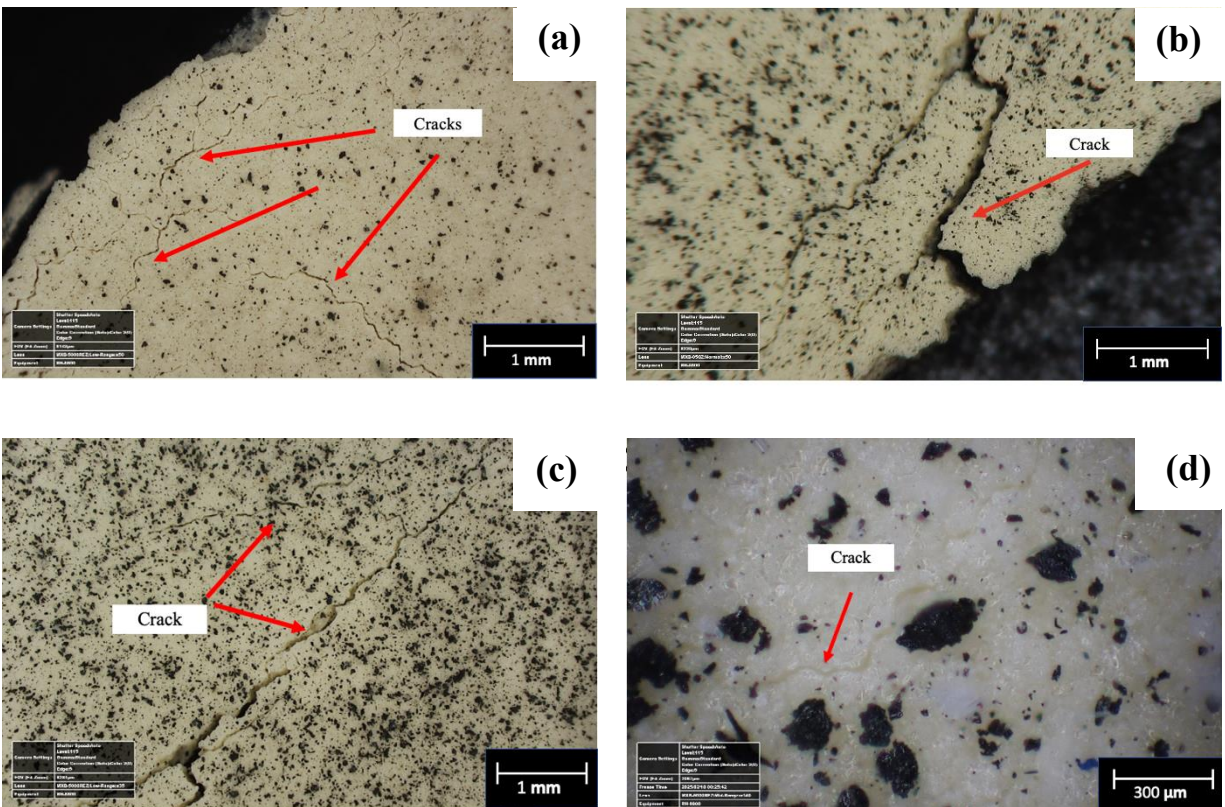


Figure 51: Optical micrographs of T1 sample surfaces after furnace cycling: (a) a sample edge showing chipping of TBC and crack profiles at 50X, (b) edge of TBC showing cracking at 50X, (c) mid-TBC surface crack at 50X, and (d) microcrack in the TBC at 3000X.

The SEM micrographs of the T1 sample (Figure 52) provide information on the failure mechanism. Within the topcoat of the furnace cycled sample, DVCs are visible. The DVCs were also visible in the T1 sample that was not furnace cycled. In this furnace cycled sample, the DVCs appear to have grown in width, indicating that during the heating and cooling, tensile stresses were exerted onto the topcoat by the bond coat and substrate, and therefore stretching the topcoat. When looking more closely at the DVC location within the topcoat, in relation to the bond coat “spikes,” the DVCs appear to fall in a uniform manner in-between the bond coat spikes. This would indicate that between these spikes, the topcoat is experiencing tensile stresses, perhaps stretching the topcoat. This tensile stress could have been exhibited during the time when the sample was heating up in the furnace as the YSZ, with a lower thermal expansion coefficient, naturally expanded less than the IN718 and bond coat which have higher thermal

expansion coefficients. However, it cannot be concluded whether these DVCs had any effect on the lifespan of the T1 sample in the furnace cycling, since the T1 samples failed first, likely due to the lack of a bond coat between the topcoat and the IN718 in the spaces between the spikes.

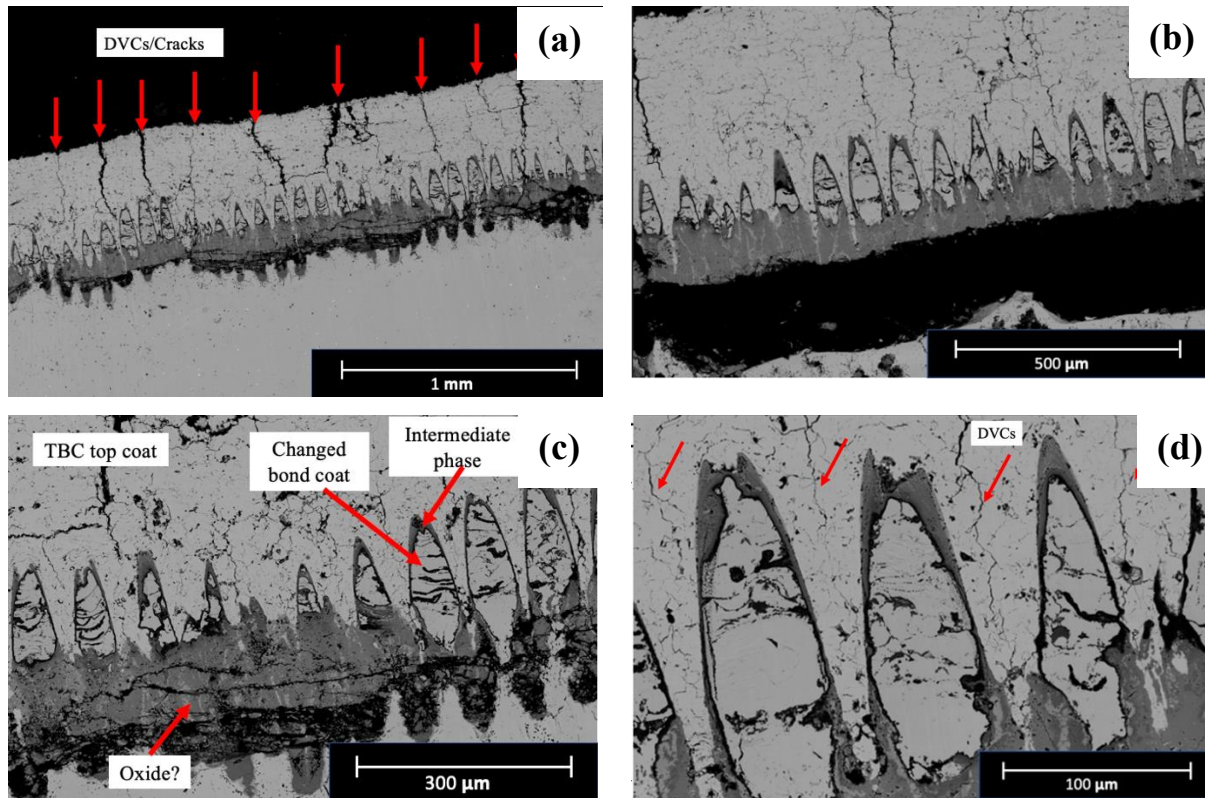


Figure 52: BSE SEM micrographs of T1 samples. A new layer formed between the substrate and the TBC, resulting in the delamination of this layer from the substrate, pinching the spikes in the process.

The bond coat separated from the IN718 substrate, along with the topcoat. The bond coat and the topcoat remain in contact. An oxide also appears to have formed on the bottom of the bond coat. On the top of the bond coat spikes, an intermediate phase appears to have formed. This is explored further in the EDS characterization section that follows. It should also be noted that within the bond coat spikes, in these BSE micrographs, the contrast of the bond coat differs from the sample which has not been cycled. There was a significant contrast difference between TBC, bond coat, and substrate in as-sprayed micrographs, and the absence of that here indicates a possible change in elemental composition sprayed sample. Due to this suspected change in the composition, EDS was completed after the SEM.

EDS map results of the cycled sample, Figure 53, show a chromium layer formed at the bottom of the trenches in between spikes. Point EDS was done on 7 regions within the sample including the TBC, intermediate layer, top of bond coat spikes, bottom of bond coat spikes, top of "oxide", bottom of "oxide", and IN718.

Table 21 includes compositional information from each point. The team assumed that the chromium layer was an oxide since TGOs are expected to grow during thermal cycling. The TBC shows minimal compositional differences compared to the as-sprayed condition. The intermediate phase has significantly less nickel and more aluminum, chromium, cobalt, and oxygen. This suggests that oxygen diffused through the TBC and the intermediate layer has become a complex oxide.

The bond coat was analyzed in two different regions, one close to the interface with the TBC and one close to the interface with the substrate. The bond coat experienced significant compositional changes, including a complete lack of aluminum, increased nickel and iron concentrations. The increased levels of nickel and iron can be explained by diffusion from the IN718 substrate into the bond coat. This can very clearly be seen in Figure 54(a) where there is a clear iron gradient from the substrate into the bond coat showing that the iron was able to diffuse about 2/3 of the way up the spikes. Aluminum segregation, also seen in Figure 54(b) confirms the lack of aluminum in the bulk bond coat, showing regions of aluminum oxide. There are also large compositional differences between the top and bottom of the bond coat. Going up the spike, there is an increase in chromium and cobalt, and decrease in nickel and iron. This is further supported by line scan EDS conducted in Figure 55 and Figure 56, where the nickel and iron concentrations are highest at the bottom of the spikes at the bond coat/substrate interface and decrease going up. The opposite effect is seen in these line scans with cobalt, where concentrations are highest in the center of the spikes and decreases moving towards interfaces with the substrate and with the coatings. This shows that there has been significant diffusion between layers during the thermal cycling process.

An additional line scan EDS was conducted to analyze the chromium rich region, shown in Figure 55 and Figure 56. It was previously asserted that the team expected this to be a chromium oxide, which has been justified by the line scan. In the central region of the line scan that correlates to the suspected oxide, chromium and oxygen are the dominant species, with some regions being richer in chromium. This chromium likely oxidized at the bottom of the spikes, resulting in the chromium deficient region in the adjacent bond coat.

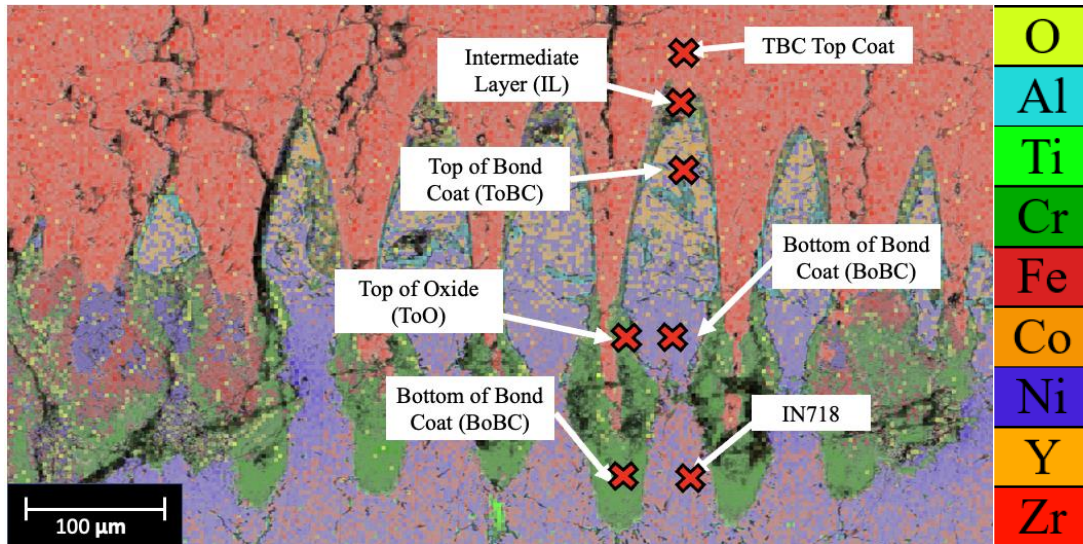


Figure 53: Map and point EDS of thermally cycled rounded spike sample. Map shows distinct chromium-rich region at substrate/bond coat interface and composition gradient in rounded spikes.

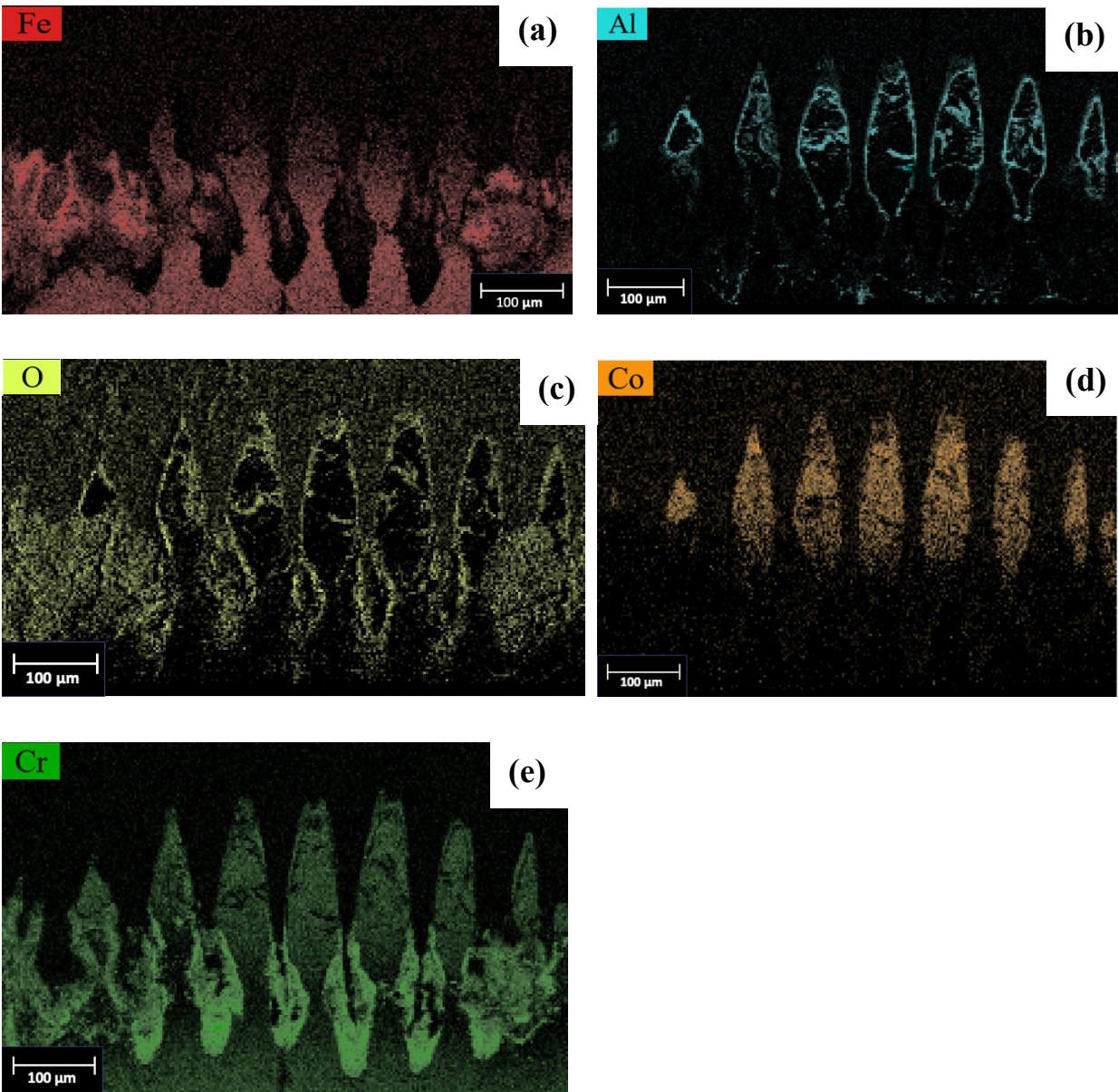


Figure 54: Select EDS maps of thermally cycled rounded spike sample. Shows concentration gradients and segregation within the spikes. (a) Iron, (b) Aluminum, (c) Oxygen, (d) Cobalt, and (e) Chromium.

Table 21: Point EDS results for thermally cycled rounded spike samples. Results shown for 7 regions on the sample.

| Element | Atomic concentration [%] | | | | | | |
|---------|--------------------------|-------|-------|-------|-------|-------|-------|
| | TBC | IL | ToBC | BoBC | ToO | BoO | IN718 |
| O | 44.72 | 33.22 | 0.00 | 0.00 | 33.17 | 8.14 | 0.00 |
| Al | 0.00 | 18.03 | 0.21 | 0.22 | 2.10 | 0.00 | 0.22 |
| Si | 0.00 | 0.81 | 0.00 | 0.00 | 2.74 | 0.00 | 0.00 |
| Cr | 0.00 | 15.44 | 21.76 | 11.24 | 51.97 | 88.15 | 9.97 |
| Mn | 0.00 | 0.00 | 0.00 | 0.00 | 0.66 | 0.82 | 0.00 |
| Fe | 0.00 | 2.77 | 0.82 | 16.00 | 4.42 | 0.00 | 25.39 |
| Co | 0.00 | 9.53 | 24.05 | 8.33 | 0.00 | 0.00 | 0.00 |
| Ni | 0.00 | 19.78 | 53.16 | 61.72 | 1.73 | 0.51 | 61.56 |
| Y | 3.51 | 0.00 | 0.00 | 0.00 | 0.00 | 0.00 | 0.00 |
| Zr | 50.80 | 0.00 | 0.00 | 0.00 | 0.00 | 0.00 | 0.00 |
| Nb | 0.00 | 0.00 | 0.00 | 0.00 | 2.75 | 2.37 | 0.00 |
| Mo | 0.00 | 0.00 | 0.00 | 1.95 | 0.00 | 0.00 | 0.00 |
| Pd | 0.98 | 0.43 | 0.00 | 0.55 | 0.46 | 0.00 | 0.90 |
| Au | 0.00 | 0.00 | 0.00 | 0.00 | 0.00 | 0.00 | 4.90 |

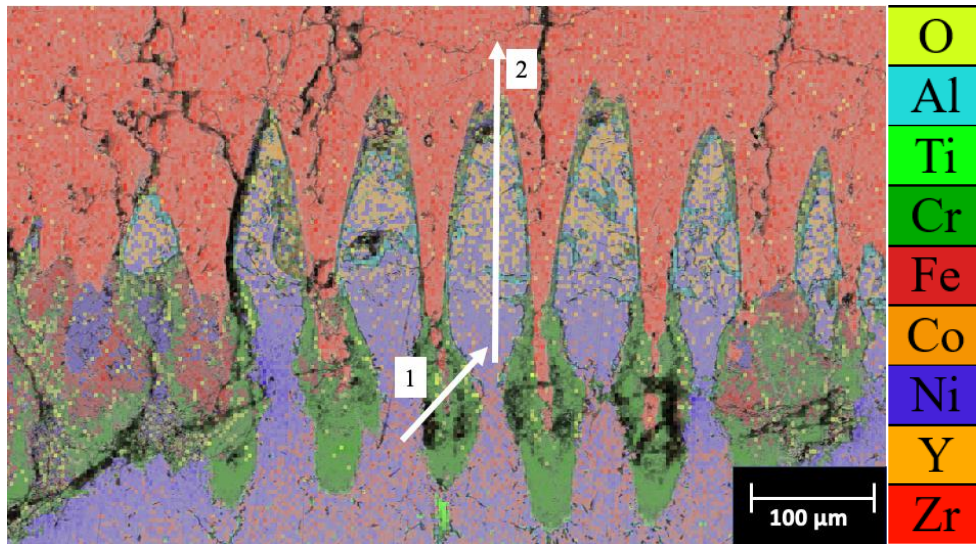


Figure 55: Line scan EDS of thermally cycled rounded spike samples. Line (1) captures chromium rich region and Line (2) captures concentration gradient up the spike.

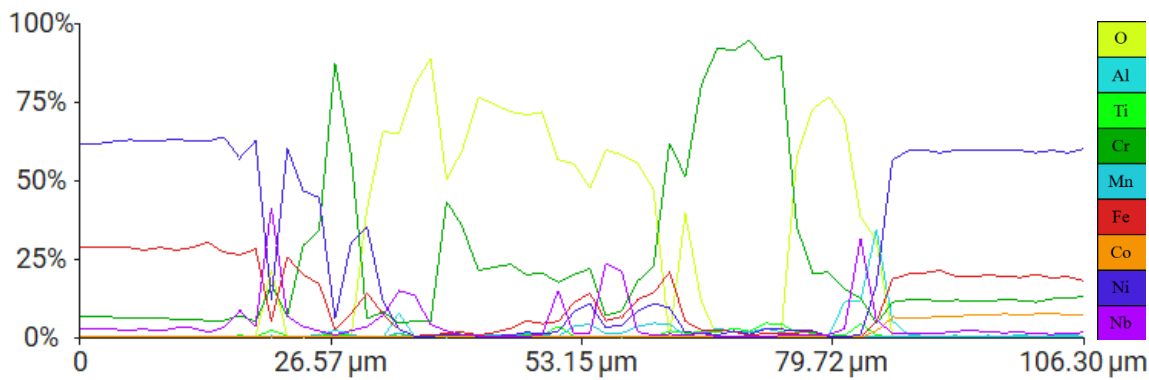


Figure 56: Line scan (1) results showing pure chromium rich region suggestion a chromium oxide.

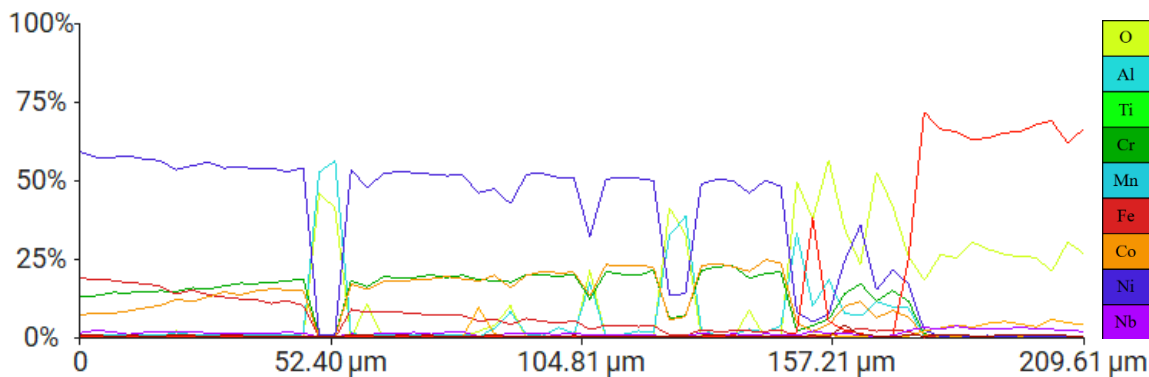


Figure 57: Line scan (2) results. Shows decrease in iron and nickel going up the spike, slight chromium deficiency at the bottom of the spike, and cobalt increase going up the spike.

3. T2

Optical micrographs of the T2 grid pattern surfaces reveal an interesting coating failure geometry. As can be seen in Figure 58(a), the TBC coating failed in 90° along the lines of the grid pattern upon which it was sprayed, Figure 58(b). In the process of spallation there are two failure mechanisms that were noticed. As seen in Figure 58(b,c), there are zones in which the topcoat remains within the trenches between raised grids, indicating a minimal depth of damage to the bond coat. However, as shown in the case of Figure 58(d), there are also cases in which the trenches are not visible, indicating that the bond coat was ripped out of that area or that the spalled top layer took a portion of the bond coat with it. This will be discussed further in the Discussion of Results section.

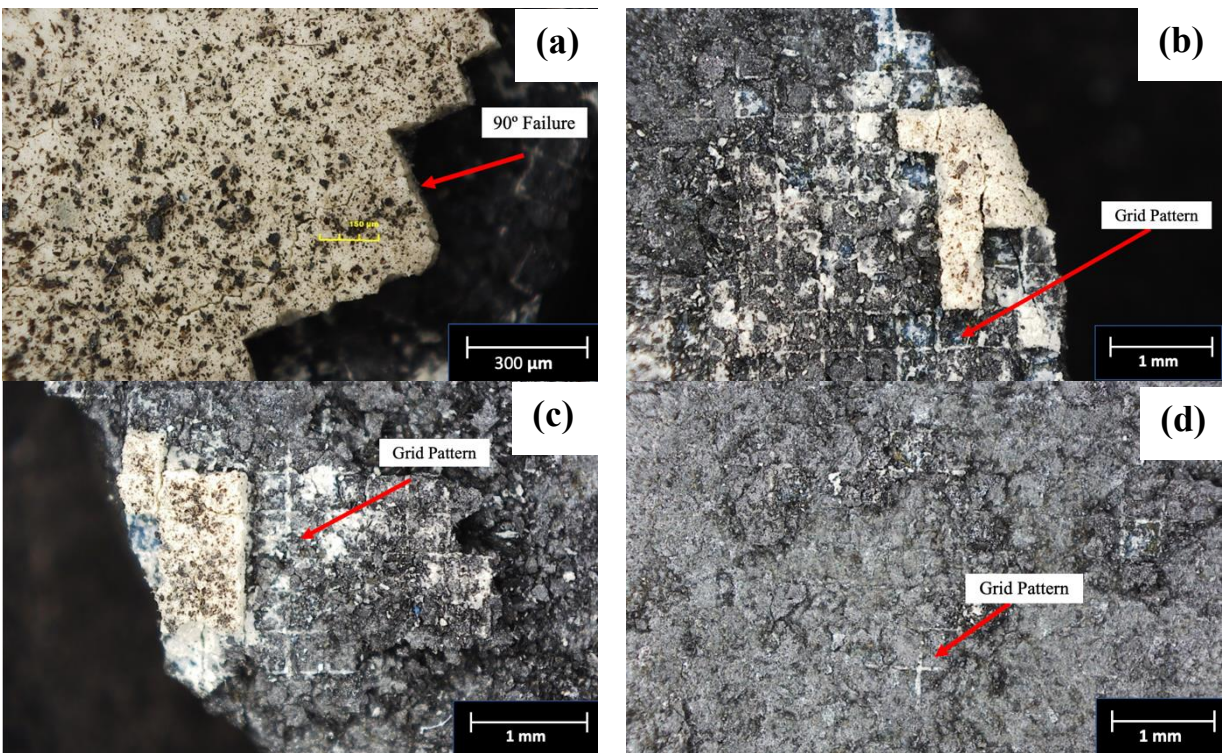


Figure 58: Optical micrographs of T2 sample surfaces after furnace cycling: (a) TBC edge showing zig-zag failure at 150X, (b) grid pattern in bond coat revealed with remaining TBC following this grid payment at 50X, (c) TBC and bond coat failure at 50X, and (d) a substrate surface where the bond coat grid pattern had been destroyed at 35X.

SEM micrographs were taken for the T2 long-furnace-cycled samples and are shown in Figure 59. The TBC had completely delaminated from the sample and most of the bond coat also came off from the substrate, with a few spots showing remaining bond coat. TGO is also observed within the trenches made by the laser when texturing. The DVCs in the delaminated TBC are noticeable and appear regularly spaced, although it is difficult to confirm if this is due to the spacing of the trenches.

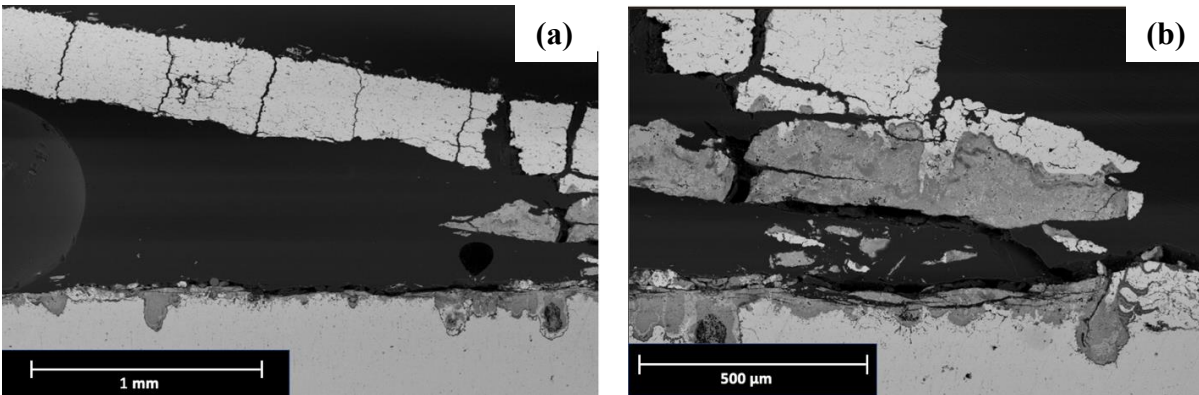


Figure 59: BSE SEM micrographs of the T2 long furnace cycled sample. The TBC completely delaminated, and the bond coat appears to have remained partially on the substrate.

EDS on cycled T2 samples revealed no residual TBC on the surface. Remaining on the sample was the substrate, some bond coat with two different oxidized regions, and dark regions within the substrate, similar to what was seen in previously characterized cycled samples. The top layer of remaining bond coat did not have the same composition as the uncycled bond coat layer, with the cycled being richer in iron and oxygen and less rich in nickel, indicating that there was diffusion between the substrate and bond coat that affected this region. At the bottom of this region is chromium oxide between the substrate and oxidized bond coat. The dark layers in the substrate were found to be aluminum oxide, which has been previously seen in cycled samples. Figure 61 shows individual EDS maps highlighting the notable regions.

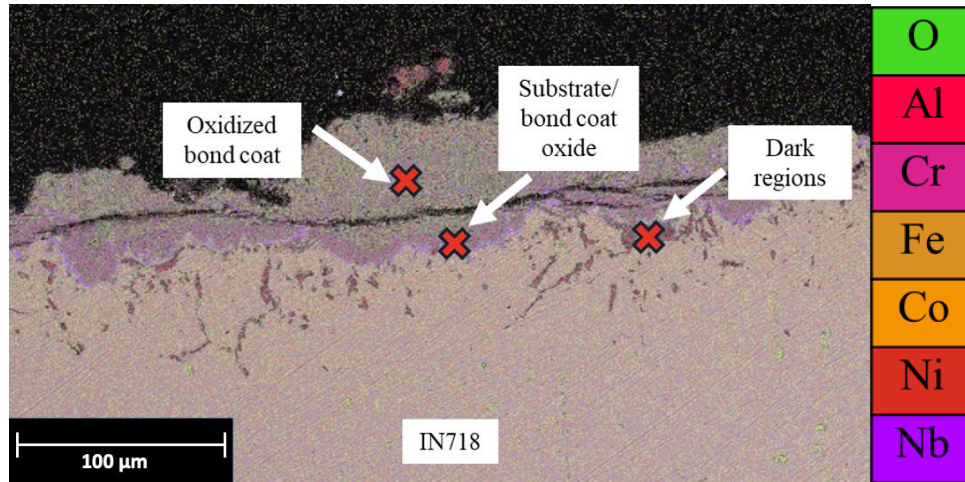


Figure 60: EDS of cycled T2 sample. Shows oxidized bond coat, substrate/bond coat oxide, dark regions within the substrate, and IN718.

Table 22: Compositional results for EDS on cycled T2 sample. Compositions given in atomic concentration (%).

| Element | Atomic Concentration [%] | | |
|---------|--------------------------|---------------------------|--------------|
| | Oxidized bond coat | Substrate/bond coat oxide | Dark regions |
| O | 26.06 | 26.24 | 39.35 |
| Al | 7.41 | 3.30 | 50.49 |
| Cr | 23.88 | 67.20 | 8.61 |
| Fe | 18.12 | 1.44 | 0.00 |
| Co | 4.27 | 0.00 | 0.00 |
| Ni | 19.61 | 1.01 | 1.13 |

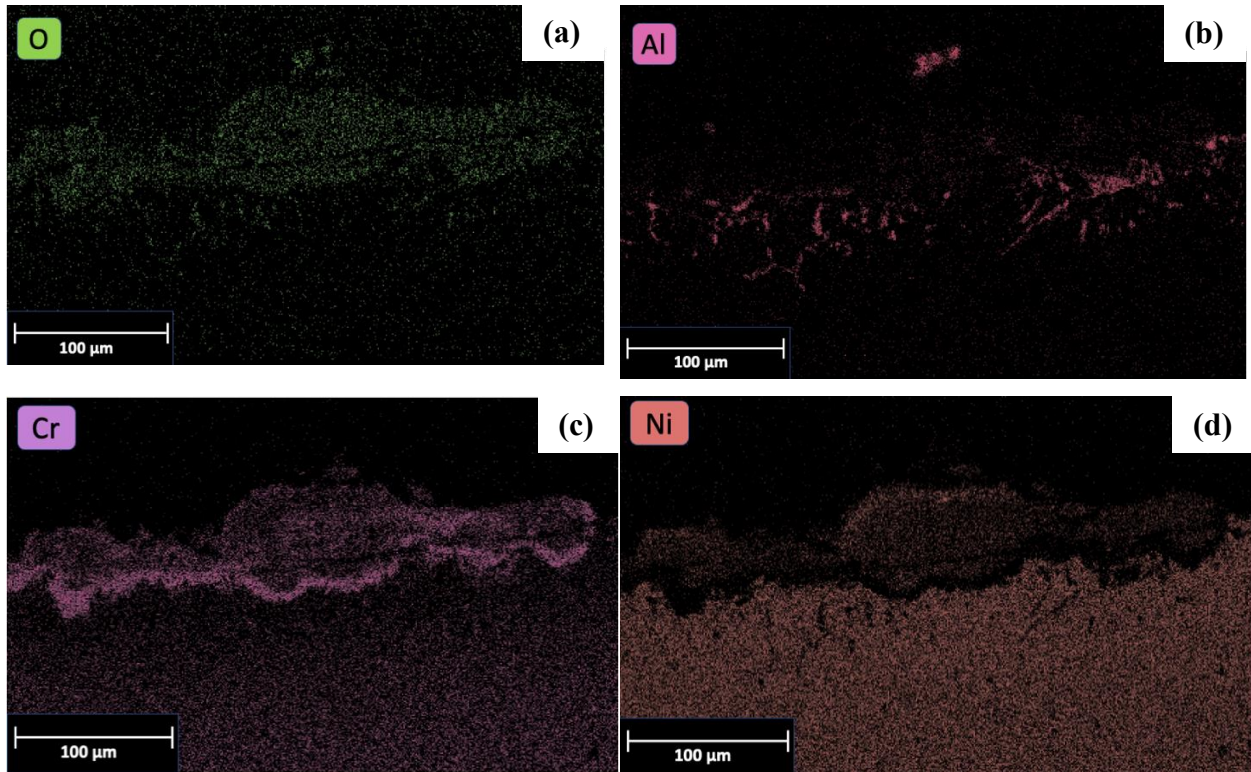


Figure 61: Cycled T2 map EDS separated by element. (a) Oxygen, (b) Aluminum, (c) Chromium, and (d) Nickel. Highlights oxidized bond coat, chromium oxide at substrate/bond coat interface, and aluminum oxide within the substrate.

4. T3

Optical micrographs of the T3, grown texture, surfaces reveal some interesting crack patterns. As shown in Figure 62(b,c), the cracks appear to follow a jagged hexagonal geometry, although the reasons for this are not understood. Figure 62(a) also shows some chips in the TBC on the edge of the samples. The substrate surface after coating failure can be seen in Figure 62(d).

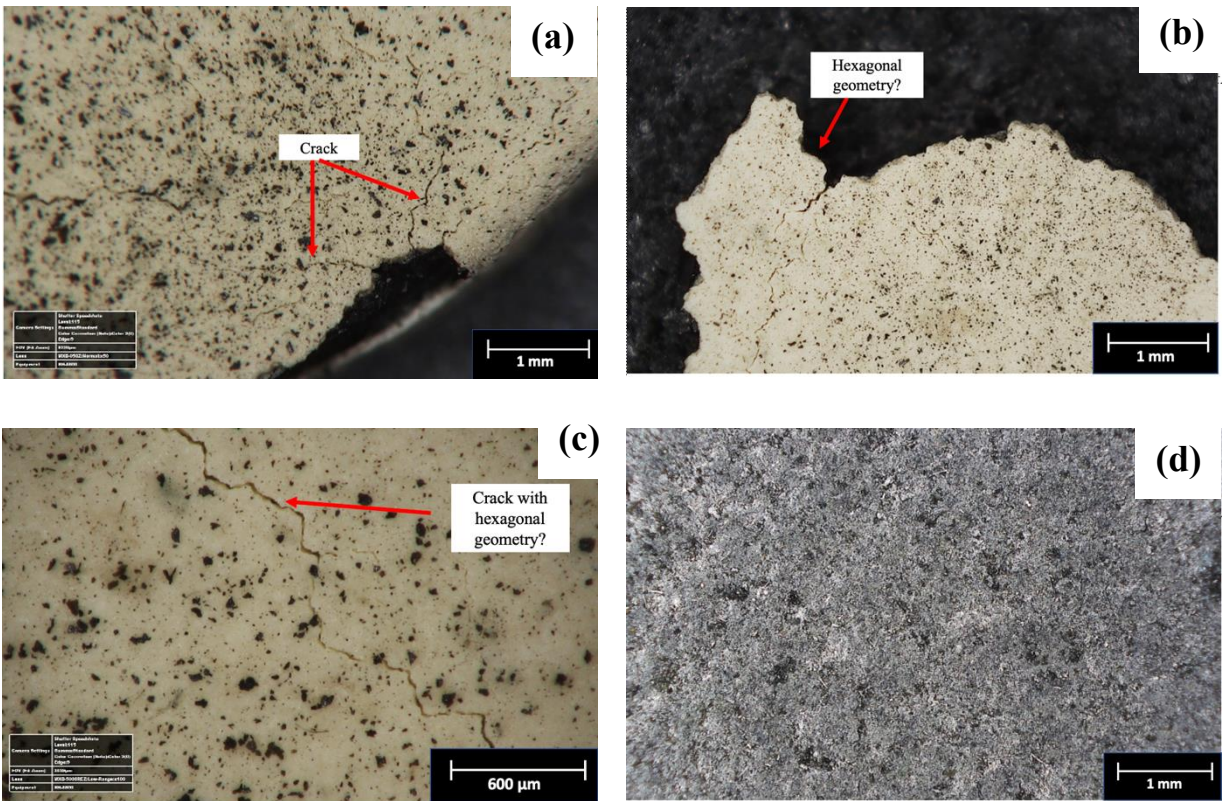


Figure 62: Optical micrographs of T3 sample surfaces after furnace cycling: (a) cracks around an area where a piece of TBC chipped off at 50X, (b) edge of TBC peeling off substrate at 50X, (c) crack geometry in TBC at 100X, and (d) base metal that TBC has come off from at 50X.

The SEM micrographs of the T3 sample provide information on the failure mechanism. The topcoat, along with most of the bond coat intact, completely delaminated from the IN718 substrate. DVCs and large cracks formed in the topcoat, wider than the DVCs in the sample that have not been furnace cycled. Since the T3 texture does not have the same uniformity as the rounded spikes in T1, the DVCs do not follow uniform spacing as they do in T1.

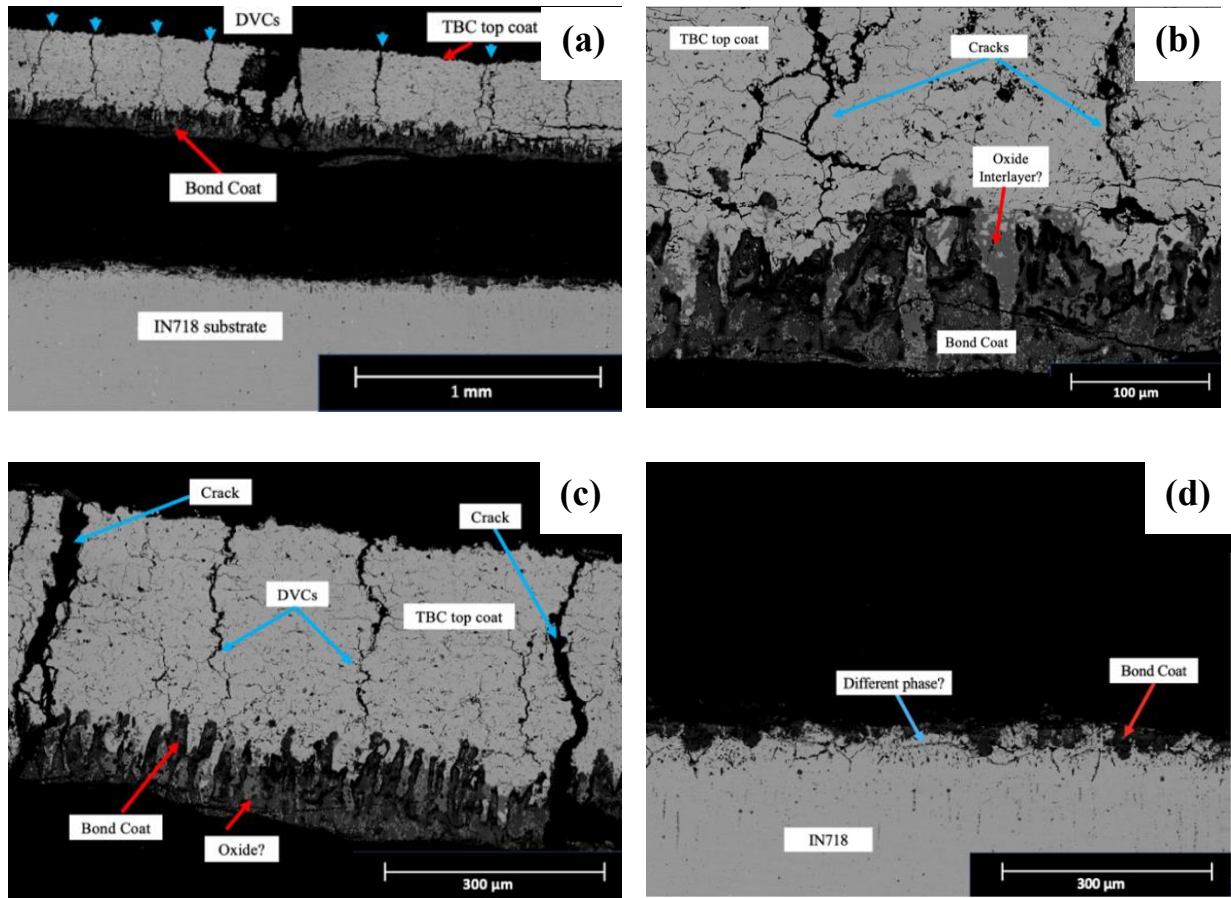


Figure 63: BSE SEM micrographs of T3 sample after furnace cycling. The delaminated topcoat/bond coat from the substrate can be observed along with the DVCs and an unknown interlayer.

Further analysis of the failed coating was done with the help of EDS. The EDS map, Figure 64, exhibits significant segregation. There are three visible regions within the spalled coating: (1) TBC, (2) lighter bond coat, and (3) darker bond coat. Point EDS was done on these regions, plus a darker region to confirm that it was porosity within the coating. The lighter region was consistent with the bond coat including oxygen diffusion, while the darker region tended to be aluminum and oxygen rich, suggesting an aluminum oxide. Individual EDS maps verifying this hypothesis are seen in **Error! Reference source not found.** The TBC did not exhibit any notable compositional changes. Since there was total delamination of the coating, it was also important to analyze the substrate for any remaining bond coat. Results of this EDS are shown in Figure 66 and Table 24. Initial inspection suggested that there was some remaining bond coat on

the surface, however EDS disproved this. The darker region was revealed to be chromium and oxygen rich (Figure 67). Furthermore, at the top of the substrate, the team observed a dark phase that looked like cracks, but EDS showed them to be aluminum rich regions. It is theorized that these are regions of aluminum oxide along the substrate grain boundaries that formed when oxygen diffusion reached the substrate.

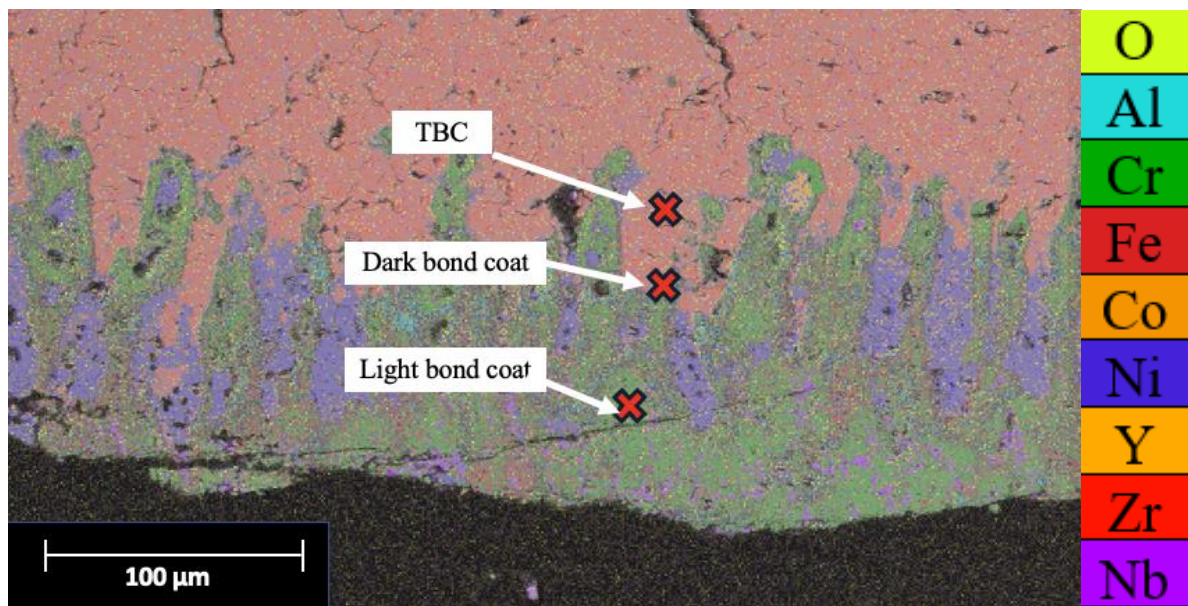


Figure 64: EDS map of spalled off coating. Shows 2 distinct regions within the bond coat, including an aluminum rich region.

Table 23: Point EDS for T3 cycled coating

| Element | Atomic concentration [%] | | |
|---------|--------------------------|-----------------|----------------|
| | TBC | Light bond coat | Dark bond coat |
| O | 51.15 | 25.88 | 33.06 |
| Al | 0.00 | 11.67 | 36.44 |
| Ti | 0.00 | 0.54 | 0.00 |
| Cr | 0.00 | 28.12 | 7.47 |
| Fe | 0.00 | 3.94 | 0.00 |
| Co | 0.00 | 13.03 | 12.02 |
| Ni | 0.72 | 13.89 | 11.01 |
| Y | 2.85 | 1.16 | 0.00 |
| Zr | 44.92 | 0.00 | 0.00 |
| Hf | 0.35 | 0.00 | 0.00 |
| Nb | 0.00 | 1.76 | 0.00 |

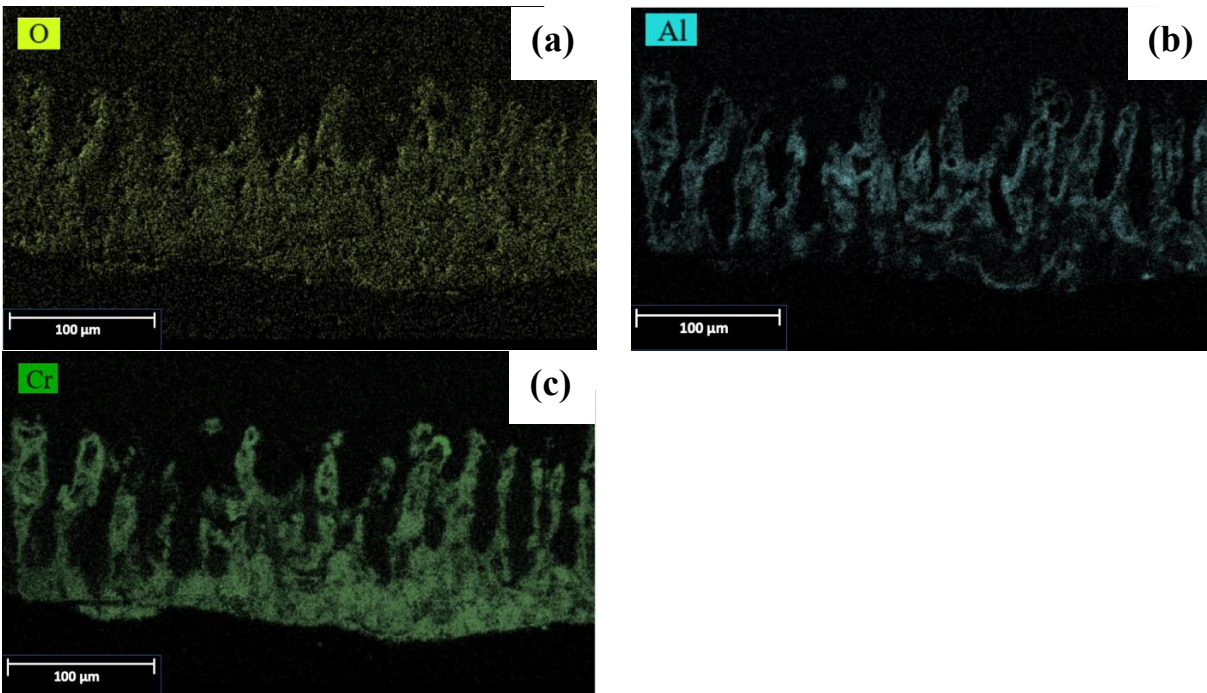


Figure 65: Individual EDS maps of T3 coating. (a) Oxygen, (b) Aluminum, and (c) Chromium.

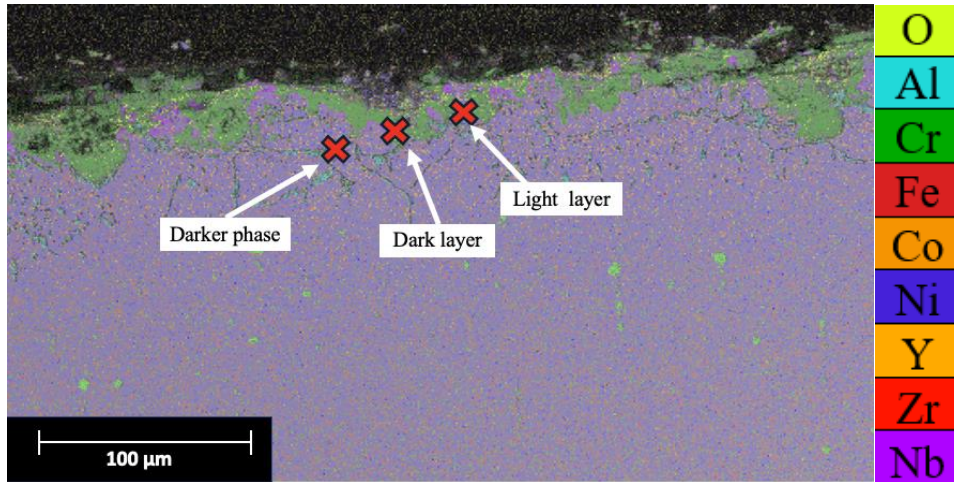


Figure 66: Substrate/bond coat interface EDS map for T3. Shows chromium remnants on surface after complete delamination.

Table 24: Point EDS for bond coat/substrate interface on failed T3 sample.

| Element | Atomic concentration [%] | | |
|---------|--------------------------|------------|------------|
| | Light layer | Dark layer | Dark phase |
| C | 9.50 | 0.00 | 0.00 |
| O | 5.84 | 22.78 | 35.65 |
| Al | 1.73 | 2.12 | 62.13 |
| Ti | 0.00 | 0.73 | 0.99 |
| Cr | 5.89 | 68.41 | 0.46 |
| Mn | 0.00 | 0.80 | 0.00 |
| Fe | 15.51 | 1.02 | 0.00 |
| Co | 7.92 | 0.00 | 0.00 |
| Ni | 49.86 | 3.14 | 0.49 |
| Nb | 3.74 | 0.99 | 0.00 |
| Pd | 0.00 | 0.00 | 0.29 |

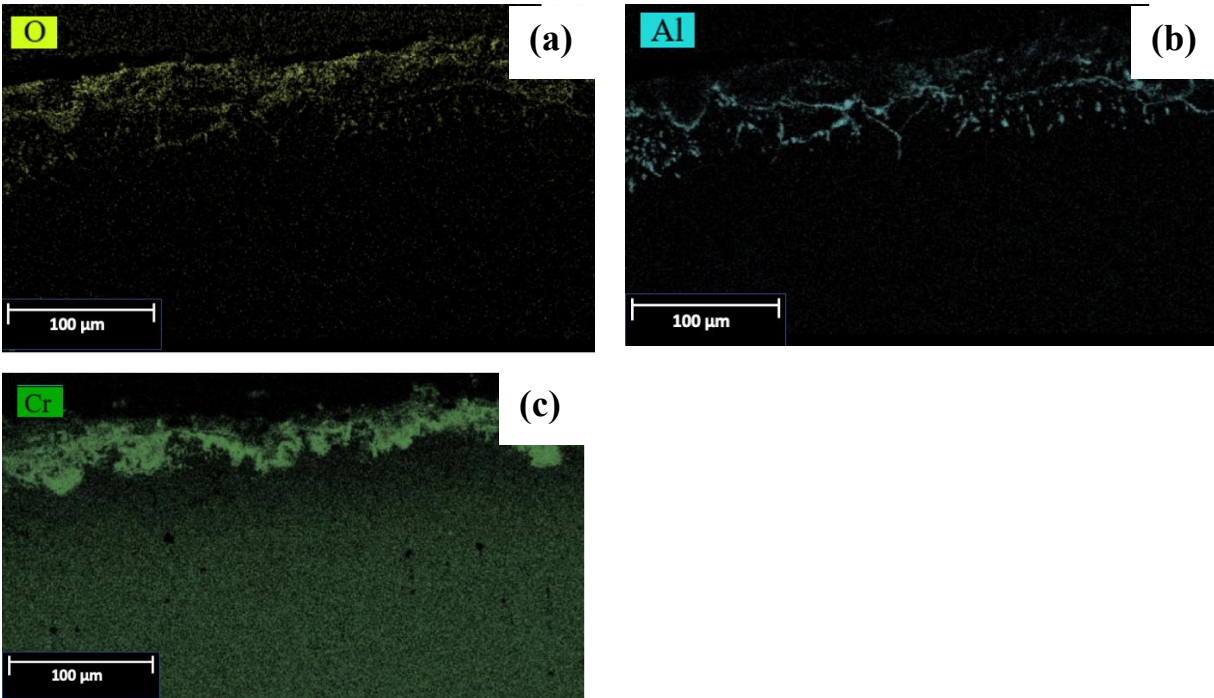


Figure 67: Individual EDS maps of T3 substrate. (a) Oxygen, (b) Aluminum, and (c) Chromium.

G. Accelerated Thermal Cycling Results

Samples were positioned in the same manner as the previous thermal cycling tests; columns 1 and 2 were cycled in furnace 2 and columns 3 and 4 were cycled in furnace 1. Based on previous thermal cycling results, it was verified that the two different furnaces were not significantly affecting results, as failure was occurring at roughly the same number of cycles for samples of the same texture being cycled in different furnaces.

- Row 1: GB, or grit blasted samples
- Row 2: T1, or rounded spike texture
- Row 3: T2, or grid texture
- Row 4: T3, or grown texture

Samples were photographed after each of the 4 accelerated thermal cycles. Overall, none of the samples experienced spallation or failure after the completion of the series of accelerated thermal cycles. Slight burning on the surface of a GB sample was noted after 3 cycles—see Figure

68(a)—but this did not seem to be significant and was likely due to debris on the surface of the coating rather than the coating itself.

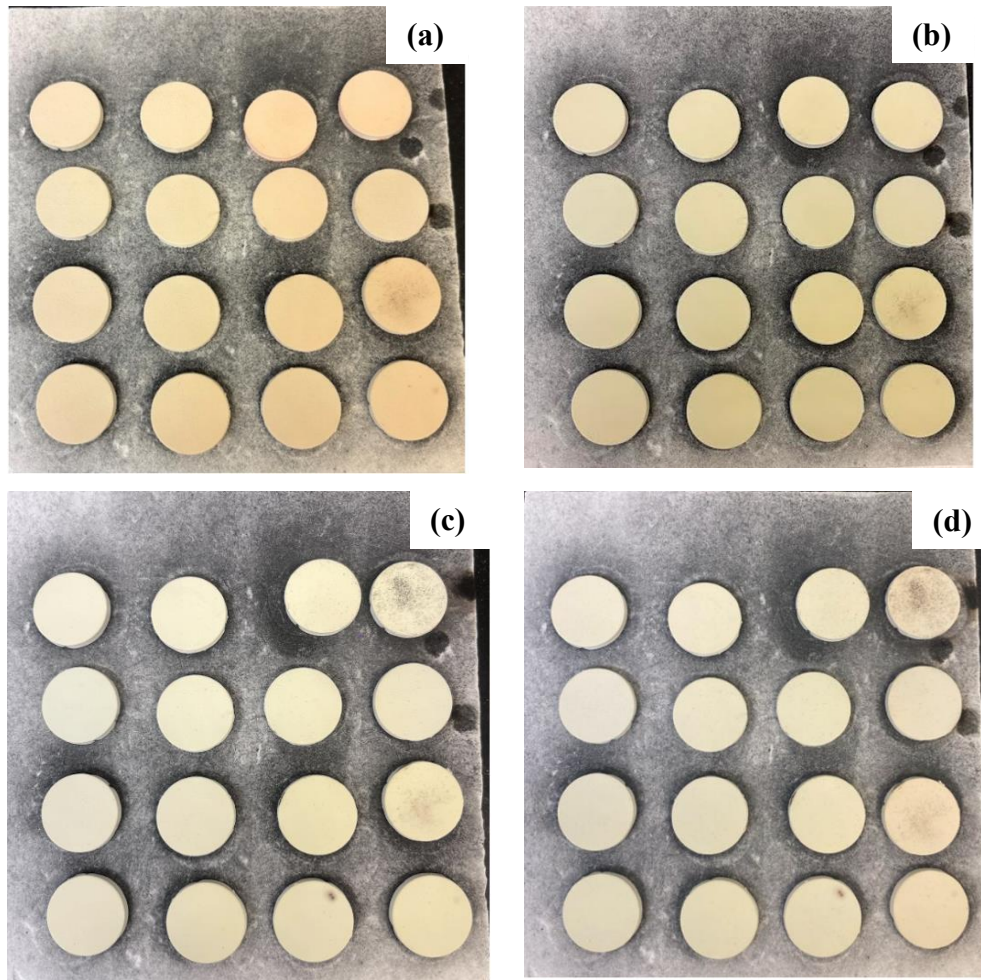


Figure 68: (a) Samples after one accelerated thermal cycle, first column retired. (b) Samples after two accelerated cycles, second column retired. (c) Samples after 3 accelerated thermal cycles, third column retired. At this point, some burning of the GB sample in the 4th column was observed. (d) Samples after 4 accelerated thermal cycles. No failure or spallation can be seen after the completion of the accelerated thermal cycling.

Due to a lack of spallation or failure, characterization began with the samples that had undergone 4 accelerated thermal cycles. After the accelerated thermal cycling, all four of the 4-cycle samples were mounted, sectioned, ground, and polished for characterization.

1. Grit Blasted

Upon initial visual inspection, the GB sample which underwent 4 short furnace cycles did not appear to experience spallation to significant coating damage. Once cross-sectioned and examined using the SEM, a TGO was shown to have started forming on the bond coat/TBC interface as shown in Figure 69. The DVCs appear to follow a random pattern as predicted.

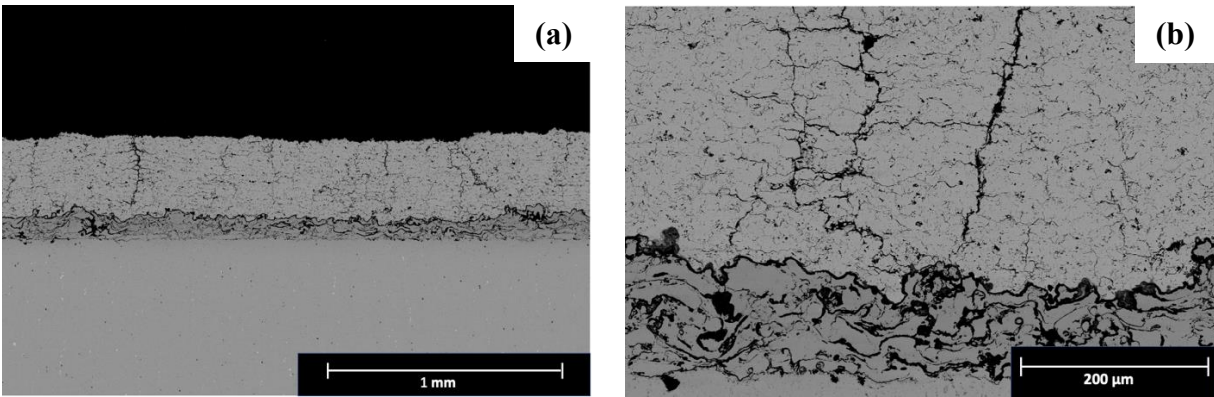
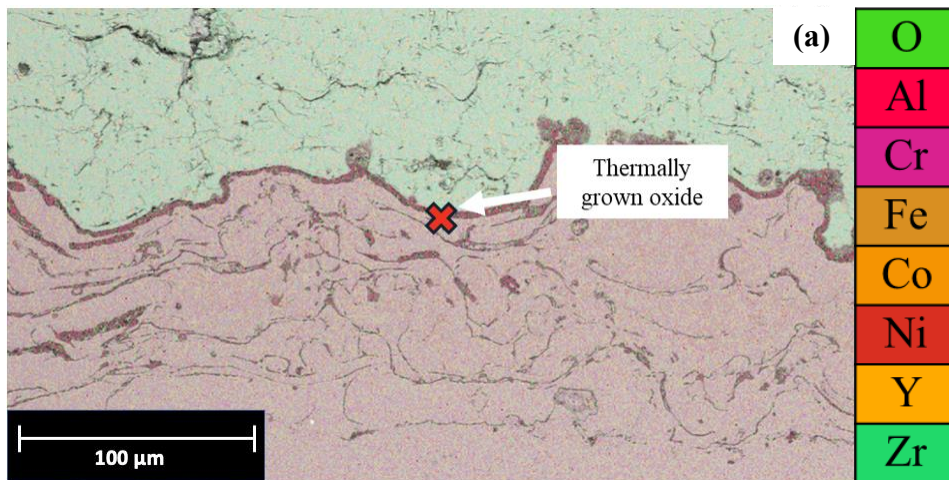


Figure 69: BSE SEM for the GB sample undergone 4 short furnace cycles. The TGO has started growing between the bond coat/TBC interface.

EDS completed on the grit blast sample after 4 cycles is displayed in Figure 70 and Table 25. These results very clearly identify the TGO at the TBC/bond coat interface as an aluminum oxide originating from aluminum within the bond coat.



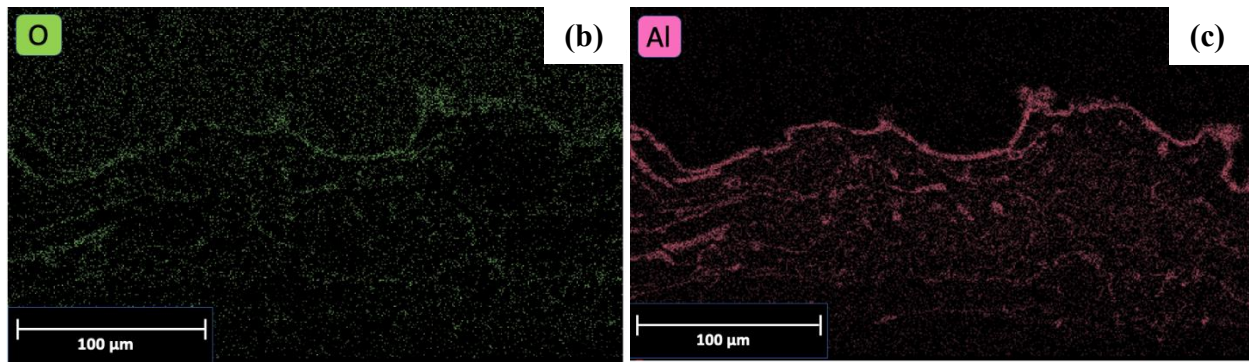


Figure 70: EDS of grit blast sample after 4 cycles. Shows early formation of aluminum oxide at TBC/bond coat interface. (a) Full EDS map, (b) Oxygen map, and (c) Aluminum map.

Table 25: Compositional results for EDS on grit blast sample after 4 cycles. Compositions given in atomic concentration (%).

| Element | Atomic Concentration [%] |
|---------|--------------------------|
| | TGO |
| O | 45.86 |
| Al | 51.17 |
| Cr | 0.97 |
| Ni | 1.41 |
| Zr | 0.58 |

2. T1

Upon initial visual inspection, the T1 sample which underwent 4 short furnace cycles did not appear to experience spallation to significant coating damage. Once cross-sectioned and examined using the SEM, a TGO was shown to have started forming in the spaces between the rounded spikes deep into the substrate as shown in Figure 71. This is consistent with the TGO observed for the T1 samples subject to long furnace cycling. A darker layer surrounding the spikes at the bond coat/TBC interface suggests the presence of another TGO, which was further investigated with EDS. The bond coat also appears to have changed composition as the contrast

between the bond coat and substrate is no longer apparent. The DVCs appear to follow a random pattern, unlike the DVC pattern observed for the T1 samples for the long furnace cycling.

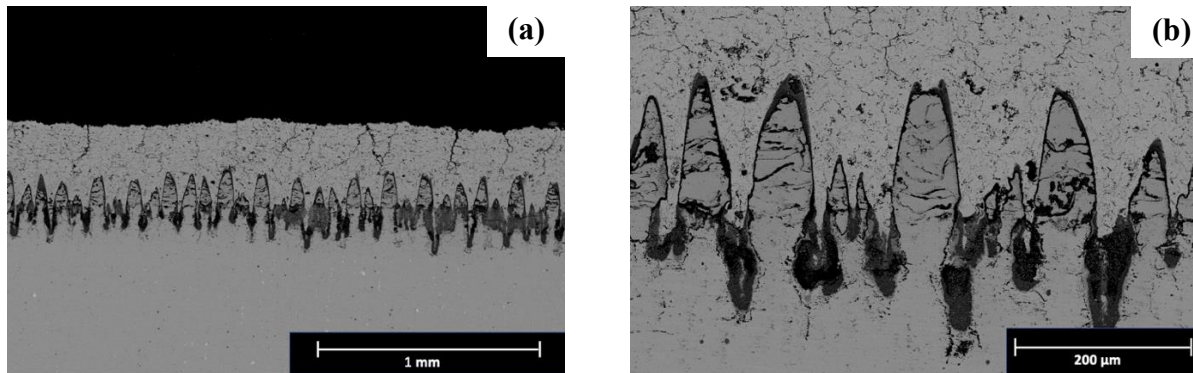


Figure 71: BSE SEM for the T1 sample subjected to 4 short furnace cycles. TGO appears to have grown in between the rounded spikes deep into the substrate along the bond coat/TBC interface.

EDS on T1 accelerated cycling is shown below in Figure 72 and Table 26

Table 26 and displays a far more complex oxidation pattern than the grit blast samples. There is a lighter TGO that sits in between the top of the textured spikes and the underlying bond coat, completely separating it in two. EDS shows this region to have higher iron and chromium concentrations, with the iron decisively coming from the substrate. The dark TGO is found between rounded spikes and are rich in chromium. A chromium deficient region in the substrate surrounding the TGO suggests that the chromium originated from the substrate and not the bond coat. As was seen in the samples cycled to failure (see Thermal Cycling Results and Characterization), oxides at the substrate/bond coat interface cut off the top of the bond coat spikes, leading to failure. However, these results indicate that the oxide formed at the TBC/bond coat interface and not at the substrate. Additionally, Figure 72(c) shows an EDS map of aluminum to be used in comparison with findings from the grit blast samples. While it seems there is a small layer of aluminum oxide covering the bond coat spikes, likely the same oxide seen at the TBC/bond coat substrate in grit blast samples, this is clearly overpowered by the chromium and iron oxides present, resulting in the premature failure previously recorded. Given that these elements originated from the substrate, the team concluded that direct exposure of the substrate to the TBC is catastrophic for thermal performance.

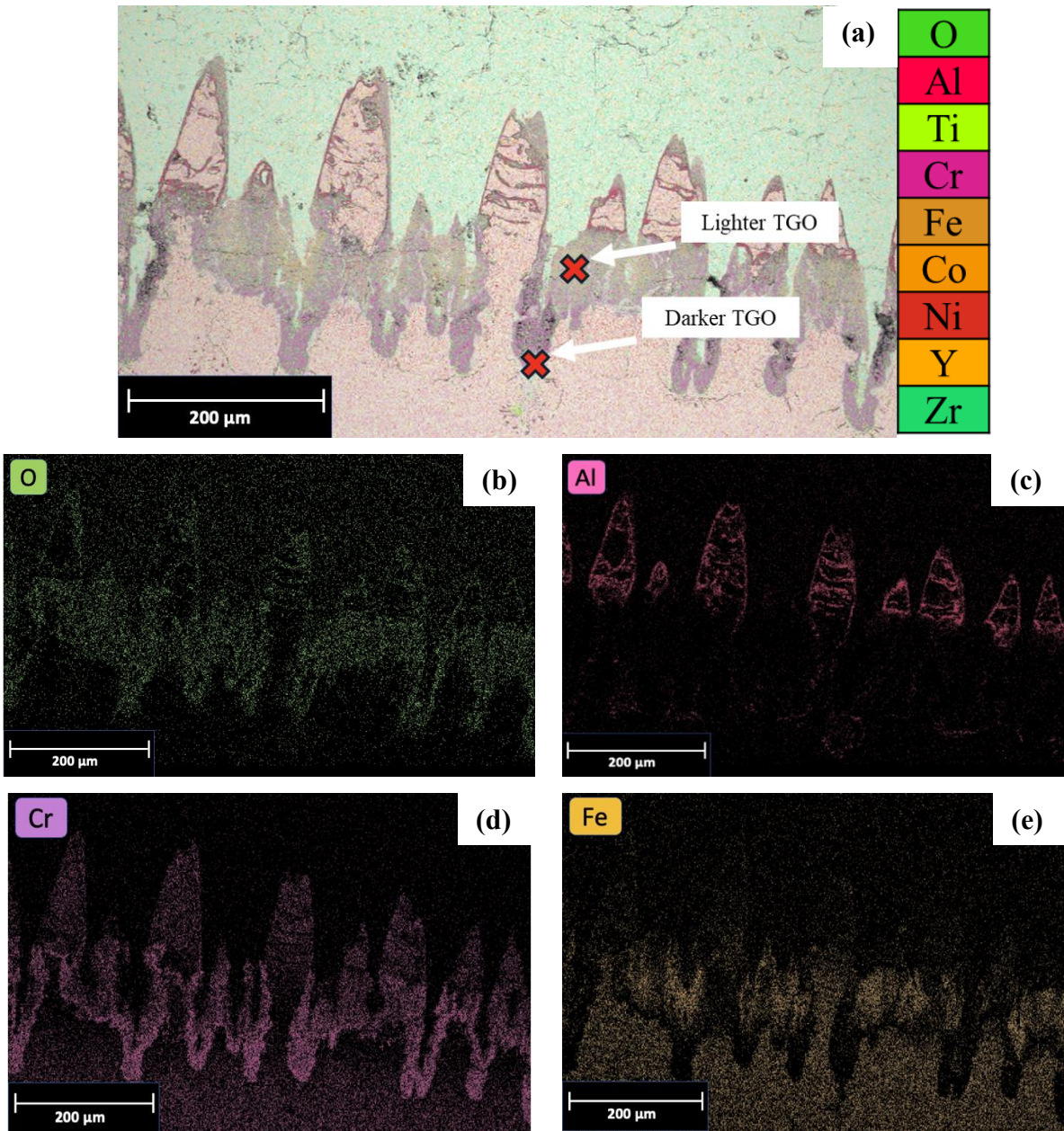


Figure 72: EDS of T1 after 4 cycles. Shows early formation of aluminum, chromium, and iron oxides at different interfaces within the coating system. (a) Full EDS map, (b) Oxygen map, (c) Aluminum map, (d) Chromium map, and (e) Iron map.

Table 26: Compositional results for EDS on T1 after 4 cycles. Compositions given in atomic concentration (%).

| Element | Atomic Concentration [%] | |
|---------|--------------------------|------------|
| | Lighter TGO | Darker TGO |
| O | 40.58 | 41.70 |
| Al | 0.74 | 0.00 |
| Cr | 2.92 | 57.84 |
| Fe | 37.89 | 0.00 |
| Ni | 18.20 | 0.46 |

3. T2

Upon initial visual inspection, the T2 sample which underwent 4 accelerated furnace cycles did not appear to experience spallation to significant coating damage. Once cross-sectioned and examined using the SEM, a TGO was observed at interface between the bond coat and the TBC, the composition of which was identified with EDS. Some TGO is also observed to have formed in the trenches at the interface with the substrate. DVCs appear to follow a very uniform pattern, falling in line with the preplanned grid “trenches” formed by the laser.

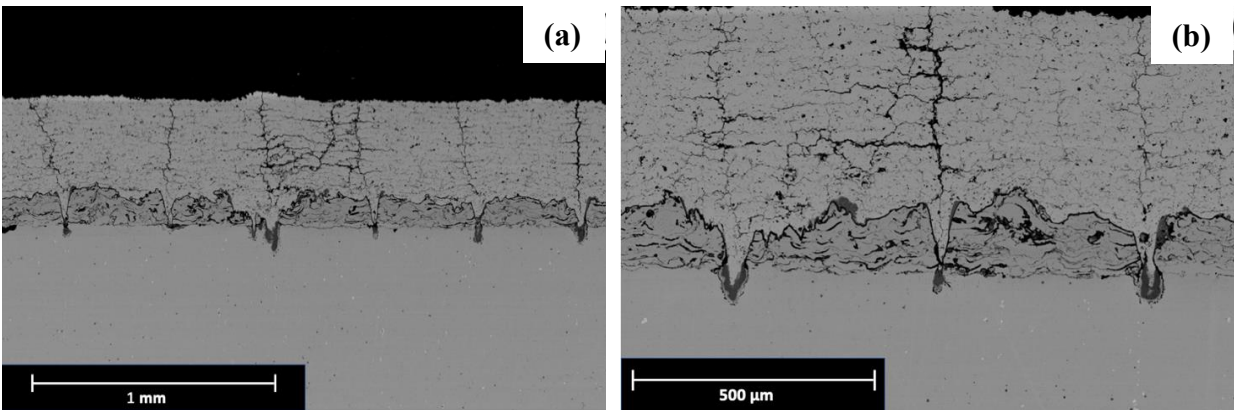


Figure 73: BSE SEM for the T2 sample subjected to 4 short furnace cycles. TGO appears to have grown in the trenches where the TBC is in contact with the substrate and in the interface between the bond coat and the TBC.

EDS of T2 after 4 short thermal cycles is seen below in Figure 74 and Table 27. Results show a thin layer of aluminum oxide formed at the interface between the bond coat and the TBC. Furthermore, the region between trenches preferentially formed chromium oxide, but there is a small layer of aluminum oxide that surrounds the chromium oxide. Both oxides can be clearly seen in individual EDS maps in Figure 74. A chromium deficient region in the substrate surrounding the chromium oxide is observed, similar to that seen in T1, suggesting that the chromium originated from the substrate.

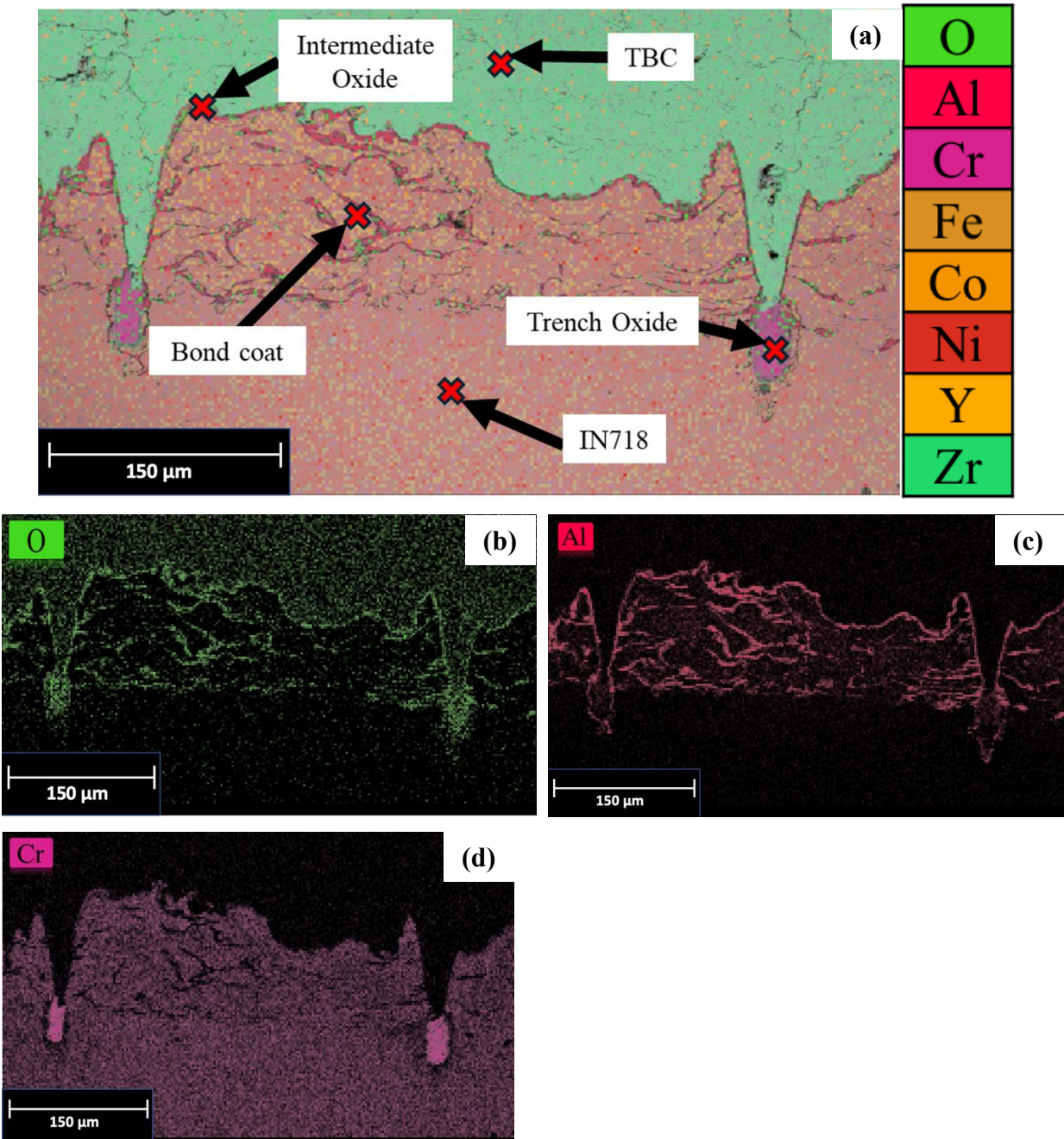


Figure 74: EDS of T2 after 4 cycles. Shows early formation of aluminum and chromium oxides at different interfaces within the coating system. (a) Full EDS map, (b) Oxygen map, (c) Aluminum map, and (d) Chromium map.

Table 27: Compositional results for EDS on T2 after 4 cycles. Compositions given in atomic concentration (%).

| Element | Atomic Concentration [%] | | | | |
|---------|--------------------------|--------------|-----------|--------------------|-------|
| | IN718 | Trench Oxide | Bond coat | Intermediate Oxide | TBC |
| O | 0.00 | 37.61 | 0.00 | 35.50 | 56.26 |
| Al | 2.56 | 15.83 | 12.62 | 16.54 | 0.00 |
| Ti | 0.84 | 1.17 | 0.00 | 0.00 | 0.00 |
| Cr | 21.47 | 45.02 | 19.53 | 13.93 | 0.00 |
| Fe | 20.71 | 0.00 | 0.00 | 1.71 | 0.00 |
| Co | 0.00 | 0.00 | 0.00 | 9.83 | 0.00 |
| Ni | 49.52 | 0.00 | 44.18 | 22.02 | 0.00 |
| Y | 0.00 | 0.00 | 1.40 | 0.00 | 3.56 |
| Zr | 0.00 | 0.00 | 0.00 | 0.00 | 39.14 |
| Nb | 4.89 | 0.00 | 0.00 | 0.00 | 0.00 |

4. T3

Upon initial visual inspection, the T3 sample which underwent 4 accelerated furnace cycles did not appear to experience spallation to significant coating damage. Once cross-sectioned and examined using the SEM, a TGO was observed at interface between the bond coat and the TBC, which was confirmed with EDS. The DVCs appear to follow a random pattern as observed for the T3 cycle which underwent long furnace cycling

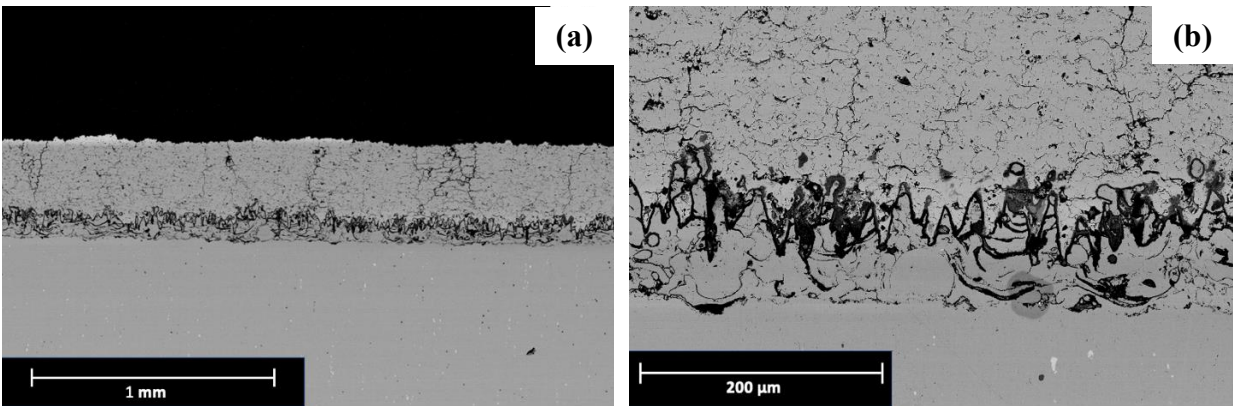


Figure 75: BSE SEM for the T3 sample subjected to 4 short furnace cycles. TGO appears to have grown on the interface between the bond coat and the TBC.

Following SEM, EDS was conducted on the accelerated cycle samples, shown below in Figure 76 and Table 28. These results show the growth of a lighter oxide and a darker oxide. The darker oxide is the preferred aluminum oxide, while the lighter oxide is rich in nickel and aluminum, suggesting early oxidation of the bond coat.

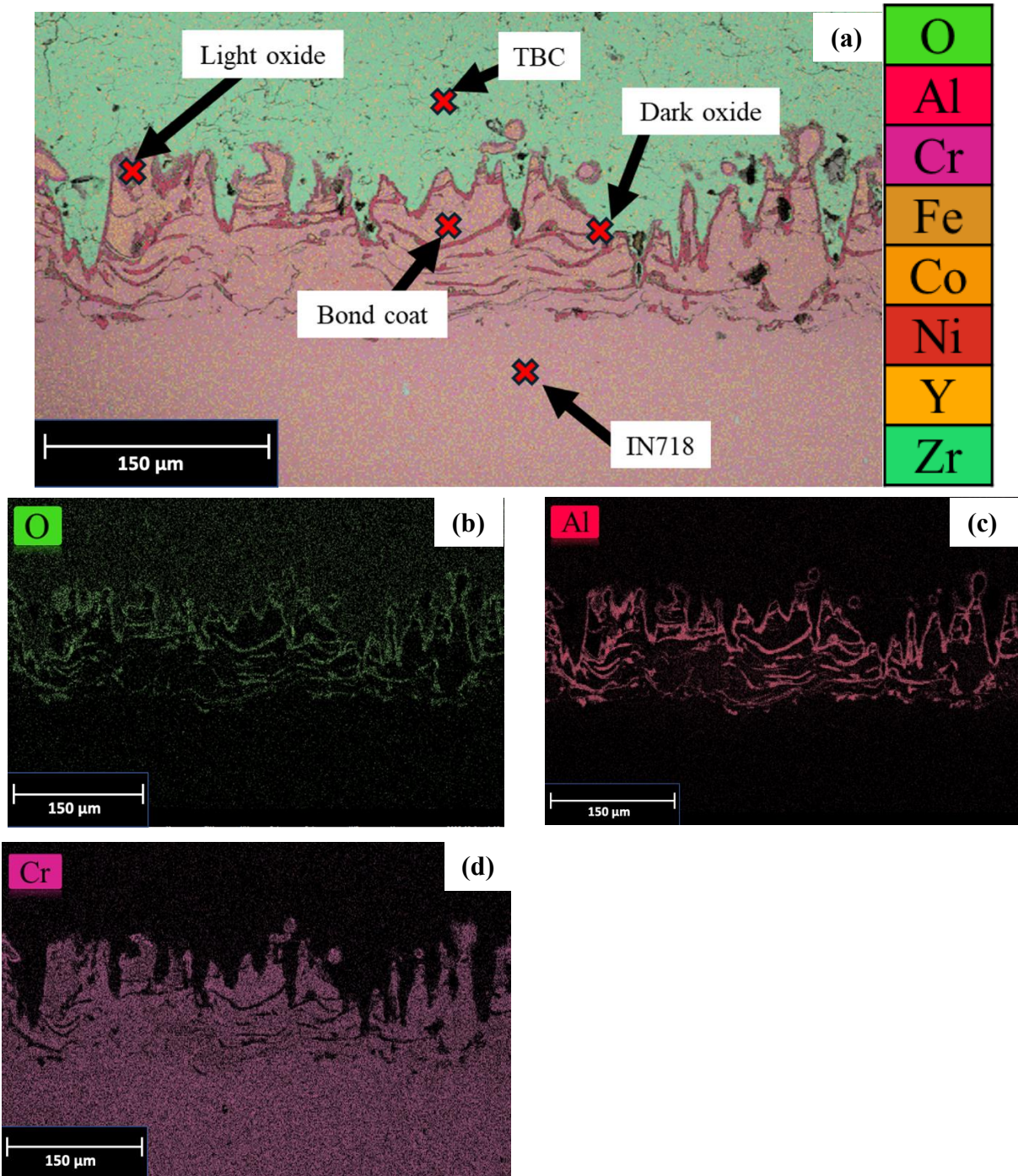


Figure 76: EDS of T3 after 4 cycles. Shows early formation of aluminum and chromium oxides at different interfaces within the coating system. (a) Full EDS map, (b) Oxygen map, (c) Aluminum map, (d) Chromium map.

Table 28: Compositional results for EDS on T3 after 4 cycles. Compositions given in atomic concentration (%).

| Element | Atomic concentration [%] | | | | |
|---------|--------------------------|-------------|-----------|------------|-------|
| | IN718 | Light oxide | Bond coat | Dark Oxide | TBC |
| O | 0.00 | 38.72 | 0.00 | 48.82 | 50.20 |
| Al | 2.56 | 21.26 | 7.51 | 47.90 | 0.00 |
| Ti | 0.84 | 0.00 | 0.00 | 0.00 | 0.00 |
| Cr | 21.37 | 5.38 | 21.19 | 0.68 | 0.00 |
| Fe | 20.62 | 0.00 | 0.00 | 0.00 | 0.00 |
| Co | 0.00 | 8.83 | 24.14 | 0.60 | 0.00 |
| Ni | 49.26 | 25.81 | 46.85 | 0.80 | 0.00 |
| Y | 0.00 | 0.00 | 0.32 | 0.66 | 4.79 |
| Zr | 0.00 | 0.00 | 0.00 | 0.00 | 43.25 |
| Nb | 5.02 | 0.00 | 0.00 | 0.00 | 0.00 |

H. Adhesion Testing Results

The team sent 12 samples to Rolls-Royce for adhesion testing. All coated samples were found to have failed at significantly lower stresses, eliminating the possibility of failure within the glue. Thus, all tested samples failed somewhere in the coating system.

Table 29: Tabulated bond strength results (psi) from adhesion testing. Largest and smallest reported values in green and red, respectively.

| | GB | T1 | T2 | T3 |
|---------|------|------|------|------|
| 1 | 3200 | 5000 | 3200 | 4800 |
| 2 | 3300 | 4900 | 5000 | 6000 |
| 3 | 3700 | 5800 | 4900 | 5500 |
| Average | 3400 | 5200 | 4400 | 5400 |
| Spread | 500 | 900 | 1800 | 1200 |

The data indicates that the textured samples generally perform better than the GB (baseline) samples. Bond strengths measured were highly variable, which was anticipated in discussions with Rolls-Royce. Variability can originate from adhesive application and defects within the designed coating system. Textured samples, specifically T2, exhibited the same minimum as GB samples, emphasizing the need for sufficient trials in the future to offer statistical significance and outweigh outliers. This work did not have the capability of testing more samples, which should be considered in future work to draw stronger conclusions.

Micrographs in Figure 77 show that T1 had the most homogeneous fracture surface that propagates through the TBC, while the other samples have regions show failure through the bond coat and the TBC. The optical microscopy that follows helped the team discern the nature of the failure.

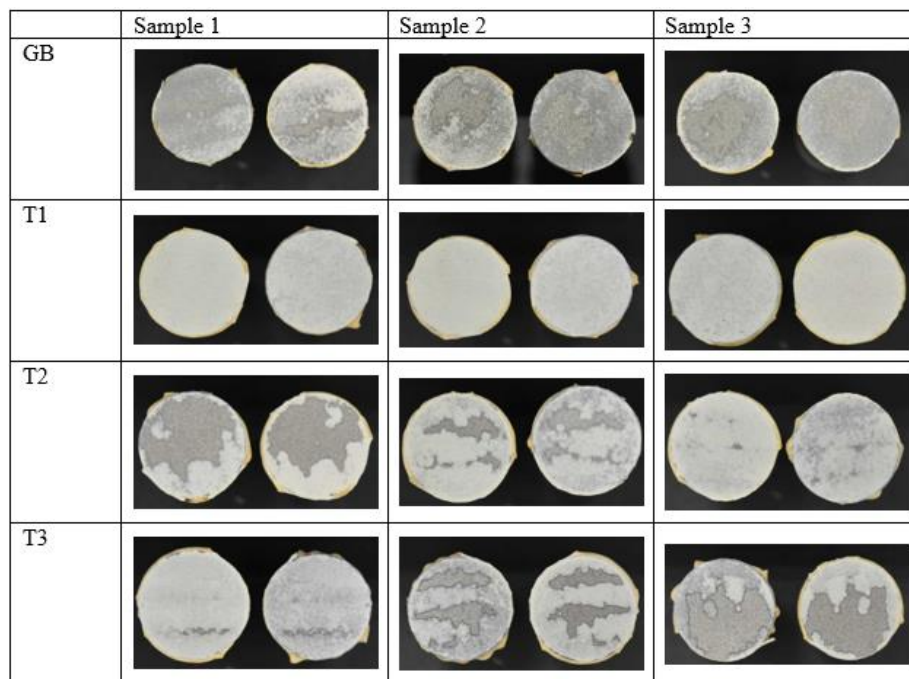


Figure 77: Fracture surfaces of adhesion tested samples. Samples exhibit failure through the TBC as well as through the bond coat.

Below are optical micrographs of the fracture surfaces taken to better understand where failure occurred during testing. Each adhesion test resulted in a metal side and coating side. Since, in most cases failure appears to have occurred within the TBC, the team focused on

imaging the metal side. Figure 78 shows the metal side of a GB sample. Most of the surface looked like what can be seen in Figure 78(a), where primary failure seems to have occurred at the TBC/bond coat interface, with some bond coat also coming out. The exception to this can be seen in Figure 78(b), where a region of bond coat has been completely torn out, indicating failure within the bond coat, perhaps extending to the bond coat/substrate interface.

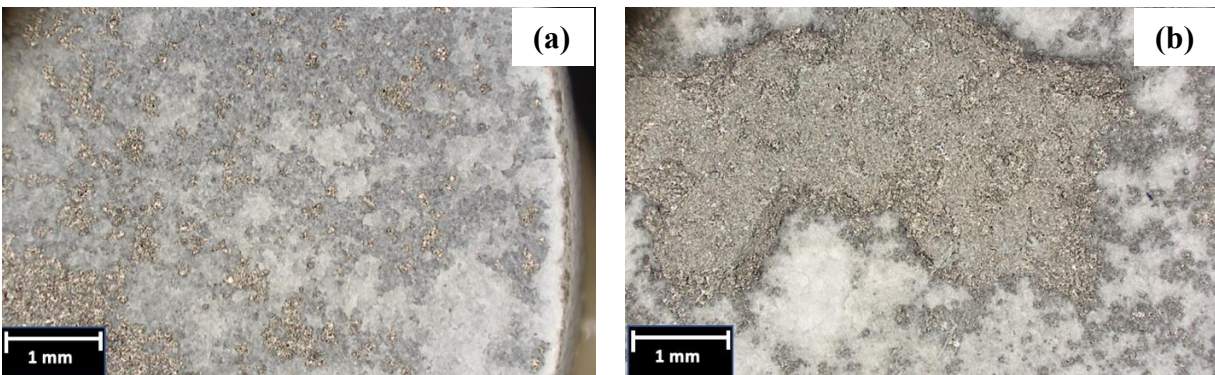


Figure 78: Optical micrographs of the metal side of a GB sample, post-adhesion testing; (a) surface showing mostly TBC failure, and (b) section of the surface where some bond coat has been torn out.

To confirm that the chunk of bond coat we observed in Figure 79(b) had come out on the coating side, the team imaged the coating side of the same GB sample. As expected, most of the coating was TBC with small speckles of bond coat, consistent with our earlier assessment of a TBC/bond coat interface failure. Indeed, the team did find the region of bond coat that had been torn out (Figure 79(b)), corroborating that there was some small degree of bond coat-substrate failure.

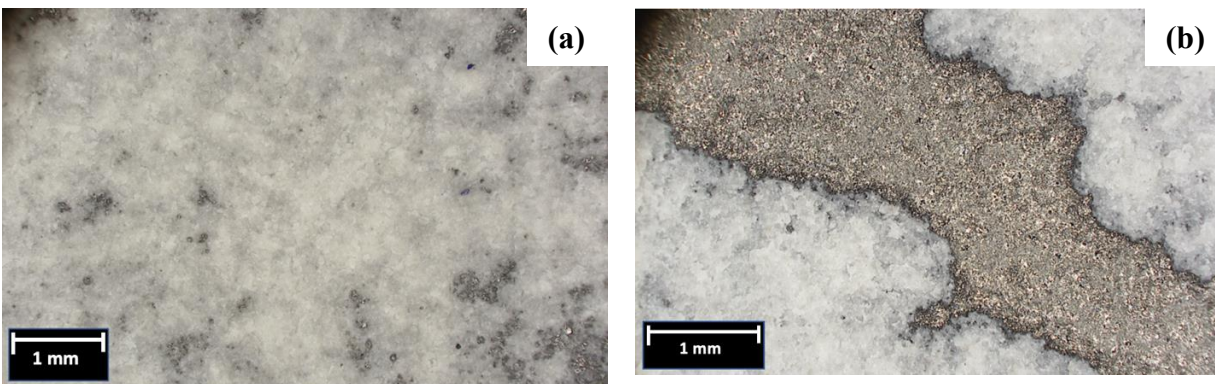


Figure 79: Optical micrographs of the coating side of a GB sample, post-adhesion testing; (a) what most of the coating-side surface looks like, showing that most of what was pulled off was coating, with only some small amounts of bond coat, and (b) a region of the coating-side surface showing a section of bond coat that was torn out – likely corresponding with the area torn out from the metal-side surface in Figure 78(b).

Figure 80 shows metal-side micrographs for a T1 sample. As TBC is continuously visible, the team has determined that this was primarily an intra-TBC failure. Figure 80(b) shows a small amount of the bond coat texture visible around an edge and confirms that the TBC texture was able to fill in the gaps of this texture.

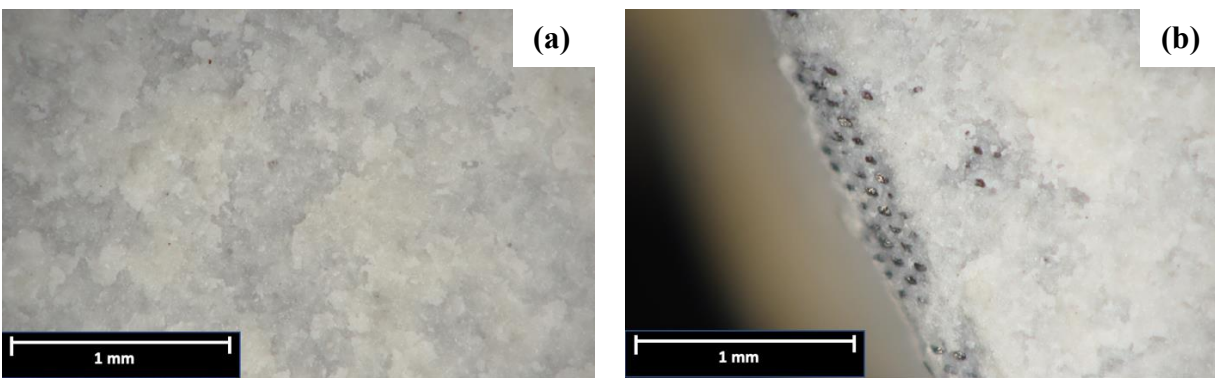


Figure 80: Optical micrographs of the metal side of a T1 sample, post-adhesion testing; (a) what most of the metal-side surface looks like, showing that virtually all failure is within the TBC, and (b) edge exposing top of bond coat texture.

Figure 81 shows the metal-side surface of a T2 sample after adhesion testing. Overall, the fracture location seems to be variable. From these views, it is clear that there was intra-TBC failure, TBC-bond coat failure, and intra-bond coat failure. Figure 81(b) shows a region of the T2 metal surface where the bond coat had been mostly removed, leaving behind only a faint outline of the grid. Based on the team's earlier observations about the T2 grid pattern texture ridges piercing through the bond coat and into the substrate, it can be deduced that this fracture occurred within the bond coat close to the substrate.

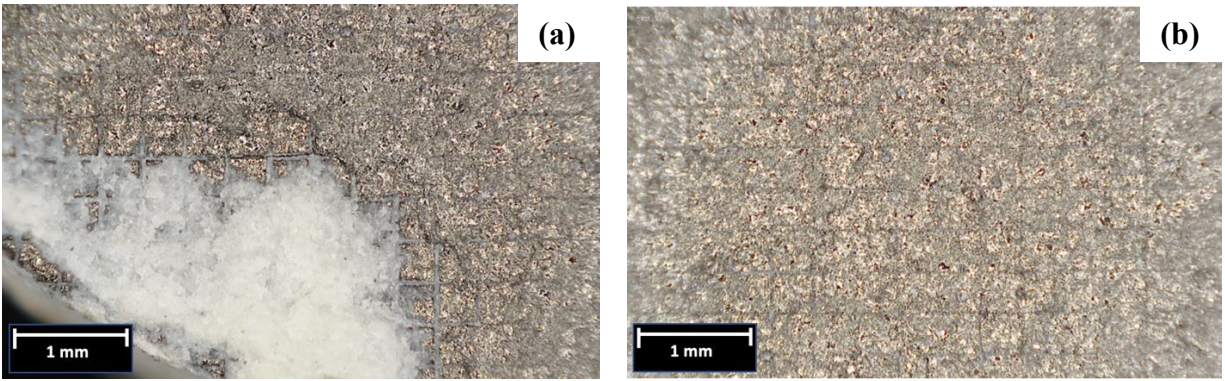


Figure 81: Optical micrographs of the metal side of a T2 sample, post-adhesion testing; (a) a region showing TBC failure, interface failure, as well as bond coat failure, and (b) what left over bond coat looked like.

Figure 82 shows micrographs of the metal-side surface of a T3 sample. Like the T2 sample, failure did not occur in just one region of the coating system. It seems that there was intra-TBC failure, as well as bond coat-substrate failure.

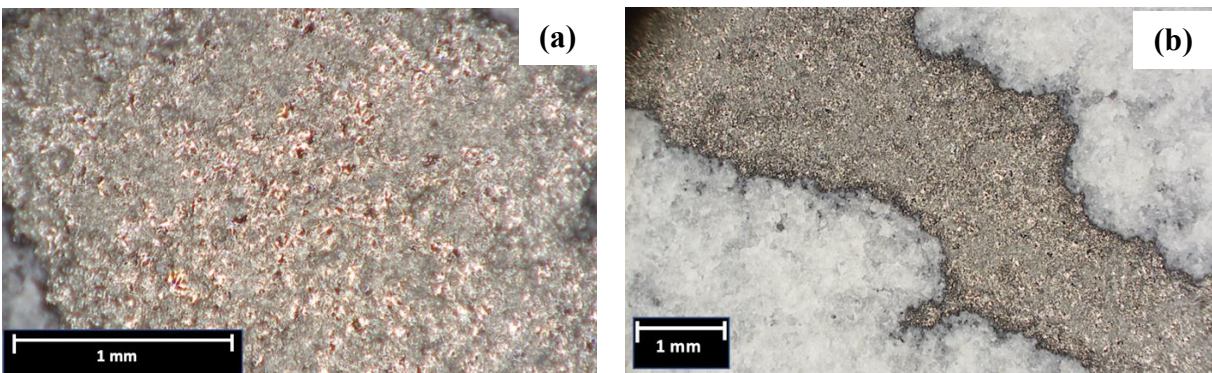


Figure 82: Optical micrographs of the metal side of a T3 sample, post-adhesion testing; (a) a region of exposed bond substrate and (b) an area showing failure within TBC as well as at the bond coat/TBC interface.

VIII. Discussion of Results

A. DVC Induction & Oxidation

1. Grit Blasted Progression

In Error! Reference source not found., a progression of the oxide growth over time for the GB (nontextured) samples is shown in the three micrographs. The as-sprayed, accelerated furnace-cycled and long furnace cycled samples for the GB morphology are shown in chronological order. Although varying in thickness, the bond coat is observed to completely cover the substrate, and the oxide begins by growing on the bond coat/topcoat interface. This oxide appears to grow to such an extent in thickness that it allows for the topcoat to delaminate from the bond coat. As observed in the EDS analysis of GB samples for long furnace cycling (Figure 49) and accelerated thermal cycling (Figure 70), the bond coat acts as an oxygen protector for the substrate. Oxides will form at the bond coat/TBC interface first, preventing the oxygen from diffusing through to the substrate. The bond coat in GB samples covered the entirety of the substrate, unlike some of the other textures. Complete coverage is expected, meaning this would be the most representative sample of actual TBC system oxidation. Because the GB samples had this full coverage, unlike the textured samples, oxide growth was limited to the bond coat/TBC interface and thus provided the second longest average furnace cycle lifetime. It is also observed that the TBC for the GB samples delaminated mostly in one piece as observed in the optical micrographs (Figure 45). The surface profile of the bond coat was relatively regular, allowing for uniform oxide growth. Uniform oxide growth across the entire bond coat/TBC interface likely resulted in a uniform stress distribution that caused complete delamination of the TBC.

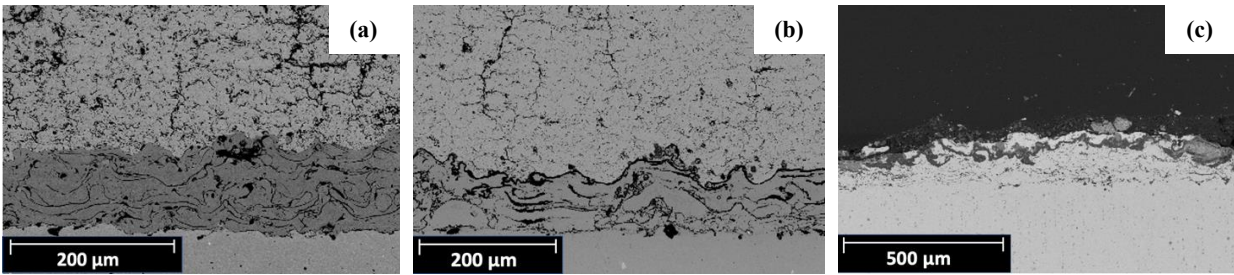


Figure 83: Bond coat/TBC interface progression of GB sample from (a) as-sprayed, (b) 4 short thermal cycles, and (c) failure after long thermal cycles. Shows TGO growth that contributed to coating failure.

The number of cycles required to reach 50% spallation of the TBC in the GB samples that underwent long furnace cycling was significantly lower than what Rolls-Royce observed in previous analyses. The average cycles to failure for the 4 samples tested was observed to be 13, however Rolls-Royce informed the team that they expected the GB samples to last between 50-100 cycles with a duration of 24 hours per cycle. The samples in this analysis underwent long furnace cycling with cycle durations at 12 hours (50% less) and an average number of cycles to failure of 74% less than the low end of the expected lifetime. This discrepancy is very significant because it indicates that something could be fundamentally different from the experiments ran between the team and Rolls-Royce. Grit blasting the substrate for the TBC system, without any laser texturing, is the industry standard. With this processing technique and experimentation method established, the team has concluded that this significant discrepancy in the lifetime of the samples is most likely due to an error in the spray parameters for the topcoat.

In Figure 84(a), an SEM micrograph of the TBC layer sprayed onto test steel sample using chosen spray parameter 4 displays a small number of DVCs that are less developed with minimal branching observed. Comparatively, the as-sprayed samples for each of the 4 texture types have shown much more DVC development and substantial branching. Figure 84(b) shows a direct comparison of DVC development in the as-sprayed grit blast sample. There is no reason for difference between Figure 84(a) and Figure 84(b), given they were both theoretically applied using the same spray parameters on the same bond coat surface – yet there is still an obvious difference. A mix-up of spray parameters is not implausible as there had already been confusion with the spray distance corresponding to spray parameter 4 earlier (the spray parameter sheet

indicated 65mm but the spray booth operator at CCAM indicated that the correct distance was 85mm).

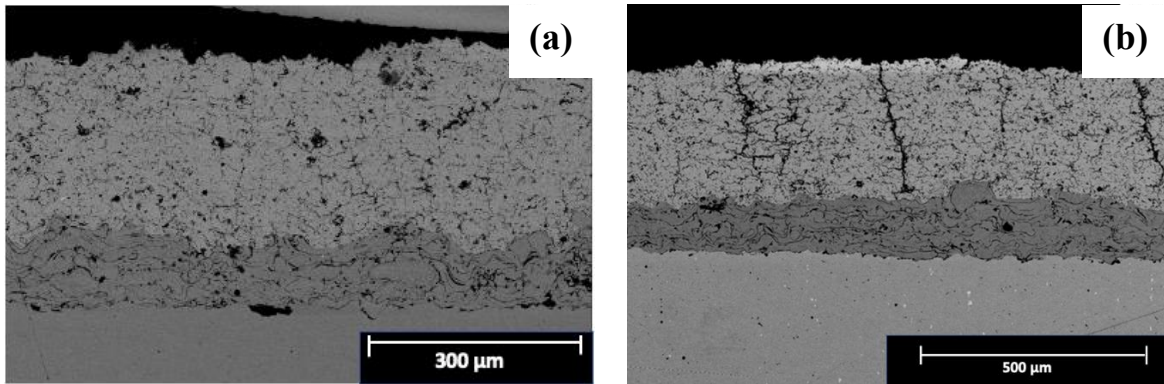


Figure 84: (a) BSE SEM micrograph of the test steel sample sprayed using spray parameter 4, and (b) BSE SEM micrograph of an as-sprayed grit blast sample which had TBC applied using supposedly the same spray parameters.

2. T1 Progression

In Figure 85, a progression of the oxide growth over time for the T1 (rounded spike texture) samples is shown in the three micrographs. The as-sprayed, accelerated furnace cycled, and long furnace cycled samples for the T1 morphology are shown in chronological order. The bond coat did not completely cover the substrate, leaving portions of the substrate in between the rounded spikes exposed directly to the topcoat. This allowed rapid chromium oxide growth in these areas between the rounded spike bond coat, since the bond coat was absent to protect from oxygen ingress. The chromium oxide initiated between bond coat spikes and quickly grew underneath the bond coat, leading to failure at the bond coat/substrate interface. This oxide growth over time is shown in the long furnace cycled sample in Figure 85(c).

Aluminum oxide forms at the interface between the bond coat spikes and TBC, as expected from behavior observed in the GB samples. This observation was validated by Rolls-Royce, stating that aluminum oxide forms first in the system, followed by chromium oxide when all aluminum has been depleted from the bond coat. This behavior, however, was not observed; chromium oxide at the substrate/bond coat interface dominates. This is caused by the lack of aluminum in the substrate, relative to the bond coat. The bond coat contains approximately 12

at% aluminum, while the IN718 substrate contains <0.5 at%. The substrate does, however, contain a significant amount of chromium (13 at%, as shown in Table 10), making it the preferred oxide former. Large regions of exposed substrate make the T1 samples susceptible to chromium oxide growth. The most important difference to note between the two oxides formed is the kinetics; aluminum oxide appears to grow slowly, while the chromium oxide growth is very rapid, causing the stress mismatch that results in coating failure to occur much faster. The team believes this is the reason for T1 samples failing at an average of 2 cycles during long furnace cycling.

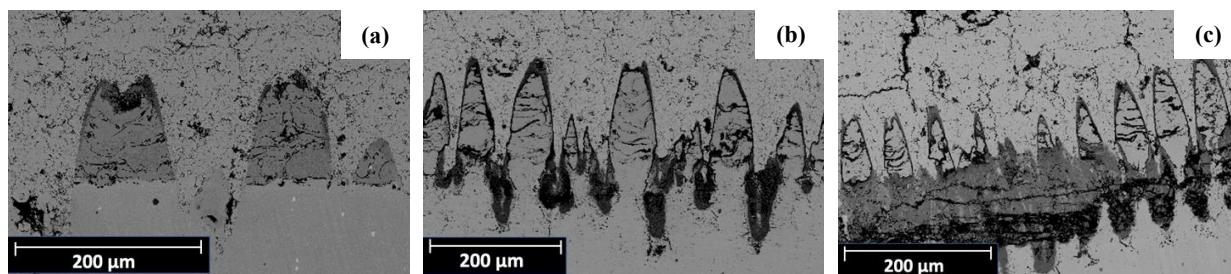


Figure 85: Bond coat/TBC interface progression of T1 from (a) as-sprayed, (b) 4 short thermal cycles, and (c) failure after long thermal cycles. Shows TGO growth that contributed to coating failure.

3. T2 Progression

In Figure 86, a progression of the oxide growth over time for the T2 (grid pattern texture) samples is shown in the three micrographs. The as-sprayed, accelerated furnace-cycled, and long furnace cycled samples for the T2 morphology are shown in chronological order. The EDS data (Figure 74) indicates that the oxide forming on the bond coat/topcoat interface is an aluminum oxide, and the oxide forming in the grid trenches is chromium oxide. The IN718 substrate, with a higher percentage of chromium than the bond coat, reacts with the oxygen, and chromium oxide grows outwards in the trenches. Delamination is observed to have occurred in most locations between the substrate and the bond coat, although more bond coat remains adhered to the substrate compared to T1. The samples with the T2 texture lasted the longest for the long furnace cycling experiment at 15 cycles, although still significantly less than the expected number of cycles of 50-100. This performance may be explained by more uniform arrangement of the DVCs. In the T2 textured samples, in both the as-sprayed and the furnace cycled samples, the

DVCs appear to fall in line with the grid line trenches. This more uniform arrangement of the DVCs may have allowed for more stress relief within the system during the heating and cooling caused by the different coefficients of thermal expansion.

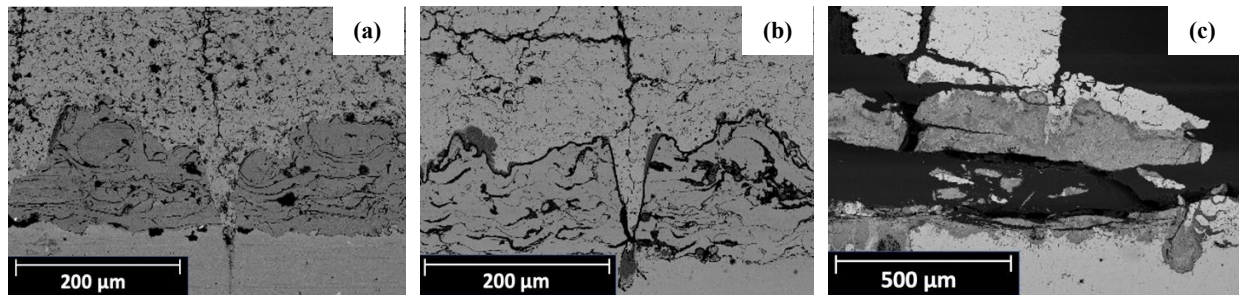


Figure 86: Bond coat/TBC interface progression of T2 from (a) as-sprayed, (b) 4 short thermal cycles, and (c) failure after long thermal cycles. Shows TGO growth that contributed to coating failure.

4. T3 Progression

In Figure 87, a progression of the oxide growth over time for the T3 (grown pattern texture) samples is shown in the three micrographs. The as-sprayed, accelerated furnace-cycled, and long furnace cycled samples for the T3 morphology are shown in chronological order. The accelerated furnace cycling micrograph shows the aluminum oxide growth on the bond coat/topcoat interface. However, the long furnace cycling shows that the bond coat mostly delaminated from the substrate and remained in contact with the TBC topcoat. This may indicate that the oxide growth occurred on the substrate/bond coat interface. The main evidence for this oxide growth allowing the delamination on the substrate/bond coat interface is in the EDS data (Figure 76) showing oxygen on the delaminated coating and the remaining substrate. The grown texture was primarily designed to increase adhesion of the bond coat and the topcoat and not make the DVC arrangement uniform. Since the DVCs are arranged randomly, this may be one factor to explain the poorer performance of the T3 samples compared to the T2 samples during long furnace cycling. The T3 samples lasted an average of 9 cycles during the long furnace cycling. The irregularity of the bond coat thickness also allowed for more oxygen ingress towards the substrate/bond coat interface, creating the fast-growing chromium oxide. The bond coat however appeared to completely cover the substrate, unlike T1 and T2, which comparatively could have protected the substrate more from the rapid oxide growth. The large number of pores between the

bond coat and the topcoat likely decreased adhesion and allowed for more rapid failure compared to the GB samples.

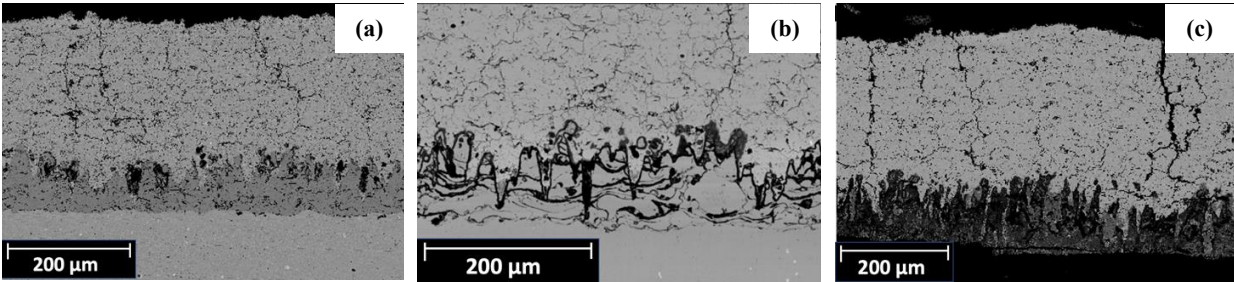


Figure 87: Bond coat/TBC interface progression of T3 from (a) as-sprayed, (b) 4 short thermal cycles, and (c) failure after long thermal cycles. Shows TGO growth that contributed to coating failure.

B. Adhesion Failure

The team's adhesion testing and analysis offers a unique opportunity to isolate the mechanical interlocking property of each bond coat texture type. Because there is no thermal aspect to this testing, there is no differential thermal expansion or dependence on DVC induction. Instead, the mechanical strength of the TBC/bond coat interface is tested with applied axial force.

Overall, the fact that all three textured samples had higher failure loads on average than the grit blast samples indicate that there was improved mechanical interlocking from all the texture geometries over the industry standard grit blasting. Specifically, after analysis of the higher-resolution optical micrographs, some patterns emerge.

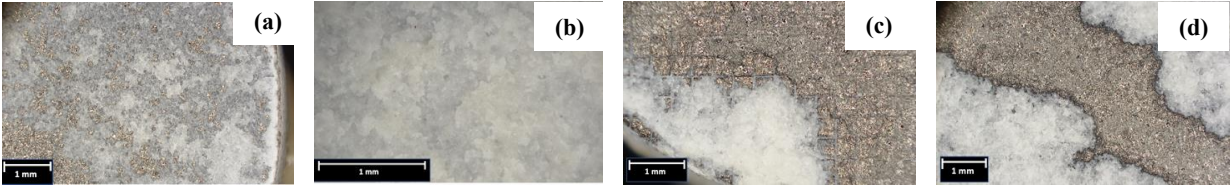


Figure 88: Comparison of adhesion tested metal surfaces; (a) GB, (b) T1, (c) T2, and (d) T3.

Of all the samples, only the GB sample failed primarily along the TBC/bond coat interface. This indicates weak mechanical interlocking between these two layers in the coating system. By contrast, T1 samples failed completely through the TBC layer. This indicates that the TBC/bond coat interface was stronger than the TBC itself due to mechanical interlocking provided by the rounded spikes. These micrographs also confirmed that TBC was successfully deposited in between the rounded spikes, as corroborated by cross-sectional SEM micrographs. The team believes that the increased rounded spike surface area covered by the TBC contributed to this increased interface strength.

The T2 and T3 samples failed in a far less homogenous way. T2 samples showed failure primarily within the TBC and within the bond coat, with a smaller fraction of the surface displayed some TBC/bond coat interface failure. This means that for most of the surface area, the TBC and bond coat strengths were lower than that of the bond coat/TBC interface, hinting at high mechanical interlocking, but not as high as was displayed in T1 samples. The T3 samples showed all failure within the TBC or at the bond coat/substrate interface. Again, this shows that the TBC and bond coat/substrate interface were weaker than the TBC/bond coat interface, indicating high mechanical interlocking.

These findings roughly align with average coating strengths. T1 and T3 samples, which displayed zero or close to zero TBC/bond coat interface failure, failed at the highest loads. T2 samples, which displayed a small amount of TBC/bond coat interface failure, failed at a slightly lower load. Finally, the GB samples, which failed almost entirely along the TBC/bond coat interface, failed at a significantly lower load. From this, the team has concluded that the rounded spike and grown textures provide the most additional mechanical interlocking between the TBC/bond coat interface. This also makes sense from a geometry standpoint, as those textures provide the most increased vertical surface contact which would oppose axial force.

IX. Conclusions and Future Work

A. Conclusions

The work completed by the team for this project has yielded important conclusions which are to be used in the continued development of this technology.

1. Bond Coat Thickness

It is known by Rolls-Royce, and has been observed in this project, that the bond coat acts as an oxygen protector. The thickness of the bond significantly affects how much it protects the substrate from oxide growth, as it is observed with the fast-growing chromium oxide in areas with little to no bond coat applied. The fast-growing chromium oxide has been shown to rapidly deteriorate the number of thermal cycles before failure. It is recommended that the bond coat be made thicker overall to account for ablation and/or the laser parameters are adjusted, so the laser does not ablate through the bond coat, leaving the substrate exposed.

2. TBC Spray Parameters

It was observed that the TBC spray parameters chosen by the group did not align with the expected TBC structure as observed in the test steel samples. This has led the group to believe that the spray parameters chosen by the group were not the same ones used on the IN718 samples. Significantly more DVCs were formed than expected, and there was cross-branching. It is recommended that the spray parameters are further tested to evaluate the spray parameters which produce fewer, less branched DVCs.

3. Mechanical Interlocking is Improved from Texturing

The adhesion results showed better performance for the textured samples compared to the GB control samples. Specifically, failure along the TBC-bond coat interface, which is how the grit blast sample failed at the lowest load, was avoided for all textured samples. T1 and T3 textured samples performed the best, with T2 close behind. This indicates that the texture allowed for better mechanical interlocking through increased vertical surface area contact –

which T1 and T3 have more of than T2 – to oppose axial force. More adhesion tests should be run to obtain statistically significant data.

4. YSZ Powder Size

It was observed, especially on the T3, grown texture, that pores existed between the bond coat and topcoat, likely contributing to decreased performance. This was likely due to the powder size of the YSZ not being small enough to fit into the small spaces created by the grown texture. It is recommended that decreasing the powder size of the YSZ would allow for fewer pores to develop, leading to more contact between the topcoat and the bond coat and better performance.

5. Regular DVC Spacing is Possible

The texture type which performed the best during thermal cycling was the T2 texture type, despite the exposed substrate in the grid trenches. The DVCs followed a relatively uniform pattern, aligning with the grid trenches. This regular DVC spacing likely increased the ability for those samples to withstand the thermal contraction and expansion throughout the cycling. It is recommended that the grid pattern is explored further, perhaps varying the spacing between the trenches to observe how it affects the performance.

B. Suggested Future Work

It is recommended that the TBC spray parameters are adjusted to decrease the number of the DVCs, the YSZ powder size be made smaller, the laser parameters be adjusted to limit depth of ablation and the bond coat be made thicker. After these four factors have been adjusted and improved results confirmed, we suggest further investigation into combining patterns. For example, the promising T2 grid pattern in conjunction with a T3 growth pattern could combine aspects of controlled DVC generation with improved mechanical interlocking. Beyond this, testing should be performed on samples with complex geometry, to mimic the complex components for which this coating system optimization research is being conducted.

X. Acknowledgements

The team could not have completed this work without the help of many individuals: Robert Golden and Matthew Gold of Rolls-Royce, Jason Kalishek of PulseTex, Grant Sowels and Kevin Childrey of CCAM, and Tanner Fitzgerald, Professors Opila, and Professor Fitz-Gerald of UVA. The consistent support, insight, and thoughtful discussions throughout the process aided in the team's success and achievements. The team would also like to thank the other UVA MSE Capstone team—Katie Anderson, Jesper Braley, and Marcus Dupart—for their invaluable support and discussion throughout the year. The facilities of the NMCF and UVA MSE Department were invaluable in this work.

XI. References

Amdry 386-4. (2023). Oerlikon; Metco. <https://mymetco.oerlikon.com/en-us/product/amdry3864>

INCONEL alloy 718. (2007). Specialmetals.Com; Special Metals Corporation.

XII. Appendices

Appendix A: Bond Coat Powder and Spray Parameters

Table A.1: Amdry 386-4 Composition.

| Element | Composition (at %) |
|---------|--------------------|
| Ni | 47.6 |
| Co | 22 |
| Cr | 17 |
| Al | 12 |
| Hf | 0.5 |
| Y | 0.5 |
| Si | 0.4 |

Table A.2: Bond coat spray parameters.

| | | | |
|--|---------------------------|--------|---------------|
| Equipment Configuration | Spray Gun | Type | Sinplex |
| | Anode | Type | Standard |
| | Electrode | Type | Standard, 9mm |
| | Gas injector | Type | Standard |
| | Powder Port | mm | 1.8 |
| | Powder Port Clamp | Type | 90,L |
| | injector standoff dist | mm | N/A |
| | # of Powder Ports | Qty | 1 |
| Powder Feed Parameters Base Station 1 | H1_Material | Type | Amdry 386-4 |
| | H1_Lot Number | # | |
| | H1_Powder feeder | Type | A |
| | H1_Suction | mm | 1.2 NL |
| | H1_Spreader | Type | 1.2 NL |
| | H1_Damper | Type | Standard |
| | H1_Stirrer Type | Type | Standard |
| | H1_Stirrer Speed | % | 60 |
| | H1_Disk Speed | % | 18 |
| | H1_Carrier Gas Flow (Ar) | NLPM | 2 |
| | H1_Powder Feed Rate | g/min | 50.128 |
| Multicoat Parameters | Jambox Voltage | V | 83.1 |
| | Gun Current (Set point) | A | 450 |
| | Gun Current (Actual) | A | 455.9 |
| | Argon Flow (Primary) | NLPM | 55 |
| | Hydrogen Flow (Secondary) | NLPM | 2 |
| | Gun Cooling Jets | Bar | 4 |
| | Water Flow | LPM | 21 |
| | Inlet Temperature | °C | 20.6 |
| | Outlet Temperature | °C | 31.5 |
| | Water Conductivity | µS | 1 |
| | Cooling Power | kW | 15.97 |
| | Gun Power | kW | 37.89 |
| Net Power | kW | 21.92 | |
| Robot | Spray Distance | mm | 130 |
| | Preheat passes | Count | 4 |
| | Number of Passes | Count | 7 |
| | Surface Speed | mm/sec | 1250 |
| | Step Size | mm | 4 |
| | Diameter (Rotation Only) | mm | N/A |
| | Cycle Time | sec | |
| | Powder Flow Timer | sec | |
| Accuraspray 4.0 | Particle Temperature | °C | 2680 |
| | Particle Velocity | m/s | 116 |
| | Intensity | A.U. | 1309 |
| | Plume Density | A.U. | 121 |
| | Plume Deviation | mm | 0 |
| | Plume Width | mm | 10.8 |
| | Exposure Time | µs | 25500 |
| | Signal Amplification | x | 24 |
| | Aggregate Powder Flow | g/min | 50 |

Appendix B: Thermal Cycling

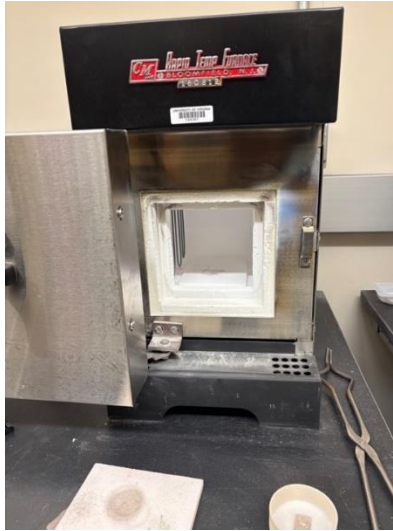


Figure B.1: One of the two furnaces in the Opila lab used for thermal cycling.

Table B.1: Furnace schedule used to divide responsibility for taking samples out of the furnace and putting them back after an hour, every 12 hours.

| | Nico | Iris | Alice | Lara | Chris |
|---------------|------|------|-------|------|-------|
| Sunday 8AM | Y | | Y | Y | |
| Sunday 8PM | | Y | Y | Y | |
| Monday 8AM | Y | | Y | Y | Y |
| Monday 8PM | | Y | | | |
| Tuesday 8AM | Y | Y | Y | Y | Y |
| Tuesday 8PM | Y | | | | |
| Wednesday 8AM | Y | | Y | Y | Y |
| Wednesday 8PM | | Y | Y | | Y |
| Thursday 8AM | Y | Y | Y | Y | Y |
| Thursday 8PM | Y | | Y | Y | Y |
| Friday 8AM | Y | | Y | Y | Y |
| Friday 8PM | Y | Y | Y | Y | Y |
| Saturday 8AM | Y | | Y | Y | Y |
| Saturday 8PM | Y | Y | Y | Y | Y |

Appendix C: Sample Preparation Equipment



Figure C.1: Samples placed in epoxy for mounting post-furnace-cycling.



Figure C.2: Image of resin bond Al₂O₃ blade.



Figure C.3: Cressington 108 Auto Sputter Coater

Appendix D: Characterization Equipment



Figure D.1: Hirox RH-8800 used for optical microscopy.



Figure D.2: (a) Phenom XL G2 SEM and (b) Quanta 650 SEM.

Appendix E: TBC Spray Parameters

Table E.1: Recorded TBC Spray Parameters

| | | |
|--|--------------------------|----------------|
| Equipment Configuration | Spray Gun | Sinplex |
| | Anode | Standard |
| | Electrode | Standard, 9mm |
| | Gas injector | Standard |
| | Powder Port | 1.8 |
| | Powder Port Clamp | 90,L |
| | injector standoff dist | N/A |
| | # of Powder Ports | 1 |
| Powder Feed Parameters Base Station 2 | H2_Material | Metco 204F |
| | H2_Lot Number | W122783 |
| | H2_Powder feeder | B |
| | H2_Suction | 1.2 L |
| | H2_Spreader | 1.2 L |
| | H2_Damper | Standard |
| | H2_Stirrer Type | Standard |
| | H2_Stirrer Speed | 50 |
| | H2_Disk Speed | 26 |
| | H2_Carrier Gas Flow (Ar) | 3.5 |
| | H2_Powder Feed Rate | 35.9 |
| | Multicoat Parameters | Jambox Voltage |
| Gun Current (Set point) | | 550 |
| Gun Current (Actual) | | 554 |
| Argon Flow (Primary) | | 45 |
| Hydrogen Flow (Secondary) | | 5 |
| Gun Cooling Jets | | 2 |
| Water Flow | | 21 |
| Inlet Temperature | | 24.2 |
| Outlet Temperature | | 40 |
| Water Conductivity | | 1 |
| Cooling Power | | 23.15 |
| Gun Power | | 49.25 |
| Net Power | 26.10 | |
| Robot | Spray Distance | 85 |
| | Preheat passes | 12 |
| | Number of Passes | 18 |
| | Surface Speed | 1000 |
| | Step Size | 4 |
| | Diameter (Rotation Only) | N/A |
| | Cycle Time | 52.1 |
| | Powder Flow Timer | 1178.6 |
| Accuraspray 4.0 | Particle Temperature | 4919 |
| | Particle Velocity | 263 |
| | Intensity | 13963 |
| | Plume Density | 1188 |
| | Plume Deviation | 0.8 |
| | Plume Width | 11.8 |
| | Exposure Time | 160 |
| | Signal Amplification | 1 |
| | Aggregate Powder Flow | 36 |

